Integrated Design of Process and Working Fluids for Organic Rankine Cycles

Von der Fakultät für Maschinenwesen der
Rheinisch-Westfälischen Technischen Hochschule Aachen
zur Erlangung des akademischen Grades eines Doktors
der Ingenieurwissenschaften genehmigte Dissertation

vorgelegt von

Matthias Hendrik Fritz Lampe

Berichter: Univ.-Prof. Dr.-Ing. André Bardow
Univ.-Prof. Dr.-Ing. Joachim Gross

Tag der mündlichen Prüfung: 02. Juli 2015

Aachener Beiträge zur Technischen Thermodynamik Band 7
Integrated Process and Organic Rankine Cycle Working Fluid Design in the Continuous-Molecular Targeting Framework

ISBN: 978-3-95886-086-5

Bibliografische Information der Deutschen Bibliothek
Die Deutsche Bibliothek verzeichnet diese Publikation in der Deutschen Nationalbibliografie; detaillierte bibliografische Daten sind im Internet über http://dnb.ddb.de abrufbar.

Herstellung & Vertrieb:

1. Auflage 2016
© Wissenschaftsverlag Mainz GmbH - Aachen
Süsterfeldstr. 83, 52072 Aachen
Tel. 0241/87 34 34
Fax 0241/87 55 77
www.Verlag-Mainz.de

ISSN: 2198-4832

Satz: nach Druckvorlage des Autors
Umschlaggestaltung: Druckerei Mainz

printed in Germany
D82 (Diss. RWTH Aachen University, 2015)

Aachener Beiträge zur Technischen Thermodynamik Band 7
Integrated Process and Organic Rankine Cycle Working Fluid Design in the Continuous-Molecular Targeting Framework

ISBN: 978-3-95886-086-5

Bibliografische Information der Deutschen Bibliothek
Die Deutsche Bibliothek verzeichnet diese Publikation in der Deutschen Nationalbibliografie; detaillierte bibliografische Daten sind im Internet über http://dnb.ddb.de abrufbar.

Herstellung & Vertrieb:

1. Auflage 2016
© Wissenschaftsverlag Mainz GmbH - Aachen
Süsterfeldstr. 83, 52072 Aachen
Tel. 0241/87 34 34
Fax 0241/87 55 77
www.Verlag-Mainz.de

ISSN: 2198-4832

Satz: nach Druckvorlage des Autors
Umschlaggestaltung: Druckerei Mainz

printed in Germany
D82 (Diss. RWTH Aachen University, 2015)

Vorwort

Die vorliegende Arbeit entstand am Lehrstuhl für Technische Thermodynamik (LTT) der RWTH Aachen im Rahmen meiner Tätigkeit als wissenschaftlicher Mitarbeiter. Ich bedanke mich bei Prof. Dr.-Ing. André Bardow, der mich im Vorhaben der Promotion ständig unterstützt und zum Gelingen dieser Arbeit maßgeblich beigetragen hat. Desweiteren gilt mein Dank Prof. Dr.-Ing. Joachim Groß sowohl für viele wertvolle Diskussionen über meine Arbeit als auch für die Übernahme des Koreferats im Promotionsverfahren. Ich danke Prof. Dr.-Ing. Heinz Günter Pitsch für die Übernahme des Vorsitzes der Prüfungskommission und für die angenehme Atmosphäre in der Prüfung. Bei Prof. Dr. ir. Piero Colonna und seiner Arbeitsgruppe möchte ich mich herzlich für die Einladung an die TU Delft bedanken, wo ich eine wundervolle und lehrreiche Zeit verbracht habe.

Ebenso möchte ich mich bei den Mitarbeitern des LTT für die tolle Atmosphäre am Lehrstuhl bedanken. Besonderer Dank gilt Dr.-Ing. Philip Voll, der mir von meiner Projektarbeit im Studium bis hin zu meiner Promotion immer mit Rat und Tat zur Seite stand, und unseren Bürokollegen Johannes Jung und Maike Hennen für eine unvergessliche Zeit im *Office*. Ich danke Niklas von der Assen für die Diskussionen zum Feinschliff dieser Arbeit und für die tolle Zusammenarbeit in der Doppelspitze der Arbeitsgruppe. Ebenso danke ich Marina Stavrou für Tage und Stunden voller spannender Diskussionen rund um die wunderschönen, kleinen Details in CoMT-CAMD. Desweiteren gilt mein Dank den Studenten, die mich in meiner Arbeit am LTT unterstützt haben. Insbesondere danke ich Christoph Kirmse, Peter Edel und Johannes Schilling für ihren Einsatz und für die wertvolle Mitarbeit.

Ich danke meinen Eltern für ihre Unterstützung und für die Ermutigung meine Ziele stets zu verfolgen. Abschließend möchte ich mich bei meiner Frau Simone bedanken, da sie mich während der gesamten Promotion immer perfekt unterstützt hat. Gerade in der Endphase hat sie mir stets Rücken frei gehalten und mich – immer im richtigen Maße – angespornt oder gebremst. Ich danke dir dafür!

Aachen, im Juli 2015 *Matthias Lampe*

Contents

List of Figures

List of Tables

Notation

Latin symbols

a	free Helmholtz energy	$\frac{\mathrm{J}}{\mathrm{mol}}$
AS	Active set	(generic)
b	blade height	m
c	absolute velocity	$\frac{\mathrm{m}}{\mathrm{s}}$
C_0	sprouting velocity	$\frac{\mathrm{m}}{\mathrm{s}}$
d	database of fluids	-
D	diameter	m
e	threshold value	(generic)
f	objective function	(generic)
F	constituting equation for molecular structure	-
g	process model	(generic)
h	specific enthalpy	$\frac{\mathrm{J}}{\mathrm{mol}}$
h	equality constraints	(generic)
I	set of groups	-
m	segment number	-
$\dot{m}$	mass flow rate	$\frac{\mathrm{kg}}{\mathrm{s}}$
p	pressure	bar
P	power	W
R	degree of reaction	-
s	specific entropy	$\frac{\mathrm{J}}{\mathrm{mol\ K}}$
T	temperature	K
T	Taylor-approximation	(generic)
U	speed of rotation	$\frac{1}{\mathrm{s}}$
v	specific volume	$\frac{\mathrm{m}^3}{\mathrm{mol}}$
v	valency	-
w	weighting factor	(generic)
w	relative velocity	$\frac{\mathrm{m}}{\mathrm{s}}$
x	process variables	(generic)

'Scientia et potentia humana in idem coincidunt,
quia ignoratio causae destituit effectum.'

Sir Francis Bacon,
"Novum Organum Scientiarum" (1620)

evap	evaporator
feas	feasible
gross	gross value
hex	hexane ring
HS	heat source
ig	ideal gas
lb	lower bound
m	meridonal
mech	mechanical
min	minimal value
max	maximal value
net	net value
opt	optimal process
pent	pentane ring
pred	prediction of thermo-physical property (where distinction necessary)
pump	pump
rel	relaxed
res	residual
regen	regenerator
s	isentropic
sh	superheating
sat	saturation
red	reduced property
tb	triple bond
turb	turbine
th	thermal
ub	upper bound
wf	working fluid

Abbreviations and Acronyms

CAMD	Computer-Aided Molecular Design
CoMT	Continuous-Molecular Targeting
const.	constant
CHP	Combined Heat and Power
FOM	Figure of Merit

GC	Group-Contribution
infeas.	infeasible
MILP	Mixed Integer Linear Program
MINLP	Mixed Integer Nonlinear Program
MIQP	Mixed Integer Quadratic Program
NLP	Nonlinear Program
ORC	Organic Rankine Cycle
OTEC	Ocean Thermal Energy Conversion
(PC-)SAFT	(Perturbed Chain) Statistically Associating Fluid Theory

Kurzfassung

Die Verstromung von Niedertemperaturwärme ist ein Schlüssel zu einer nachhaltigen Energieversorgung. Eine der wesentlichen Technologien für die Erzeugung von Strom aus Niedertemperaturwärme sind Organic Rankine Cycles (ORC). Die in ORCs eingesetzten Arbeitsmittel werden heute in einem zweischrittigen Verfahren ausgewählt: Zuerst werden mit heuristischem Wissen geeignete Kandidaten ausgesucht. Im zweiten Schritt bewertet eine Prozessoptimierung jeden dieser Kandidaten. Dadurch kann der Beste unter den ausgewählten Kandidaten identifiziert werden. Wird das optimale Arbeitsmittel bei der Vorauswahl von den Heuristiken nicht erfasst, führt das zweischrittige Verfahren zu suboptimalen Lösungen. Dies kann durch eine simultane Optimierung von Arbeitsmittel und Prozess vermieden werden. Eine simultane Optimierung führt allerdings auf ein gemischt-ganzzahliges nicht-lineares Optimierungsproblem, dass aufgrund seiner Größe und Komplexität nicht direkt lösbar ist.

In dieser Arbeit wird eine systematische Methode für die simultane Optimierung von Arbeitsmittel und Prozess vorgestellt. Die Methode basiert auf der Darstellung der Arbeitsmittel in einem physikalisch-basierten Stoffmodell, der PC-SAFT (perturbed chain statistical associating fluid theory) Zustandsgleichung. Mit PC-SAFT werden hier Reinstoffe durch einen Satz von drei Parametern charakterisiert. Die Optimierung wird durch eine Relaxierung der Reinstoffparameter ermöglicht. Dadurch können Prozess und Arbeitsmittel simultan in einem Schritt, dem *Continuous-Molecular Targeting* (CoMT), optimiert werden. Durch die Relaxierung entsprechen die optimalen Werte der Reinstoffparameter im Allgemeinen keinem realen Fluid. Daher werden im nachgeschalteten *Structure-Mapping* reale Stoffe gesucht, deren Eigenschaften den Eigenschaften des optimalen Arbeitsmittels nahe kommen. Dazu wird mittels einer Taylor-Approximation der Zielfunktion aus dem CoMT-Schritt eine Bewertung von Stoffen aus einer Datenbank durchgeführt. Die Methode erlaubt somit die gleichzeitige Optimierung von ORC Prozessen und den darin eingesetzten Arbeitsmitteln.

Das Structure-Mapping zur Suche nach optimalen Fluiden aus einer Datenbank erlaubt es nicht neue Arbeitsmittel zu identifizieren. Daher wird die Methode durch einen Computer-Aided Molecular Design (CAMD) Ansatz erweitert, der die Datenbanksuche ersetzt. Dabei werden die Reinstoffparameter durch eine Gruppenbeitrags-

methode berechnet: Das Fluid wird als Zusammensetzung aus verschiedenen Bausteinen, den sogenannten Gruppen dargestellt. Die Gruppen können einzelne Atome oder kleinere Verbindungen von Atomen sein (z.B. eine Methylgruppe). Im CAMD wird dann eine Kombination aus diesen Gruppen gesucht, die entsprechend der Taylor-Approximation die optimale Molekularstruktur darstellt. Somit ist die Suche nach optimalen Arbeitsmitteln nicht mehr auf eine Datenbank beschränkt sondern erlaubt auch die systematische Suche nach neuen Arbeitsmitteln. Die Anwendung auf das Beispiel eines solar-betriebenen ORC zeigt, dass für realistische Anwendungen tatsächlich neue Arbeitsmittel besser geeignet sein können als die bisher eingestzten.

Für die Arbeitsmittelauswahl werden in der Regel konstante Wirkungsgrade für die Turbine angenommen. Der Wirkungsgrad der Turbine hat einen entscheidenden Einfluss auf die Wahl von Arbeitsmitteln. Umgekehrt ist der erreichbare Wirkungsgrad der Turbine ist abhängig vom eingesetzten Arbeitsmittel. Daher wird das Prozessmodell des ORC um ein Turbinenmodell erweitert. Dieses eindimensionale Modell für eine Radialturbine erlaubt eine Berechnung des Wirkungsgrades und ein vorläufiges Design der Turbine. Das Design der Turbine kann dazu genutzt werden, um nicht erlaubte Wertebereiche für Designparameter (z.B. niedrige Blatthöhe oder hohe Rotationsgeschwindigkeit) auszuschließen. Die Ergebnisse zeigen, dass die Beschränkung der Designparameter einen wesentlichen Einfluss auf die Wahl des Arbeitsmittels hat.

Die bisher aufgeführten Arbeiten beziehen sich auf die Auswahl eines Reinstoffes als Arbeitsmittel im Kreisprozess. In der Literatur werden aktuell vermehrt auch Gemische als Arbeitsmittel vorgeschlagen, um den Wirkungsgrad des Prozesses weiter zu steigern. Daher wird die vorgestellte Methode für simultane Optimierung von Arbeitsmittel und Prozess auf Gemische erweitert. Die Optimierung identifiziert analog zu den Reinstoffen ein optimales, hypothetisches Arbeitsmittelgemisch, das wiederum keinem realen Gemisch entspricht. Das Optimum stellt allerdings eine obere Schranke für die Güte des Prozesses dar. Kein reales Gemisch kann besser sein, als das hypothetische, optimale Arbeitsmittelgemisch. Diese Beobachtung erlaubt einen konzeptionellen Vergleich von Gemischen und Reinstoffen als Arbeitsmitteln, der losgelöst von einzelnen Fluiden erfolgen kann. Dabei wird der Prozess jeweils mit einem Gemisch und einem Reinstoff als Arbeitsmittel optimiert. Die Differenz der Ergebnisse erlaubt es, die Vorteile des Einsatzes von Gemischen zu quantifizieren.

Die vorgestellte Methode eine glichzeitige Optimierung von Arbeitsmitteln und ORC Prozessen. Dabei können sowohl bereits existierende Stoffe aus Datenbanken berücksichtigt werden als auch neue Arbeitsmittel, die bisher nicht bekannt waren. Des Weiteren können auch Gemische aus Arbetsmitteln in der Optimierung berücksichtigt werden, was die Wirkungsgrade der ORC Prozesse noch weiter erhöhen kann.

Chapter 1

Introduction

The depletion of fossil fuels is a well-known problem (Shafiee and Topal, 2009) and the concluding increase in energy cost (Nel and Cooper, 2009) leads to a trend to a more rational use of resources. Furthermore, the limited fossil fuel reserves urge the need to identify regenerative energy sources as a replacement. Here, this thesis is going to focus on systems used for the exploitation of heat sources.

Renewable heat sources are mainly used in two fashions: the direct use of heat and the conversion of heat to power. Direct use of renewable sources for heating is possible for many heat sources and allows for recovery of heat on high as well as low temperature levels. Most common is the direct use of geothermal heat. The highest share of geothermal heat directly used is heat pump systems (71 % of the installed capacities worldwide) as reviewed by Lund et al. (2011). The same authors identify bathing and swimming applications (13 %) and space heating (11 %) as major applications. However, the direct use of heat is only possible, if the heat source and the consumer are close to each other. Furthermore, the focus on heating limits the plant operation mainly to cold days. For this reason, the limited consumption can be the limiting factor for the exploitation of heat sources. Accordingly, the use factor for the direct use is estimated to be 27 % (Lund et al., 2011). In this work, the focus is on the indirect use of renewable heat, where the heat is converted to electrical power. The conversion allows for the efficient transportation using the existing power grid.

One conversion technology allowing for small-scale systems with high flexibility is the Organic Rankine Cycle (ORC). The ORC is based on the Rankine Cycle, which is used for the conversion of heat to power in almost every fossil-based power plant. The Rankine Cycle exploits a temperature difference between a heat source (e.g., hot flue gas from combustion) and a heat sink (e.g., the environment via a cooling tower). For this purpose, a pressurized working fluid is evaporated using heat from the heat source and run over a turbine, where work is extracted. After the turbine, the working

fluid is condensed and pressurized again.

As for every conversion between different forms of energy, there is a limit to the possible rate of conversion from heat to power. Carnot derived an upper bound for the efficiency of the conversion. Under his assumptions,

> "the motive power of heat is independent of the agents employed to realize it; its quantity is fixed solely by the temperatures of the bodies between which is effected, finally, the transfer of the caloric." Carnot (1824)

Thus, the efficiency of conversion directly depends on the temperature of the heat source. Once again, this observation favors fossil-based systems, as the high temperature level achieved by combustion allows for high efficiency. Another interesting observation in Carnot's statement is that efficiency does not depend on the agents employed to realize it. This statement is true under the idealizing assumptions Carnot made to derive an upper bound. However, in non-ideal, real world applications there is a significant influence of the working fluid on the performance of the conversion.

In large-scale power plants, water is used as a working fluid in the Rankine Cycle. Water can be handled easily, it is safe (i.e., not flammable, not toxic, not hazardous), available and cheap. However, the ORC is used for small-scale conversion of low-temperature heat to power. Technical restrictions prevent the usage of water for these applications. The low temperature level of the heat sources would lead to low turbine efficiency and low pressure levels enforcing vacuum technology for the condensation (Vankeirsbilck et al., 2011). Therefore, water is replaced by organic working fluids in the ORC. Organic fluids are typically more volatile than water, which allows for practical pressure levels. Furthermore, the higher molar mass of organic compounds allows for the design of more efficient turbine.

On the one hand side, turning away from water as a working fluid is a challenge for the design of the system. Additional to the design of the cycle itself (e.g., identification of optimal pressure and temperature levels, mass flow rates), a suitable working fluid has to be identified. The search-space of organic fluids is virtually unlimited. Estimates on the number of organic substances range from 10^{20} to 10^{24} (Ertl, 2003). Limited down to stable substances below a certain molar mass (160 Da) Fink et al. (2005) estimate $13,892,436$ compounds still leaving the designer of a system with an virtually unlimited number of options. On the other hand, the working fluid selection adds a new degree of freedom to the design. Thus, the design of the system becomes even more flexible allowing for a design specifically tailored to the application. Additional flexibility and gain in performance are awarded for overcoming the challenges of integrated working fluid and process design.

1.1 Structure of this thesis

In this thesis, the challenge of an integrated working fluid and process design is tackled. In chapter 2, methods are introduced allowing for the design of ORC and working fluids. As the problem of selecting a fluid for a process is not only relevant for the design of ORC systems, a generic problem formulation for the integrated fluid and process design is derived. Methods for solving the problem are presented and shortcomings in the existing methods are identified. Furthermore, the scientific contribution of this thesis is outlined.

A method is presented allowing for the integrated design of fluids and processes in chapter 3. The integrated design exploits the underlying perturbed chain statistical associating fluid theory (PC-SAFT) equation of state in a so-called continuous-molecular targeting (CoMT). The PC-SAFT equation is further supplemented with methods to calculate the ideal gas heat capacity and the molar mass of working fluids. The integrated design method is applied to the design of a geothermal ORC system.

In the chapter 3, the proposed method for the integrated working fluid and process design is based on the selection of working fluids from a database of known PC-SAFT pure component parameters. In chapter 4, the method is extended by computer-aided molecular design (CAMD) allowing for the systematic design of novel molecular structures of working fluids. As illustrative example, the geothermal system from chapter 3 is revisited and the design of working fluids is performed for this example.

The model of the process used for the working fluid selection is based on the common assumption that the turbine efficiency is a constant parameter. In chapter 5, a preliminary design model of the turbine is presented enabling to consider the efficiency and key design parameters of the turbine in the selection of working fluids. The results of a case-study for a small-scale solar ORC system show that the turbine design is a relevant parameter for the selection of working fluids and encourage the use of preliminary design models for the turbine in an early stage of the working fluid design.

The working fluid selection is not only limited to pure components. Similar to the working fluid design of pure components, the consideration of a mixture adds a new degree of freedom to the design problem and allows for the design of more efficient systems. Thus, the method for the working fluid design is extended towards the optimization of working fluid mixtures in chapter 6. The optimization of the zeotropic mixtures is exploited for a comparison between the performance of pure component working fluids and working fluid mixtures.

Chapter 7 presents a brief summary of the thesis and conclusions are drawn. Furthermore, perspectives for future research are given and categorized.

et al., 2011). In OTEC applications, the amount of available heat counteracts the low temperature. The ORC power capacities are limited by the design of the expander. In the small kilowatt-scale, turbo-machinery cannot be employed efficiently, because the size of the equipment is too small to allow for manufacturing under sufficient tolerances. Thus, volumetric expanders are used aiming for micro-scale ORCs ($1 - 10$ kW) suitable for domestic applications (Qiu et al., 2011). For power capacities above $P_{\text{net}} \approx 20$ MW, commonly more ORC units of a smaller capacity are employed, which allows for the use of standardized equipment and security of production.

Various heat sources fall into the application ranges of ORC systems. The largest share of existing ORC systems is used in biomass applications (57 %) (Quoilin et al., 2013). In these systems, waste-heat from a biomass-fired combined heat and power (CHP) engine is used as heat source (Qiu et al., 2012), or a biomass-burner is used to heat the ORC via an intermediate thermo-oil cycle (Drescher and Brüggemann, 2007). Here, the hot flue-gas has high temperatures allowing for high efficiency of the conversion. The second largest field of application is geothermal energy (22 %) followed by waste heat recovery (20 %) with roughly the same number of installed units (Quoilin et al., 2013). Besides these applications that are well established, some fields are emerging, i.e., small-scale (Paepe et al., 2006; Qiu et al., 2011), solar (Tchanche et al., 2009; Delgado-Torres and García-Rodríguez, 2010) and automotive (Bombarda et al., 2010; Lang et al., 2013) applications.

The list of working fluids that are considered for these applications is long and diverse. The classes of considered working fluids include: hydrocarbons (e.g., alkanes, aromatics, and alcohols), flourocarbons (e.g., per-, and hydrofluorocarbons), and linear or cyclic siloxanes. Bao and Zhao (2013) reviewed different studies on ORC systems and give an exhaustive list of approximately 90 working fluids considered in literature.

2.2 Interdependency of process and working fluid

The temperature and power ranges introduced in the previous section can be covered by ORC systems, as the system can be tailored to the application. The key parameters for tailoring the ORC to an application can be identified by considering the flowsheet of the ORC. The ORC is based on the Rankine Cycle. The only difference is that water is replaced by an organic working fluid. A typical ORC (figure 2.1) consists of four major process steps to convert heat to electric power: The heat is transferred to the cycle in the evaporator. Herein, the liquid working fluid is heated up to the

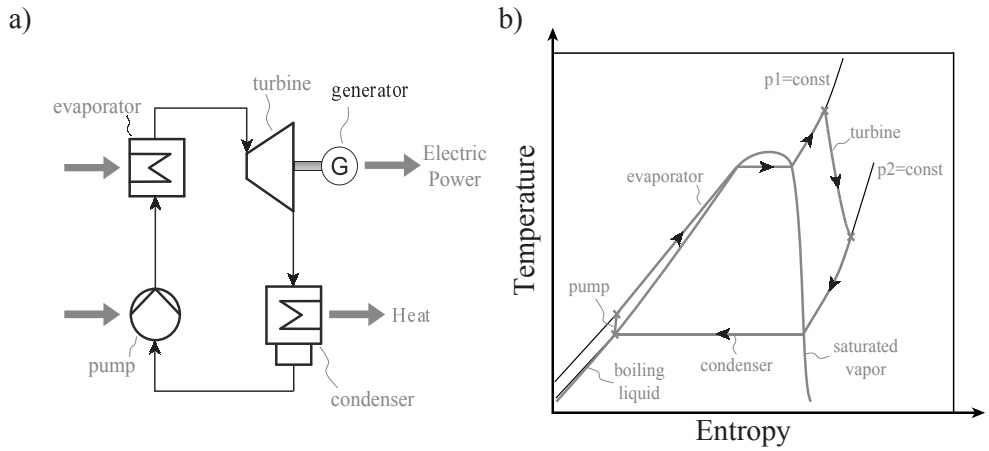

Figure 2.1: Schematic of an Organic Rankine Cycle: a) flowsheet of the ORC process and b) corresponding temperature–entropy diagram.

boiling point, evaporated and superheated at a constant high pressure p_1. The high pressure working fluid vapor leaves the evaporator and drives a turbine. Thereby, the turbine withdraws energy from the working fluid and drives a generator to produce electricity. While the working fluid passes the turbine, the pressure is lowered and the working fluid leaves the turbine as superheated vapor on the lower pressure-level p_2. The superheated vapor is then condensed on the lower pressure-level in the condenser, where heat is emitted from the cycle to the ambient. The low pressure liquid leaving the condenser is fed to a pump, where the liquid working fluid is pressurized again. The working fluid leaves the pump and enters the evaporator again.

The ORC as shown in figure 2.1 has three key parameters that can be tailored to the application: the two pressure levels and the mass flow rate of the working fluid. The pressure levels are a key parameter, as the temperature of condensation and evaporization are set by adjusting the pressure levels. The mass flow rate is decisive for the amount of heat withdrawn from the heat source as well as for the power output of the cycle.

The range of possible applications can be extended by changing the working fluid in the process. The temperature of the phase changes is fixed by setting the corresponding pressure level for a certain working fluid. When the working fluid is replaced, the boiling point of the fluid changes accordingly. This allows adjusting the temperature and the pressure of the phase change. In an integrated design of working fluid and process, this degree of freedom can be exploited to tailor the ORC to an application.

ORC working fluids are commonly categorized in three classes (Chen et al., 2010; Aljundi, 2011): wet, isentropic or dry fluids (figure 2.2). The working fluids are

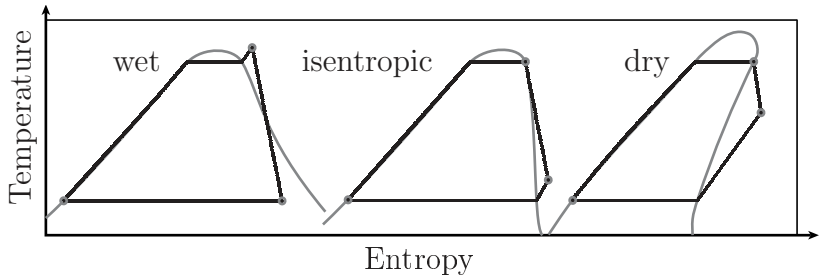

Figure 2.2: Categorization of working fluids according to the slope of the saturated vapor line in a temperature–entropy diagram: wet fluids with negative slope, isentropic fluids with a vertical line, and dry fluids with positive slope. A typical ORC is shown for each type of fluid for comparison.

categorized by comparing the slope of the saturated vapor line in the temperature–entropy diagram (T–s diagram). Wet fluids have a negative slope. Thus, the expansion of the working fluid in the turbine can end in the two-phase region of the fluid leading to formation of droplets and erosion of the turbine. To prevent damages of the turbine, wet fluids are usually superheated. In contrast, isentropic fluids have a vertical slope and superheating is not needed. Dry fluids[1] have an overhanging two-phase region in a T–s diagram (Aljundi, 2011). A dry fluid leaves the turbine as superheated vapor without the need of superheating the fluid in the evaporator.

The working fluid properties enable or prohibit certain cycle conditions as well as certain configurations of the cycle. Branchini et al. (2013) present a systematic comparison of different cycle configurations for 13 working fluids. The least complex configuration is the subcritical, non-recuperated cycle (figure 2.3a). Throughout this work, this configuration is referred to as the *basic ORC*. Depending on the type of fluid, the working fluid can be superheated after the evaporator (dotted line in figure 2.3a). The main degrees of freedom for the basic ORC are the pressure levels at which the cycle is operated, as the pressure levels correspond to temperatures for evaporation and condensation. The dependency of the boiling points on the pressure is one of the most obvious inter-dependencies of working fluid and process.

A dry fluid leaves the turbine as superheated vapor without the need of superheating the fluid in the evaporator (figure 2.2). Additionally, the temperature of the superheated vapor leaving the turbine is higher than the temperature of the boiling liquid allowing for preheating (figure 2.3b). Preheating in a *regenerator* (or *internal heat exchanger*, IHE) can enhance the efficiency of the cycle, when dry fluids are selected as working fluids. Lai et al. (2011) report a positive effect on the efficiency for

[1] also referred to as *o-type* fluids (Chen et al., 2010)

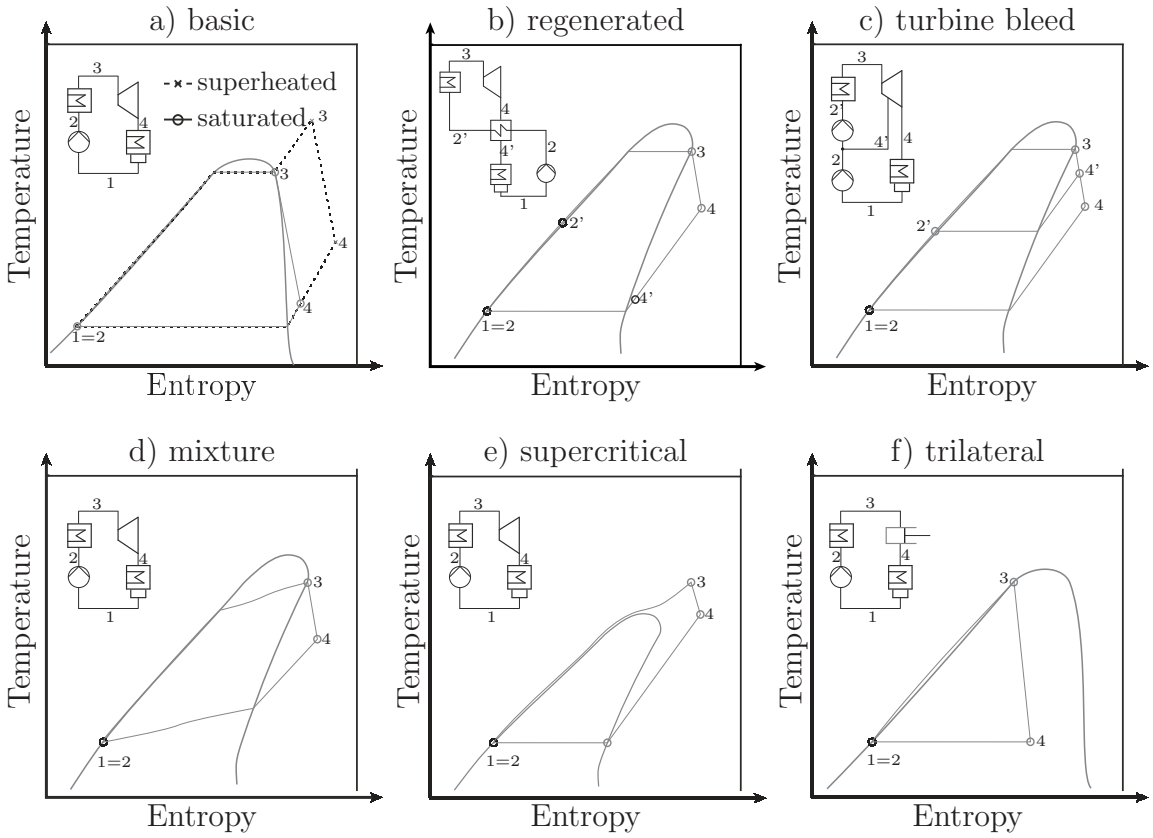

Figure 2.3: Common configurations of ORC systems in a temperature–entropy diagram along with a flowsheet.

various fluids in high-temperature applications. However, Dai et al. (2009) report no enhancement under the considered specifications of waste heat recovery. Desai and Bandyopadhyay (2009) and Branchini et al. (2013) propose turbine bleeding (figure 2.3c) to allow for preheating of the liquid. For this purpose, a part of the working fluid is extracted from the turbine at a mid-pressure level and mixed with the working fluid after the pump.

Besides exploiting preheating, different cycle designs aim for a better match of the temperature curves of working fluid and heat source. This matching limits the exergy losses due to heat transfer. Better match can be achieved by mixtures as working fluids (Angelino and Colonna, 1998; Heberle et al., 2012; Oyewunmi et al., 2014; Mavrou et al., 2015) (figure 2.3d) or by supercritical cycle configurations (Casati et al., 2011; Chen et al., 2011) (figure 2.3e). Another configuration limiting exergy losses for the heating of the cycle is the trilateral cycle (Fischer, 2011). In the trilateral cycle, the

working fluid is not evaporated. Instead, boiling liquid is expanded into the two-phase region (figure 2.3f). The trilateral cycle is preferable for the better match of temperature profiles, but the design of efficient expanders is complex and commercial solutions are not available yet (Löffler, 2008; Fischer, 2011).

Different cycle designs are enabled by the selection of suitable working fluids: e.g., regenerated ORCs can only be employed for dry fluids; supercritical cycles are driven by working fluids with low critical pressure. Furthermore, the variety of applications spans heat source temperatures from 90 °C to 400 °C and more than 4 orders of magnitude in power output. Thus, no single working fluid can be optimal for all configurations and applications at the same time and systematic methods for the selection of a working fluid are needed (Bao and Zhao, 2013; Quoilin et al., 2013). Moreover, the cycle design has to be taken into account as only a combination of process and working fluid enables optimal utilization of the heat source.

2.3 ORC working fluid selection

Working fluid selection is generally recognized as a crucial decision in the design of an ORC, since the performance of the cycle directly depends on the thermo-physical properties of the working fluid (Wang et al., 2012; Stijepovic et al., 2012; Borsukiewicz-Gozdur, 2013; Chen et al., 2010). However, the dependency of thermo-physical properties of the working fluid and the corresponding optimal process parameters is complex and working fluid selection today still depends on experience and heuristic knowledge. In the following, current approaches for working fluid selection specifically used for ORC systems are presented.

Quoilin et al. (2013) showed in their review that different studies recommend different working fluids for the same temperature levels. The recommendation of different working fluids can either be due to different objective functions or different sets of preselected working fluids. Quoilin et al. (2013) therefore conclude that the working fluid selection should be directly integrated into the design process of any ORC system. Such an integrated design approach is missing today for the design of ORCs.

2.3.1 Two-step approach

A typical protocol for ORC working fluid selection (figure 2.4) consists of a preselection step, where a component database is screened for working fluid candidates (Wang et al., 2012; Tchanche et al., 2009; Kosmadakis et al., 2009). The candidates are

Vorwort

Die vorliegende Arbeit entstand am Lehrstuhl für Technische Thermodynamik (LTT) der RWTH Aachen im Rahmen meiner Tätigkeit als wissenschaftlicher Mitarbeiter. Ich bedanke mich bei Prof. Dr.-Ing. André Bardow, der mich im Vorhaben der Promotion ständig unterstützt und zum Gelingen dieser Arbeit maßgeblich beigetragen hat. Desweiteren gilt mein Dank Prof. Dr.-Ing. Joachim Groß sowohl für viele wertvolle Diskussionen über meine Arbeit als auch für die Übernahme des Koreferats im Promotionsverfahren. Ich danke Prof. Dr.-Ing. Heinz Günter Pitsch für die Übernahme des Vorsitzes der Prüfungskommission und für die angenehme Atmosphäre in der Prüfung. Bei Prof. Dr. ir. Piero Colonna und seiner Arbeitsgruppe möchte ich mich herzlich für die Einladung an die TU Delft bedanken, wo ich eine wundervolle und lehrreiche Zeit verbracht habe.

Ebenso möchte ich mich bei den Mitarbeitern des LTT für die tolle Atmosphäre am Lehrstuhl bedanken. Besonderer Dank gilt Dr.-Ing. Philip Voll, der mir von meiner Projektarbeit im Studium bis hin zu meiner Promotion immer mit Rat und Tat zur Seite stand, und unseren Bürokollegen Johannes Jung und Maike Hennen für eine unvergessliche Zeit im *Office*. Ich danke Niklas von der Assen für die Diskussionen zum Feinschliff dieser Arbeit und für die tolle Zusammenarbeit in der Doppelspitze der Arbeitsgruppe. Ebenso danke ich Marina Stavrou für Tage und Stunden voller spannender Diskussionen rund um die wunderschönen, kleinen Details in CoMT-CAMD. Desweiteren gilt mein Dank den Studenten, die mich in meiner Arbeit am LTT unterstützt haben. Insbesondere danke ich Christoph Kirmse, Peter Edel und Johannes Schilling für ihren Einsatz und für die wertvolle Mitarbeit.

Ich danke meinen Eltern für ihre Unterstützung und für die Ermutigung meine Ziele stets zu verfolgen. Abschließend möchte ich mich bei meiner Frau Simone bedanken, da sie mich während der gesamten Promotion immer perfekt unterstützt hat. Gerade in der Endphase hat sie mir stets Rücken frei gehalten und mich – immer im richtigen Maße – angespornt oder gebremst. Ich danke dir dafür!

Aachen, im Juli 2015 *Matthias Lampe*

candidates—and even the optimal fluid—are discarded if the heuristics underlying the metaobjective fail. The definition of a metaobjective for the preselection of working fluid candidates requires the engineer to decide a priori which thermo-physical properties are most important for process performance. In many publications, rules, guidelines or rationales are given which properties of the working fluid are to be considered: Maizza and Maizza (2001); Saleh et al. (2007); Kosmadakis et al. (2009); Tchanche et al. (2009); Mikielewicz and Mikielewicz (2010); Papadopoulos et al. (2010); Kuo et al. (2011); Li et al. (2011); Rayegan and Tao (2011); Siddiqi and Atakan (2011); Stijepovic et al. (2012); Quoilin et al. (2013); Zhai et al. (2014); Palma-Flores et al. (2015).

In this work, the focus is on the thermodynamic properties of the working fluids. However, besides the thermo-physical properties of the working fluids, technical restrictions, laws and regulations apply regarding

- chemical and thermal stability
  (Kosmadakis et al., 2009; Maizza and Maizza, 2001),
- corrosiveness
  (Kosmadakis et al., 2009; Maizza and Maizza, 2001; Kuo et al., 2011),
- compatibility with the employed material
  (Kosmadakis et al., 2009; Maizza and Maizza, 2001),
- properties as a lubricant
  (Kosmadakis et al., 2009),
- toxicity
  (Kosmadakis et al., 2009; Maizza and Maizza, 2001; Tchanche et al., 2009; Papadopoulos et al., 2010; Kuo et al., 2011),
- flammability
  (Kosmadakis et al., 2009; Tchanche et al., 2009; Papadopoulos et al., 2010; Kuo et al., 2011),
- global warming potential GWP
  (Tchanche et al., 2009; Papadopoulos et al., 2010; Kuo et al., 2011),
- ozone depletion potential ODP
  (Maizza and Maizza, 2001; Kosmadakis et al., 2009; Tchanche et al., 2009; Papadopoulos et al., 2010; Kuo et al., 2011).

These restrictions are important for the working fluid selection, as some working fluids are excluded by these criteria. However, the thermo-physical properties of the working fluids enable their use in the ORC in first place. Many rules of thumb and guidelines

for the selection of working fluids are proposed.

Maizza and Maizza (1996, 2001) suggest low critical temperature T_c and pressure p_c, small specific volume v, low viscosity μ and surface tension γ, and high thermal conductivity λ as desirable properties for a working fluid:

$$\max\ p_\mathrm{c}, \lambda; \quad \min T_\mathrm{c}, \mu, \gamma, v \tag{2.1}$$

They conclude that the efficiency for a waste heat ORC application depends mainly on the location of the critical point, and shape and slope of the saturation curves.

For high temperature applications of the ORC, Kosmadakis et al. (2009) propose to select fluids with appropriate critical temperature T_c and pressure p_c, and proper vapor pressure $p^\mathrm{sat}(T)$. Furthermore, a high thermal conductivity λ, a high enthalpy drop in the turbine $\Delta h_{\mathrm{Q}=0}$, and high heat capacity c_p are proposed

$$\max\ \lambda, \Delta h_{\mathrm{Q}=0}, c_p; \quad \min v, \mu, \Delta h_v \tag{2.2}$$

Kosmadakis et al. (2009) conclude from consideration of these criteria that the working fluid selection driven by these properties is a non-trivial problem: the process objective function (e.g., efficiency or net power output) that is mapped by the metaobjective depends not only on the fluid properties, but also on the process parameters assumed for the calculation of the cycle.

Papadopoulos et al. (2010) discuss many of the proposed properties for the design of working fluids and state guidelines for the selection of the criteria. They propose to consider the following objective functions:

$$\max\ \rho, \Delta H_v, \lambda; \quad \min c_p^\mathrm{liq}, \mu\ , \tag{2.3}$$

while constraining the values for melting point T_m, critical point (T_c and p_c), and boiling point of the fluid p^sat.

A small scale ORC system is analyzed by Kuo et al. (2011). They propose differed properties to consider in the selection of a working fluid. They finally conclude that the so-called Figure of Merit ($FOM = \frac{c_p\, T}{\Delta h_\mathrm{evap}}$) is a suitable performance indicator for a working fluid:

$$\min FOM, \mu, v, p^\mathrm{sat}\ . \tag{2.4}$$

Also the critical temperature T_c of the working fluid has to be considered.

Similar guidelines are continuously discussed in literature (Saleh et al., 2007; Li et al., 2011; Rayegan and Tao, 2011; Siddiqi and Atakan, 2011; Stijepovic et al., 2012; Quoilin et al., 2013; Zhai et al., 2014; Palma-Flores et al., 2015).

The key thermo-physical properties considered are: the critical temperature T_c, the specific volume v, the specific heat c_p, and the specific enthalpy of vaporization Δh_v. These properties are important for the design of the ORC system. The critical temperature is chosen since it is known to correlate with the systems thermal efficiency (Aljundi, 2011; Liu et al., 2004). The specific volume is considered for the effect on the sizing and accordingly on the cost of the ORC (Kuo et al., 2011). The heat capacity and the enthalpy of vaporization are often considered simultaneously by the calculation of the Figure of Merit (FOM = $\frac{c_p T}{\Delta h_{\text{evap}}}$) (Kuo et al., 2011). The Figure of Merit has been shown to correlate well with the thermal efficiency of the cycle (Kuo et al., 2011; Mikielewicz and Mikielewicz, 2010). In summary, the definition of the meta-objective for the preselection still depends on experience of the designer.

Besides the complexity of identifying design targets that will lead to optimal efficiency of the ORC, the preselection is not able to cover tradeoffs in the desired values. Tradeoffs occur, when a working fluid has one parameter with a preferable value and one parameter with a sub-optimal value. Such tradeoffs occur frequently and some are inevitable, when the properties of the fluids are assessed independently: The thermophysical properties of working fluids are coupled to each other, as all properties ultimately result from molecular structure and the bonding of the atoms (Poling et al., 2001). For example, bigger molecules have higher critical temperatures (Guo et al., 2011; Qiu, 2012). Furthermore, these molecules have a lower vapor-pressure, and a higher enthalpy of vaporization. These trends are not a direct correlation between size and the properties. However, in figure 2.5, enthalpy of vaporization $\Delta h_v(400\ \text{K})$ and saturation pressure $p^{\text{sat}}(400\ \text{K})$ are plotted each against the critical temperature T_c for 200 different organic substances. Both show a strong correlation to the critical temperature. This observation limits the definition of property targets as metaobjective. When targets are defined for all three properties independently, the design targets cannot be fulfilled by a single fluid.

2.3.1.2 Assessment of candidate working fluids

The definition of the metaobjectives is used to identify a list of candidate working fluids. In the second step of the two-step approach, a process simulation or process optimization is performed for each working fluid. A process model is employed and the process objective function is used for the evaluation of the performance of a working fluid. Different objective functions are used in the design of ORC systems including net power output P_{net} and thermal efficiency η_{th} as important design objectives. The

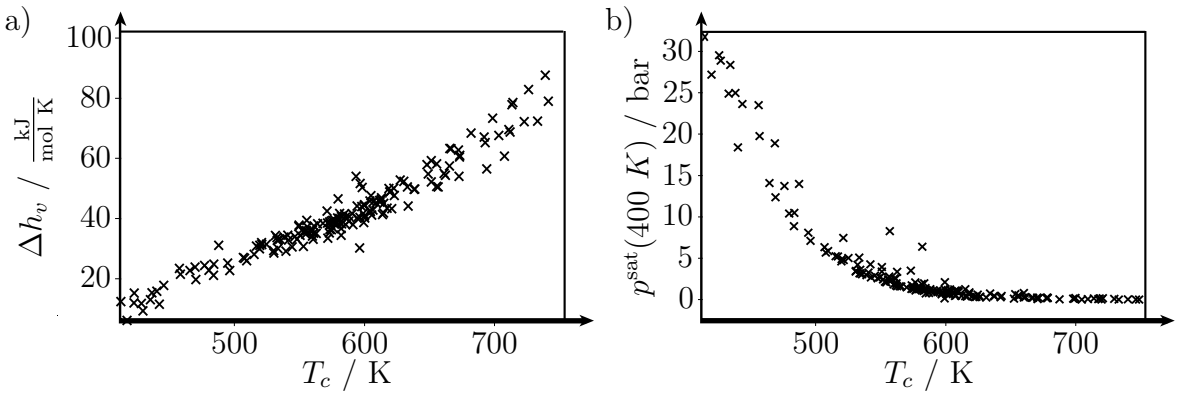

Figure 2.5: Correlations of thermo-physical properties and the critical temperature T_c of organic substances: a) enthalpy of vaporization $\Delta h_v(400\ \text{K})$ and b) saturation pressure $p^{\text{sat}}(400\ \text{K})$.

net power output is defined as

$$P_{\text{net}} = |P_{\text{gross}}| - |P_{\text{pump}}| \ , \tag{2.5}$$

where the power production from the turbine P_{gross} and the power consumption of the pump P_{pump} are considered[2]. The thermal efficiency

$$\eta_{\text{th}} = \frac{P_{\text{net}}}{\dot{Q}_{\text{HS}}} \tag{2.6}$$

considers also the amount of heat supplied to the system by the heat source $\dot{Q}_{\text{HS}}$. Furthermore, the second-law efficiency of the system η_{II} is used to prevent exergy-destruction in the system. The second-law efficiency is defined as (Heberle and Brüggemann, 2010)

$$\eta_{\text{II}} = \frac{P_{\text{net}}}{\dot{E}_{\text{HS}}} \ , \tag{2.7}$$

with $\dot{E}_{\text{HS}}$ is the exergy-flow from the heat source. The models for the calculation of work and heat contribution of the different parts of the cycle, are mainly based on steady-state models under assumptions of constant efficiency for the components. These models allow for an efficient and fast simulation or optimization of ORC systems.

Which of the objective functions is the most important for the design of the system, depends on the application. If the heat is available at no or low cost (i.e., waste heat),

[2]Depending on the sign convention, taking absolute values can be omitted. Here, they are written for clarity.

the amount of heat supplied to the system is less relevant for the revenue of the ORC system and the net power should be used as objective function for the design. For applications, where the heat is connected with cost (e.g., biomass fired ORC systems) the efficiency gains importance. The amount of heat supplied to the cycle can further be relevant, when investment-costs are considered. The heat exchangers—especially the condenser—can contribute a major share of the overall investment of an ORC system (Quoilin et al., 2011; Coskun et al., 2011). Economic objective functions are used to reflect such trade-offs (Quoilin et al., 2011; Coskun et al., 2011; Li et al., 2012; Nafey and Sharaf, 2010; Preißinger, 2014).

2.4 Integrated process and fluid design

As already seen for the design of an ORC system in section 2.3, the inherent difficulty in designing a fluid specifically for a process is the interdependency of process and fluid. The process can be adapted to a specific fluid by adjustment of the process parameters (e.g., pressure, temperature, or mass flow rate) or even the structure of the process (e.g., different reaction scheme, or separation sequence) (Seader and Henley, 2006). In turn, a fluid can be selected to fulfill a specific task in the process under fixed process conditions. However, integrating these two design problems is complex: the number of fluids that are already employed or could be employed in general is high. For each of these fluids, there are optimal process conditions. To ensure a sound comparison the fluids, they have to be compared on the basis of optimal process conditions for each fluid.

In general, the integrated fluid and process design can be formulated as mixed-integer nonlinear program (Gani, 2004), where f is an objective function depending on two types of variables: a vector x representing the variables of the process model and a vector θ of fluid properties (e.g., enthalpies, entropies, densities) at different state points. The objective is to minimize f

$$\min f(x, \theta) \ . \tag{2.8}$$

The integrated design of fluid and process requires a model of the process. The process model introduces two types of constraints: inequality constraints $g_1(x, \theta)$ and equality constraints $g_2(x, \theta)$ depending on the same variables as the objective:

$$g_1(x, \theta) \leq 0 \tag{2.9}$$

$$g_2(x, \theta) = 0 \ . \tag{2.10}$$

In this generic formulation of the problem, the fluid occurs via the vector θ of fluid properties calculated by a general model h . The fluid properties to be calculated depend, in general, on the process variables x. Furthermore, there is a dependency on some parameter-set z to represent the fluid in the fluid model (e.g., pure component parameters). These parameters z depend, in turn, on the fluid selected. The selection is represented by a vector of integer variables y^{s}. The fluid model can thus be formulated as

$$\theta = h\left(x, z(y^{\mathrm{s}})\right) \ . \tag{2.11}$$

The vector y^{s} can either represent an index selecting between predefined fluids or a selection of groups constituting a molecular structure of the considered fluid. In the latter case, y^{s} is restricted by additional constraints to ensure the feasibility of the molecular structure. As these constraints are commonly linear, they are represented by a matrix F:

$$F\, y^{\mathrm{s}} = 0 \ . \tag{2.12}$$

Finally, the formulation of the integrated design of fluid and process is given by eqs. (2.8)-(2.12) as

$$\begin{aligned} \min_{x, y^{\mathrm{s}}} \quad & f(x, \theta) \\ \text{s.t.} \quad & g_1(x, \theta) \leq 0 \\ & g_2(x, \theta) = 0 \\ & \theta = h\left(x, z(y^{\mathrm{s}})\right) \\ & F\, y^{\mathrm{s}} = 0 \\ & x_{\mathrm{lb}} \leq x \leq x_{\mathrm{ub}} \in \mathbb{R}^n \times \mathbb{Z}^m \\ & y^{\mathrm{s}}_{\mathrm{lb}} \leq y^{\mathrm{s}} \leq y^{\mathrm{s}}_{\mathrm{ub}} \in \mathbb{Z}^l \ . \end{aligned} \tag{2.13}$$

This integrated optimization problem allows for selecting an optimal fluid as well as optimal process conditions from a single MINLP optimization problem. The integrated process and fluid design allows for a tailor-made design of a fluid specifically for the process. However, the integrated problem is of prohibitive size and complexity. The combinatorial complexity of the fluid selection and their interdependency with the process variables prevents eq. (2.13) from being solved for the integrated design.

However, in the last two decades much progress has been made towards solving eq. (2.13). Different approaches are presented in the following.

as the normal boiling point.

Following the above definition of CAMD means to solve problem (2.15), where the objective function f_p is a measure of how the *specified set of target properties* is matched by the properties θ

$$\begin{aligned} \min_{y^\mathrm{s}} \quad & f_\mathrm{p}(\theta) \\ s.t. \quad & \theta = GC\left(y^\mathrm{s}\right) \\ & F\, y^\mathrm{s} = 0 \ . \end{aligned} \tag{2.16}$$

Here, the model of the fluid is a group-contribution method GC that only depends on the selection of *building blocks* represented by y^s.

Implementations of the problem differ in the methods for the representation of the molecular structure: The methods depend on a selection of *building blocks*, the so-called groups, from which the molecular structure is build. These groups can either be single atoms or small groups of atoms inside a molecular structure. In a group-contribution method, each of these groups has a certain, predefined contribution to a physical property of the molecular structure. Thus, the value of the property can be calculated as sum over all group-contributions of the molecular structure.

Group-contribution methods are classified by the usage of topological information exploited for the property prediction. First order implementations use only information on the number of groups of each type (Gani et al., 2003). Therefore, the usage of first order groups is preferable from a computational point of view. However, the arrangement of the groups inside the molecular structure has significant impact on the properties of the molecule. Thus, information on the neighborhood of a group can enhance the estimation accuracy. Therefore, higher-order groups are proposed (Marrero and Gani, 2001). A higher-order group is, in principle, a group of groups, i.e., a certain combination of groups, which are adjacent in the molecular structure. Complete topological information can further enhance the accuracy of the employed GC-methods. The information can be stored in the connectivity index (Kier and Hall, 1986; Bicerano, 2002). The full structural information can be exploited, when graph-theoretic approaches are employed (Churi and Achenie, Luke E. K., 1996; Raman and Maranas, 1998). Also a combination of classical group-contribution methods with molecular simulations has been proposed to enhance accuracy (Harper et al., 1999). Employing molecular simulations in a CAMD approach can be exploited for the prediction of numerous properties, e.g., identification of solvents enhancing reactions (Struebing et al., 2013). However, the computational effort for solving problem (2.16) is considerably higher, when topological information is introduced or molecular simulations are employed.

To solve optimization problem (2.16), two types of approaches are commonly employed: *generate–and–test* and *optimization-based* approach. In generate-and-test approaches (as discussed in detail by Brignole and Cismondi (2003)), all molecular structures fulfilling the structural constraints $F\,y^{s} = 0$ are generated. In a second step, the properties for these feasible structures are tested for their performance, i.e., their properties are compared with the targets. This approach is suitable for the generation of small molecules consisting of a limited number of groups. For larger structures consisting of more types of groups, *optimization-based* approaches are used to enable implicit search of the space of solutions (Apostolakou and Adjiman, 2003). For larger search spaces, the optimization-based approach is more efficient compared to a full enumeration in the generate-and-test approach. The optimization can be performed either by rigorous optimization (Apostolakou and Adjiman, 2003; Samudra and Sahinidis, 2013) or stochastic optimization (Marcoulaki and Kokossis, 2000). The use of stochastic optimization allows to incorporate structural alterations to a flowsheet (Marcoulaki and Kokossis, 2000).

Property-based CAMD methods are widely used for the fluid design. Systematic frameworks and methods are proposed (Gani et al., 1991; Friedler et al., 1998; Marcoulaki and Kokossis, 2000; Samudra and Sahinidis, 2013) allowing for the application in many fields. CAMD was applied successfully for, e.g., solvent selection (Odele and Macchietto, 1993; Naser and Fournier, 1991; Pistikopoulos and Stefanis, 1998; Marcoulaki and Kokossis, 2000; Papadopoulos and Linke, 2009), polymer design (Derringer and Markham, 1985; Gani, 2007; Vaidyanathan and El-Halwagi, 1994), or refrigerant design (Duvedi and Achenie, 1996; Gani, 2007; Sahinidis et al., 2003; Samudra and Sahinidis, 2013; Marcoulaki and Kokossis, 2000). Papadopoulos et al. (2010) present a property-based CAMD method for the design of ORC working fluids.

A major obstacle for the application of the property-based CAMD method is the sound definition of target properties. The target properties in this approach are independent from the process conditions due to the decoupling of the optimization problem. Thus, predefined properties cannot incorporate different process conditions, e.g., different pressure levels. Harper (2000) points out the importance of a sound definition of the property targets considered and concludes that their definition should be considered an aim for the design of new CAMD-frameworks.

In ORC systems, the optimal fluid depends inherently on the considered process conditions (sec. 2.2). In an a priori definition of thermo-physical design targets, their dependency on the considered process conditions is not taken into account. The proposed guidelines for the working fluid selection (sec. 2.3.1) reflect the challenge of defining a suitable design objective for ORC working fluids.

2.4.1.2 Targeting approaches

Targeting approaches have been developed allowing for the identification of favorable fluid properties (Eden et al., 2003, 2004; Bommareddy et al., 2010; Roskosch and Atakan, 2015). The targeting allows for efficient approximate solution of problem (2.13) by omitting the equations enforcing the feasibility of a fluid, the so-called constituting equations. For targets based on the thermo-physical properties of the fluid the optimal values are identified in

$$\begin{aligned} \min_{x,\theta} \quad & f(x,\theta) \\ \text{s.t.} \quad & \theta = h(x) \\ & g_1(x,\theta) \leq 0 \\ & g_2(x,\theta) = 0 \ . \end{aligned} \tag{2.17}$$

This optimization yields optimal thermo-physical properties of the fluid θ^* and optimal process parameters x^*. In this way, real fluids are not identified in the targeting, but properties of a fluid that indicate a favorable performance are found. These design targets θ^* are conceptually different from the pre-defined properties of simple approaches. The targeting allows for the identification of desirable properties, while considering the process and options for the adaption of the process to the fluid in a sound and systematic way. The objective function in the targeting can be a process-based measure of the performance (e.g., thermodynamic efficiency, exergy loss) or even an economic objective function (e.g., sales revenue, product cost, net capital cost) based on the data gathered from the process design. When constituting equations for the feasibility of the fluid are neglected, the complexity of the optimization problem is reduced and the degrees of freedom on the process can be considered in the optimization for the identification of the optimal properties of the fluid.

However, any targeting approach relies on the ability to characterize the working fluid sufficiently in the targeting. This ability ensures that fluids with the identified optimal properties can be found in a second step. Two aspects have to be considered: First, the optimized properties of the fluid have to reflect the effect of the fluid on the process sufficiently. Second, the optimal properties of the fluid might be contradicting, if the fluid model lacks consistency. If one of these two aspects is not considered, the targets identified in the first step do not characterize an optimal fluid.

Bardow et al. (2010) proposed a targeting approach exploiting the coarse-grained molecular model of the physically-based PCP-SAFT equation of state (Gross and Sadowski, 2001, 2002; Gross, 2005; Gross and Vrabec, 2006). The so-called continuous-molecular targeting (CoMT) aims at solving the integrated design problem by re-

Contents

mutations. The locality of the mutation exploits that solutions that are near in the search space are likely to lead to similar objective function. This is not the case for database-indexes. These properties of the problem render the complexity of solving the problem to optimality as the same complexity as a complete enumeration of the (fluid) search space.

In their pioneering work, Papadopoulos et al. (2010) introduced methods to avoid the preselection of candidates by using CAMD and multi-objective optimization. The multi-objective optimization allows to account for more than one property or metaobjective as objective function. In a more recent work on the design of working fluid mixtures (Papadopoulos et al., 2013), the same authors show that the use of process-related objective functions (thermal and exergetic efficiency) in their design approach is possible. The calculation of these process-related objective functions is achieved by applying a cubic equation of state and a process model. The authors clearly demonstrate the merits of a design approach for ORC incorporating both working fluid and process. The problem is solved for one of the mixture components, while skipping the constituting equations for the second. Then, the solution for the first mixture component is fixed and the problem is solved again to identify an optimal second component of the mixtures.

The integrated design problem can be solved in sound and detailed implementation of process and fluid model, when the fluid search space is compact. Pereira et al. (2011) use an optimization-based approach for the integrated solvent and process design, where the fluid is represented in the SAFT-VR equation of state and a detailed process model for the optimization is employed. As degree of freedom for the fluid selection, the number of C-Atoms for an alkane is used. The combination of the number of C-Atoms as a degree of freedom and the SAFT-family of equations of state is promising, as physical properties of fluids scale well with the parameters employed for the representation of the fluid (Blas and Galindo, 2002). However, this approach is limited to the selection from a single family of fluids.

2.5 Contribution of this thesis

The literature review reveals remaining challenges in the selection of ORC working fluids: The interdependency of the optimal working fluid properties and the process should be reflected. Thus, in this thesis a design framework is presented allowing for the simultaneous optimization of working fluid and process based on the CoMT-CAMD concept (Bardow et al., 2010). The framework is extended to (1) allow for the

design of new working fluids by employing a CAMD method and (2) the consideration of mixtures as working fluids.

The process models used for the working fluid selection are commonly assuming a constant turbine efficiency for all considered working fluids. Assuming the same turbine efficiency for all working fluids is justified when only similar working fluids are considered. In CoMT-CAMD, the search space of the working fluids is extended to consider more existing and even novel working fluids. Thus, measures have to be employed to ensure the existence of an efficient turbine. Here, a preliminary model for the turbine design is proposed that allows for constraining the search space of working fluids to those fluids allowing for an efficient turbine design. These contributions and merits of the thesis outlined in the following.

Integrated design of ORC working fluids and processes In chapter 3, a method is presented for the design of ORC working fluids based on the integrated design of process and working fluid. The presented approach is based on a continuous-molecular targeting. Here, the targeted variables are not the thermo-physical properties of the working fluid, but the pure component parameters describing the working fluid molecule are used. In the presented approach, the PC-SAFT equation of state is used as a single and consistent model for the working fluid properties. Based on the design targets, a structure-mapping is performed in a second step to identify real working fluids with a similar performance as the target. Different strategies for the structure-mapping and the explicit consideration of constraints for the process are presented and discussed. The method is presented in a numerical example for the selection of an ORC working fluid to present the merits of the integrated design of working fluids and processes.

Computer-aided molecular design based on continuous-molecular targets The structure-mapping presented chapter 3 is based on a database of existing working fluids; thus, the design of new working fluids is not possible. In chapter 4, a CAMD method based on continuous-molecular targets is presented. This CAMD method is based on parameters that are identified in the CoMT-optimization rather than from heuristic definition. Furthermore, the design objective in the presented CAMD approach is a process-based objective function instead of working fluid properties.

Considering turbine design in working fluid selection The design of suitable expanders for ORC systems is regarded as one of the major challenges for the design of ORC systems (Bao and Zhao, 2013; Quoilin et al., 2013; Colonna et al., 2015). The design of the turbine is commonly postponed to later stages of the design of an ORC system. Here, a preliminary design model is integrated into the process model allowing for the consideration of the turbine design already in the working fluid selection. For

this purpose, a radial turbine model is included into the proposed integrated design of process and working fluid in chapter 5. The turbine model extends the model for the process and allows for a preliminary design. In such a holistic model, working fluid process and turbine can be considered all at the same time.

Extending the design approach towards mixtures The proposed design approach for the integrated optimization of working fluids and process is extended to allow for the design of working fluid mixtures. The extension is based on introducing a second set of pure component parameters and the mixture composition as new degrees of freedom. The optimization of optimal hypothetical working fluid mixtures is achieved. Here, the focus is not on the selection of real mixtures for a specific application. Instead, the results of the optimization are compared to optimal pure components to assess the potential improvement in performance using binary working fluid mixtures.

Chapter 3

Continuous-molecular targeting for Organic Rankine Cycles

In this chapter, a method for the integrated design of ORC process and working fluid is presented. The integrated design of working fluid and ORC process (Fig. 3.1) begins with the typical specifications of the ORC application. For the design of an ORC, at least temperature and mass flow rate of the heat source have to be defined. Furthermore, information on, e.g., allowable pressure levels, or information on the cooling system can be used to specify the application. These specifications lead to the definition of constraints and parameters in the process optimization. The integrated design requires a model for both the process and the working fluid (sec. 2.4). Thereby, the working fluid and process are both optimized using the same objective function; the definition of heuristics for preselecting a working fluid is overcome. The solution is an optimal pair of working fluid and process. Such a simultaneous optimization directly captures all trade-offs between the process and the working fluid properties.

A mathematical formulation of the integrated design leads to a MINLP of prohibitive size and complexity, because a discrete degree of freedom is added to the problem for each working fluid (sec. 2.4). In the presented approach, the working fluid is represented by a thermodynamic model (Fig. 3.1). Herein, the working fluid

---

Contents of this chapter have been published in:

Lampe, M., Stavrou, M., Bücker, H. M., Gross, J., and Bardow, A. (2014). "Simultaneous Optimization of Working Fluid and Process for Organic Rankine Cycles Using PC-SAFT". *Industrial & Engineering Chemistry Research*,53(21):8821–8830.

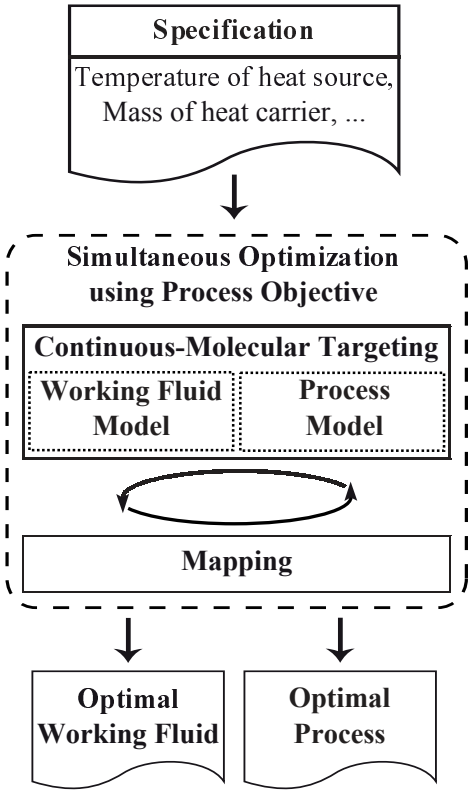

Figure 3.1: Framework for simultaneously optimizing process conditions and working fluid. The scheme shows the continuous-molecular targeting step and the structure-mapping step.

properties are defined by a set of pure component parameters. The working fluid model employed in the presented framework is PC-SAFT (section 3.3). PC-SAFT is a model for the residual Helmholtz energy and thus gives a consistent picture of all equilibrium properties of the working fluid. The integrated design of working fluid and process is enabled by relaxation of the pure component parameters for the working fluid in PC-SAFT from their discrete to continuous values. The relaxation allows for a simple gradient-based optimization of the objective function with respect to both, the pure component parameters and process conditions. The result of the optimization, the so-called continuous-molecular targeting, is an optimal process and an optimal, hypothetical working fluid described by its PC-SAFT pure component parameters. Since these parameters usually do not coincide with a real fluid, real working fluids with similar properties are identified in the subsequent so-called structure-mapping. The continuous-molecular targeting concept has been introduced by (Bardow et al., 2010) for the simultaneous solvent and process design.

3.1 Continuous-molecular targeting

In PC-SAFT, the properties of a pure component are entirely defined by a vector z of pure component parameters, each specifying molecular attributes of the component, such as van der Waals attraction or hydrogen-bonding energy. In the suggested approach, the pure component parameters are relaxed from discrete to continuous values to allow for an integrated design of process and working fluid. The relaxation of the pure component parameters transforms the mathematical problem of integrated working fluid and process design (sec. 2.4) into a nonlinear program (NLP) solvable with standard solvers. The resulting problem consists of two types of variables: the vector z of pure component parameters and a vector x of key process parameters. The NLP formulation

$$
\begin{aligned}
&\min_{x,z} f(x,\theta) \\
&\text{s.t. } g_1(x,\theta) \leq 0 && \text{process model (inequalities)} \\
&\quad g_2(x,\theta) = 0 && \text{process model (equalities)} \\
&\quad \theta = h(x,z) && \text{PC-SAFT} \\
&\quad A(d)\, z \leq b(d) && \text{convex hull} \\
&\quad x_{\min} \leq x \leq x_{\max} \\
&\quad z_{\min} \leq z \leq z_{\max} \\
&\quad x \in \mathbb{R}^n,\ z \in \mathbb{R}^l
\end{aligned}
\tag{3.1}
$$

allows for an optimization of the objective function $f(x,\theta)$. The degrees of freedom are the key process parameters x and the pure component parameters z of the working fluid. The formulation in (eq. (3.1)) has two sets of constraints: The set $g(x,\theta)$ contains the model of the process itself consisting of inequalities $g_1(x,\theta)$ and equalities $g_2(x,\theta)$. The equations $h(x,z)$ represent the PC-SAFT model calculating the thermo-physical properties θ needed for the process model (e.g., enthalpies, entropies, or densities). For the ORC process, any model based on thermo-physical equilibrium properties can be used in the current implementation of the framework. The proposed approach allows for different objective functions, constraints, and specifications. Discrete design decisions (e.g., use of regeneration) could directly be integrated into the process model by introducing binary variables.

The problem of introducing discrete degrees of freedom to describe the working fluid in a simultaneous optimization is overcome. The pure component parameters of the working fluid and the process conditions are degrees of freedom on an equal footing to the optimization. A simple (gradient-based) optimization leads to the

could be used as an indicator for the performance of the working fluid i. However, the distance $dist(z_i)$ is affected by scaling and units chosen for the pure component parameters. Moreover, the sensitivity of the objective function with respect to the different pure component parameters is not reflected. Thus, the simple distance is not employed, but a Taylor-approximation of the objective function estimates the performance. The Taylor-approximation based on the Hessian and Jacobian of the objective function with respect to the pure component parameters. Thus, the Taylor-approximation incorporates the influence of the parameters on the objective function.

The estimation based on this Taylor-approximation is the basic structure-mapping and discussed in sec. 3.2.1. Furthermore, shortcomings of the basic structure-mapping are identified and improvements of the basic approach are introduced in sections 3.2.2 - 3.2.4.

3.2.1 Basic structure-mapping

The key idea of the structure-mapping is to estimate the performance of a working fluid with given parameters z using a Taylor-approximation (Bardow et al., 2010). As each working fluid is solely described by its pure component parameters, a Taylor-approximation in the pure component parameters is used. However, the process parameters x have to be considered. For this purpose, a process optimization is employed, which allows for optimizing the process variables x for given pure component parameters $\bar{z}$. The process optimization can directly be derived from eq. (3.1), where the constraints for the pure component parameters z are neglected.

$$\begin{aligned} f^{\mathrm{opt}}(\bar{z}) := \min_{x} & f(x,\theta) \\ \text{s.t. } & g_1(x,\theta) \leq 0 \\ & g_2(x,\theta) = 0 \\ & \theta = h(x,\bar{z}) \\ & x_{\min} \leq x \leq x_{\max} \in \mathbb{R}^n \ . \end{aligned} \tag{3.4}$$

The process optimization (3.4) yields the optimal performance of the working fluid, i.e., the value of the objective function f^{opt} for the optimal values of the process variables x^{opt}. The Taylor-approximation of f^{opt} depends only on the pure component parameters z of the working fluid and is used as performance estimate

$$\hat{f}(z) := f^{\mathrm{opt}}(z^*) + \frac{\partial f^{\mathrm{opt}}}{\partial z}\,(z_i - z^*) + \frac{1}{2}\,(z_i - z^*)^{\mathrm{T}}\,\frac{\partial^2 f^{\mathrm{opt}}}{\partial z^2}\,(z_i - z^*)\ , \tag{3.5}$$

where the Hessian $\frac{\partial^2 f^{\text{opt}}}{\partial z^2}$ and the Jacobian $\frac{\partial f^{\text{opt}}}{\partial z}$ of the objective function as well as the optimal hypothetical working fluid z^* are independent of the working fluid z_i. Thus, the estimate $\hat{f}$ can be evaluated efficiently for the complete database of pure component parameters z_i to estimate of the performance of each working fluid.

However, changes in the active-set of constraints are not considered in the Taylor-approximation $\hat{f}(z_i)$ in eq. (3.5): for the optimal hypothetical working fluid, a subset of constraints is active after the process-optimization using eq. (3.4), e.g., the upper pressure is at bound. For working fluids near the hypothetical optimal working fluid, the same subset of constraints is active. For a working fluid in another region of the search space, the pressure might be limited by another constraint, e.g., critical pressure limiting the pressure level. The Taylor-approximation in eq. (3.5) is based on local information from the optimal hypothetical working fluid. The effect of changes in the active-set is not captured by the Taylor-approximation. The active-set of constraints is defined as the subset of inequality constraints that are at their bound in the optimal solution.

$$AS(\bar{z}) := \left\{ i : g_{1,i}\left(x^{\text{opt}}, h(x, \bar{z})\right) = 0 \right\} \ , \tag{3.6}$$

where $g_{1,i}\left(x^{\text{opt}}, h(x, \bar{z})\right)$ denotes the i-th entry of the inequality constraint vector g_1. For the process optimization problem in eq. (3.4), the active set depends on the pure component parameters used; for different working fluids, different constraints will be active in the optimal process. Using eq. (3.5) for the ranking of different working fluids implicitly assumes that the active set of constraints from the optimal values will be the active set of constraints for each combination of pure component parameters. If the assumption holds, the ranking based on eq. (3.5) is close to the correct ranking of the working fluids[1]. However, three different situations are illustrated in fig. 3.2, where the assumption fails for a one dimensional problem. In situation a), a change in the active-set occurs for $z > z^*$ enforcing a sub-optimal value for x. Thus, the constraint becoming active prevents the objective function from reaching the estimated value. This situation can be handled by a Taylor-approximation for each of the inactive constraints as described in sec. 3.2.2. A similar situation is shown in 3.2b), but the constraint becoming active makes the problem infeasible for all values of x. Though the problem can be overcome in the same way as problem a), a more effective approach is presented in sec. 3.2.3. Finally, in situation c), the active-set changes exactly at the optimal value of the objective function. For such situations, an iterative approach for the structure-mapping is presented in sec 3.2.4.

[1] I.e., a ranking based on the true performance of the working fluid

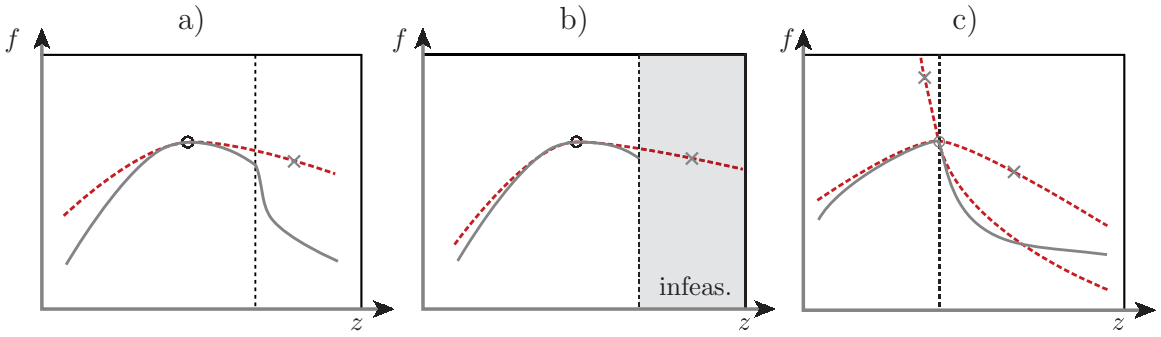

Figure 3.2: Problems for the basic structure-mapping: The Taylor-approximation (dashed line) at the optimal value (o) overestimates the performance (x) of a working fluid. a) Constraints becoming active and limiting $f^{\mathrm{opt}}(z)$, b) Constraints becoming active and rendering the problem infeasible, c) Constraints becoming active directly at the optimal value.

3.2.2 Inactive constraints

The Taylor-approximation from eq. (3.5) is determined at the optimum. In the case of constraints becoming active for some point, which is not the optimal value, the Taylor-approximation does not account for this constraint. When the constraint becomes active, the working fluids performance is over- or underestimated. The presented refinement aims at excluding the regions of the search space, in which the constraint is expected to be active.

The inequality constraints g_1 of the process are treated in a similar way as the objective function itself. Consider the case of any inactive inequality constraint $g_{1,i}(x^*, z^*) < 0$, such that $i \notin AS(z^*)$: When the pure component parameters change, the value of constraint $g_{1,i}$ will change accordingly. This change in the value of $g_{1,i}$ can lead to the constraint becoming active. This can change the behavior of the objective function considerably (figure 3.2). These changes are not captured by the Taylor-approximation in eq. (3.5). An additional constraint for the mapping can prevent this effect. The new constraint excludes regions of pure component parameters z, in which the constraint is expected to become active. The region is estimated by a Taylor-approximation of $g_{1,i}^{\mathrm{opt}}$ similar to eq. (3.5) as

$$0 \leq g_{1,i}^{\mathrm{opt}}(z^*) + \frac{\partial g_{1,i}^{\mathrm{opt}}}{\partial z}(z_i - z^*) + \frac{1}{2}(z_i - z^*)^{\mathrm{T}} \frac{\partial^2 g_{1,i}^{\mathrm{opt}}}{\partial z^2}(z_i - z^*) \quad i \notin AS(z^*)\ . \tag{3.7}$$

The general procedure of the structure-mapping remains the same as the procedure explained for the basic structure-mapping (sec. 3.2.1). For each working fluid, eq. (3.5) is evaluated and the working fluids are ranked according to the estimated objective

function $\hat{f}(z_i)$. Additionally, constraint (3.7) is evaluated for each working fluid. Working fluids, violating the constraint are excluded from the ranking. This procedure can be used for the database as well as for the design of new fluids, as only the pure component parameters of the fluid are used.

The exclusion of parameter regions using the constraint from eq. (3.7) is useful for excluding overestimated working fluids from the final ranking provided by the structure mapping. However, the approach might also exclude promising working fluids, if the approximation of the constraint by the Taylor-approximation of eq. (3.7) is insufficient or the performance of the working fluid is not affected significantly by the active constraint. Thus, the approach should be used only, if the basic structure mapping is corrupted by overestimated fluids due to a constraint becoming active.

3.2.3 Tightening convex hull

Changes in the active-set of constraints not only prevent better objective function values for the working fluid, but can also render the problem infeasible for any combination of process parameters, e.g., a fluid with a critical pressure p_c below the lower bound for the pressure $p_c \leq p_{\min}$ for a subcritical ORC. There is no feasible pressure level for this fluid and any process based on this working fluid violates at least one constraint. However, as the taylor-approximation (3.5) does not capture the change in the active-set, an infeasible working fluid can still enter the final ranking. The procedure for handling of the inactive constraints from the previous section overcomes this shortcoming of the Taylor-approximation already. However, regions in the parameter-space, where the process is infeasible for all values of the process parameters, can be identified in advance and exploited for tightening of the search-space.

If a set of constraints $g_s(z) \leq 0$ is independent of the process variables x, it can directly be assessed for fluids in the database. Based on these constraints, the database is refined before the convex hull is generated. g_s can contain constraints from g or be derived from g by elimination of process variables. For example, consider a subcritical cycle with the constraints $p_{\mathrm{c}} \geq p_{\mathrm{evap}} \geq p_{\mathrm{cond}} \geq p_{\min}$, where the evaporation pressure p_{evap} and the condensation pressure p_{cond} of the cycle process depend on x, the minimal pressure $p_{\min}$ is a constant and the critical pressure p_{c} is a function of the pure component parameters z. Combining these constraints yields $p_{\mathrm{c}} > p_{\min}$, which is independent of x and can be added to g_s. The feasible components are gathered in the set d_{feas} , such that

$$d_{\mathrm{feas}} = \{z_i \in d : g_s(z_i) \leq 0\} \tag{3.8}$$

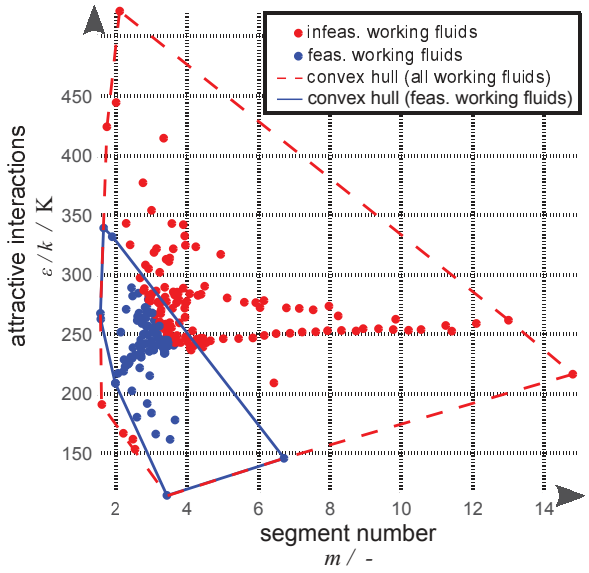

Figure 3.3: Convex hull constraints projected in a 2-dimensional plane of PC-SAFT parameters representing working fluid candidates. The dashed line is the convex hull around all pure component parameters (set d). The solid line is the refined convex hull around feasible pure components only (set d_{feas}, see text for details).

Infeasible compounds are excluded from the database before the generation of the convex hull. The relevant parameter range of the PC-SAFT model is defined by the convex hull around the remaining, feasible substances in d_{feas}. Fig. 3.3 shows the actual database used in the illustrative example and the resulting feasible set by removing infeasible compounds. The feasible working fluids are contained in a region of the parameter space, where there are no infeasible working fluids in between them. Thus, the search space for the optimization is reduced. This behavior is not only useful from a numerical point of view but also demonstrates the strong physical nature of the underlying PC-SAFT model: The parameters directly relate to physical properties and reverse, which is an important feature for the proposed design approach, as it can be exploited for relating the pure component parameters to real working fluids.

3.2.4 Adaptive structure-mapping

The approaches for structure-mapping approximate inactive constraints (sec. 3.2.2) and tighten the search space of working fluids (sec. 3.2.3). However, the approximation relies only on local information from the hypothetical optimal working fluid. If a local

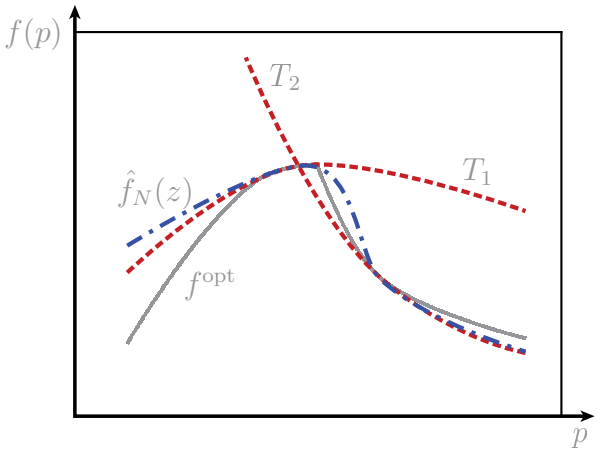

Figure 3.4: Adaptive structure-mapping: at points with insufficient approximation of the objective function f^{opt} (solid, grey line) by Taylor-approximation (dashed, red lines) T_1, the approximation is refined. A new Taylor-approximation T_2 is calculated yielding the combination T_{comb} (dash-dotted, blue line).

Peng-Robinson (Peng and Robinson, 1976). Additionally, the g^{E}-models based on the, so-called, (quasi-)chemical theory, e.g., non-random two liquids (Renon and Prausnitz, 1968) or universal quasi-chemical (Abrams and Prausnitz, 1975), are excluded for the same reason. For the ORC systems considered here, mainly simple and well-known substances are employed as working fluids. These fluids can be modeled with the aforementioned models. However, for the identification of new molecules the lack of data for fitting such models and the low predictive power urges the need for a physically-based model for the working fluid. Furthermore, the CoMT-CAMD approach for the design of working fluids considered in this work exploits the physical meaning of the pure component parameters.

The molecular model of the PC-SAFT equation of state considers molecules as chains of spherical segments that interact through van der Waals interactions, hydrogen bonds, and polar interactions. Two parameters characterize the geometry of the molecule: the segment number and a segment diameter parameter . The van der Waals attraction between segments is defined by a third parameter, the segment dispersion energy ϵ/k. In this work, these three parameters $z = (m, \sigma, \epsilon/k)^{\text{T}}$ are used to describe the working fluid. The extension of the model to account for hydrogen bonding and polar interactions is straight-forward (Bardow et al., 2010; Stavrou et al., 2014; Lampe et al., 2015). It has been shown that interpretations of the parameters hold well. E.g., for homologous series, linear relationships of the model parameters with chain length

have been obtained (Pedrosa et al., 2006; Nannan et al., 2013; Gross and Sadowski, 2001; Solms et al., 2003). PC-SAFT has already successfully been employed for the design of ORC systems (Lai et al., 2009, 2011; Vatani et al., 2013).

The PC-SAFT equation of state is based on the thermodynamic perturbation theory of order 1, i.e., the TPT1 (Wertheim, 1984a,b, 1986a,b), applied by Chapman et al. (1988, 1990) to develop the statistical associating fluid theory (SAFT). Based on this work, many modifications have been developed, e.g., SAFT-LJ using Lennard-Jones chains with association sites (Müller et al., 1994), SAFT-VR allowing for attractive potentials of variable range (Gil-Villegas et al., 1997), and PC-SAFT used here (Gross and Sadowski, 2001, 2002; Gross, 2005; Gross and Vrabec, 2006). SAFT-based equations of state are extensively used for modeling pure components and mixtures. The prediction of mixture properties by SAFT-based equations of state allows for the calculation of properties for complex fluid mixtures as reviewed in Chapman et al. (2004); Spyriouni and Economou (2005); Tan et al. (2008).

In PC-SAFT, fluid mixtures are modeled by a set of pure component parameters for each fluid and an additional parameter (k_{ij}) for each pairwise interaction between fluids i and j. If sufficient data is available for the mixture, k_{ij} is fitted to the data. However, in the presented CoMT-CAMD method for the design of fluids, a fluid mixture is only represented by the pure component parameters and the k_{ij} values are set to zero (Bardow et al., 2010; Stavrou et al., 2014).

3.3.1 Quantitative structure property relationship for molar mass and ideal gas heat capacity

PC-SAFT is a model for the residual Helmholtz-energy of pure substances or mixtures. For the simulation or optimization of a process, additional data of the fluid is needed. Typically, the molar mass of the fluid is needed for calculation of specific numerical values. Moreover, for the cycle optimization, the caloric properties of the fluid are of major importance. For calculating caloric properties (e.g., enthalpies), the ideal gas heat capacity is needed. When a single fluid is modeled for the simulation of a cycle, these parameters can be obtained from a database. The ideal gas heat capacity and molar mass of a working fluid are easily measurable and vastly available. For fluids, where no data is available, the molar mass can directly be obtained from the molecular structure. The ideal gas heat capacity can be predicted with good accuracy from the structure via group-contribution methods (Joback and Reid, 1987; Constantinou and Gani, 1994; Coniglio and Daridon, 1997; Ceriani et al., 2009). However, in the CoMT-framework, the fluid is only represented by a set of pure component parameters. Thus,

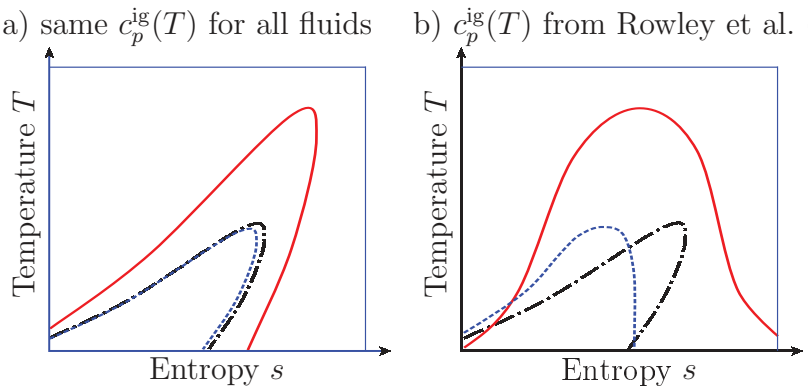

Figure 3.5: 2-phase-regions for n-pentane (dash-dotted), water (solid) and R11 (dashed) from PC-SAFT: a) $c_p^{ig,n-pentane}$ is assumed for all components b) c_p^{ig} relations specific for each substance are used (Rowley et al., 2006)

database values cannot be employed and the molecular structure is unknown. In the following, QSPR-methods are presented for the calculation of the molar mass and the ideal gas heat capacity based on the PC-SAFT pure component parameters.

3.3.1.1 Ideal gas heat capacity

In the ORC application, the ideal gas heat capacity is strongly affecting the process performance (Stijepovic et al., 2012; Tchanche et al., 2009; Bao and Zhao, 2013). The influence of the ideal gas heat capacity on the ORC process design can be appreciated by comparing the 2-phase-region of different working fluids. In Fig. 3.5, the 2-phase-regions of three working fluids are shown in a T–s diagram. In Fig. 3.5 a), the ideal gas heat capacity is the same for all components to $c_p^{ig,n-pentane}$, while the pure component parameters of PC-SAFT change for all three working fluids. In Fig. 3.5 b) literature values (Rowley et al., 2006) for c_p^{ig} for each component are employed. The ideal gas heat capacity substantially influences the shape of the 2-phase-region and thereby the ORC process performance (Li et al., 2011; Kuo et al., 2011; Zhai et al., 2014) (see also sec. 2.3.1.1).

When PC-SAFT is used for a known fluid, c_p^{ig} can be taken from a database. In the CoMT framework, a novel fluid is only characterized by its PC-SAFT parameters. These parameters are therefore used to employ a quantitative structure property relationship (QSPR) for the ideal gas heat capacity[2] (Stavrou et al., 2014). A QSPR for estimating the ideal gas heat capacity is appealing in the presented approach because

[2]The QSPR method for the calculation of the ideal gas heat capacity is a result of joint work in collaboration with Marina Stavrou (Universität Stuttgart).

not only the residual but the full equilibrium properties of a component can then be obtained from PC-SAFT pure component parameters. This gives a consistent and sound model for the working fluid selection.

The ideal gas heat capacity for organic components is mainly determined by the energies associated with the translational, rotational and vibrational degrees of freedom of the molecule (Coniglio and Daridon, 1997). For the expectation that a QSPR approach based on PC-SAFT parameters is promising, the following rationale can be provided: The energy stored in translation and rotation of the molecule depends on the size of the molecule, which is represented by the geometric parameters m and σ in PC-SAFT. The energy associated with vibrations within a molecule additionally depends on the magnitude of the forces between the atoms of the molecule, which, to some extent, scales with the segment dispersion energy ϵ/k. In the developed QSPR, the ideal gas heat capacity is calculated as a sum of structural descriptors d_i,which are combinations of the pure component parameters z, and coefficients γ_i

$$c_p^{\mathrm{ig}} = \sum_{i=0}^{n} \gamma_i \, d_i \ . \tag{3.10}$$

The structural descriptors d_i are empirically derived from the equations of PC-SAFT. The final expression used in this work is

$$c_p^{\mathrm{ig}}(300\ \mathrm{K}) = \gamma_0^{300} + \gamma_1^{300}\ (m\,\epsilon/k) + \gamma_2^{300}\ \left(m\,\sigma^3\right) + \gamma_3^{300}\ \left(m\,\epsilon/k\,\sigma^3\right) \tag{3.11}$$

$$c_p^{\mathrm{ig}}(400\ \mathrm{K}) = \gamma_0^{400} + \gamma_1^{400}\ (m\,\epsilon/k) + \gamma_2^{400}\ \left(m\,\sigma^3\right) + \gamma_3^{400}\ \left(m\,\epsilon/k\,\sigma^3\right)\ . \tag{3.12}$$

The coefficients γ_i are fitted to a set of approximately 500 pure components for 300 K and 400 K (data from Rowley et al. (2006), table 3.1). The QSPR correlates the ideal gas heat capacity with a determination coefficient of 0.99 for both 300 K (Fig. 3.6) and 400 K. The temperature dependency of c_p^{ig} is accounted for by linear interpolation between the two predicted values.

To assess how the error of the QSPR method for c_p^{ig} effects the objective function, a sensitivity analysis is performed. The results of the cycle optimization for the 50 best organic fluids from the database are analyzed (Fig. 3.7). For each of the fluids, an artifical error of ± 10 % was added to the calculated c_p^{ig} and the cycle was optimized again. The result of these optimization is depict as errorbars in figure 3.7. The results of the optimization depart from those using the correct values. Nevertheless, the order of the fluids as predicted by the process optimization remains. Thus, it can be concluded that the QSPR-method for the ideal gas heat capacity has an accuracy, which allows for the selection of working fluids. A highly precise cycle calculation for single fluids in the latter stages of the process design should be based on the aforementioned methods using a database or group-contributions.

Table 3.1: Coefficients for calculating ideal gas heat capacity in the QSPR model from eq. (3.10)

parameter	value for 300 K	value for 400 K
γ_0 / $\mathrm{J\,kmol^{-1}}$	-15174	-19389
γ_1 / $\mathrm{J\,kmol^{-1}\,K^{-2}}$	-5763	-8171
γ_2 / $\mathrm{J\,kmol^{-1}\,K^{-1}\,\mathring{A}^{-3}}$	1232	1498
γ_3 / $\mathrm{J\,kmol^{-1}\,K^{-2}\,\mathring{A}^{-3}}$	-239	-315

Table 3.2: Coefficients for calculating molar mass M in the QSPR model from eq. (3.13)

parameter	value
β_1 / $\mathrm{kg\,kmol^{-1}\,K^{-1}}$	0.0255
β_2 / $\mathrm{kg\,kmol^{-1}\,\mathring{A}^{-3}}$	0.0560
β_3 / $\mathrm{kg\,kmol^{-1}\,K^{-1}\,\mathring{A}^{-3}}$	0.0015

3.3.1.2 Molar mass

The molar mass of the working fluid is also of importance for the design of the ORC. The high molar mass of the organic working fluids compared to water allows for compact system sizes and improves the efficiency of the turbine. For the calculation of the molar mass in the CoMT-framework, a similar rationale as for the heat capacity can be applied: though the molar mass can readily be calculated, or looked up in databases, in the CoMT-framework the molar mass can only be calculated from the PC-SAFT pure component properties. Analogously to the heat capacity in the previous section, the molar mass M for the fluid is calculated using QSPR from the same structural descriptors d_i and coefficients β_i (Stavrou et al., 2014). For the calculation of M, constant term β_0 is unused as it shows no improvement for the test group. Thus the calculation is

$$M = \beta_1 \, (m\,\epsilon/k) + \beta_2 \, \left(m\,\sigma^3\right) + \beta_3 \, \left(m\,\epsilon/k\,\sigma^3\right) \ , \tag{3.13}$$

which provides an estimate for the molar mass of the fluid based on the PC-SAFT pure component parameters without introducing new parameters.

3.3.2 PC-SAFT as fundamental equation

PC-SAFT is chosen as a model for the working fluid properties. The coarse-grained molecular picture underlying PC-SAFT allows for a sound description of the working fluid based on pure component parameters with a physical meaning.

PC-SAFT is a thermal equation of state for the residual Helmholtz energy a^{res}. For the calculation of the fluid properties an ideal gas contribution is needed to calculate

$$a(T,\rho) = a^{\mathrm{res}}(T,\rho) + a^{\mathrm{ig}}(T,\rho)\ . \tag{3.14}$$

With the QSPR calculations for c_p^{ig}, the ideal gas contribution a^{ig} can be calculated and PC-SAFT is transformed into a fundamental equation allowing for the calculation of all equilibrium properties of a working fluid solely described by the pure component parameters.

3.4 Geothermal example and application of the basic CoMT-CAMD framework

Throughout this work, the methods that are discussed and presented are all accompanied by an illustrative example. The example is chosen as a representative application for an ORC. In this work, two examples are used for the assessment: a geothermal and a solar example. The examples are based on the definition of a heat source and sink (sec. 3.4.1), and a process-model for optimization (sec. 3.4.3). Additionally, a database of fluids for the structure-mapping (sec. 3.4.2). These parts are described in detail in the next sections before the methodology is applied to the example in section 3.4.4.

3.4.1 Specification of the heat source

The example is based on data and specifications of a geothermal ORC. Geothermal applications are one of the most established applications for the ORC. Quoilin et al. (2013) collected data on installed units and reveal that 22 % of the installed ORC systems use geothermal heat sources. The temperature of the geothermal heat source is varying depending on the location and the depth of the production drill-hole. At temperatures above 90 °C, a conversion to electricity is possible. This corresponds to a potential for geothermal energy production from 25 GW heat in europe (Quoilin et al., 2013). For these applications, a *binary cycle* is employed. Here, the geothermal

Table 3.3: Potential for geothermal energy in Europe for different heat source temperature ranges (data from Quoilin et al. (2013)).

Temperature / °C	Potential / MW
65-90	10,462
90-120	7,503
120-150	1,268
150-225	4,745
225-300	11,150

water runs through a heat exchanger, where the heat is transferred to a working fluid that, in turn, is used for running the power cycle. Furthermore, it is possible to use the heat from the geothermal water for power production but also for a direct use in heating applications (Heberle and Brüggemann, 2010; Guo et al., 2010). This *combined heat and power* option is not considered further in this thesis.

In this thesis, the geothermal heat source is considered as described by Heberle et al. (2012). The example is used to show the merits and the outcome of the methodology. Real data is used to provide a realistic example. The geothermal source is represented mainly by the properties of the heat carrier coming from the production drill-hole (table 3.4). The heat carrier considered here has a fixed temperature at the exit of the production drill-hole $T_{\mathrm{HC}}^{\mathrm{in}}$ and a constant specific heat capacity $c_{\mathrm{l,HC}}$. Furthermore, the mass flow rate $\dot{m}_{\mathrm{HC}}$ is considered a constant parameter.

For the cold side of the ORC system, the cooling of the condenser has to be considered. In this work, an air cooled system is considered.

Table 3.4: Geothermal source specification for the illustrative example (adopted from Heberle et al. (2012)).

Property of heat carrier	Symbol	Value
mass flow rate	$\dot{m}_{\mathrm{HC}}$	66 $\frac{\mathrm{kg}}{\mathrm{s}}$
inlet temperature	$T_{\mathrm{HC}}^{\mathrm{in}}$	120 °C
heat capacity	$c_{\mathrm{l,HC}}$	4.2 $\frac{\mathrm{kJ}}{\mathrm{kg\ K}}$

List of Figures

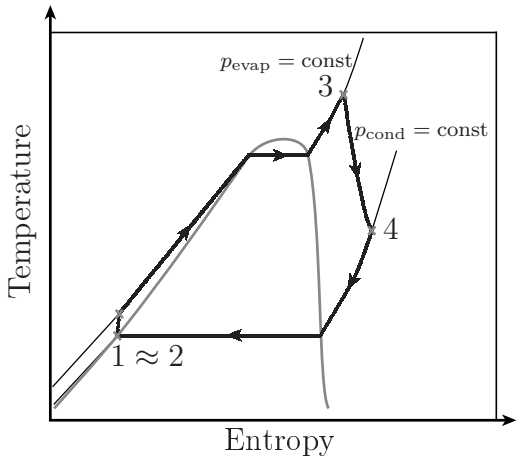

Figure 3.8: Simple ORC in a temperature-entropy chart

The vector $x = (p_{\text{cond}}^{\text{red}}, p_{\text{evap}}^{\text{red}}, \Delta T_{\text{sh}}, \dot{m}_{\text{WF}})^{\text{T}}$ represents the variables for the process and vector $z = \left(m, \sigma, \frac{\epsilon}{k}\right)^{\text{T}}$ the relaxed PC-SAFT pure component parameters. Energy balances around turbine and pump, and the definition of the isentropic efficiency yield

$$P_{\text{net}} = \dot{m}_{\text{wf}} \left[\eta_{s,\text{turb}} \left(h_{4s} - h_3\right) - \eta_{s,\text{pump}}^{-1} \left(h_{2s} - h_1\right)\right] \ . \tag{3.16}$$

The efficiencies $\eta_{s,\text{pump}}$ and $\eta_{s,\text{turb}}$ are constant. The state points are calculated as

$$h_{4s} = \text{h}(p_{\text{cond}}, \text{s}(p_{\text{evap}}, \text{T}^{\text{sat}}(p_{\text{evap}}, z) + \Delta T_{\text{sh}}, z), z) \tag{3.17}$$
$$h_3 = \text{h}(p_{\text{evap}}, \text{T}^{\text{sat}}(p_{\text{evap}} + \Delta T_{\text{sh}}, z), z) \tag{3.18}$$
$$h_{2s} = \text{h}(p_{\text{evap}}, \text{s}'(p_{\text{cond}}, z), z) \tag{3.19}$$
$$h_1 = \text{h}'(p_{\text{cond}}, z) \ , \tag{3.20}$$

using the PC-SAFT model for the calculations[3] of enthalpies $\text{h}(p, T, z)$ and $\text{h}(p, s, z)$, saturation temperature $\text{T}^{\text{sat}}(p, z)$, and entropy $\text{s}(p, T, z)$. These values depend on the state of the fluid and variable vector z consisting of the pure component parameters of the working fluid.

The optimized variables in the process model are $x = (p_{\text{cond}}^{\text{red}}, p_{\text{evap}}^{\text{red}}, \Delta T_{\text{sh}}, \dot{m}_{\text{WF}})^{\text{T}}$: pressure of the condenser p_{cond}, pressure of the evaporator p_{evap}, degree of superheating ΔT_{sh}, and mass flow rate of the working fluid $\dot{m}_{\text{WF}}$. As only subcritical processes

[3]Note that upright letters are used for PC-SAFT functions, whereas italic letters are used for the corresponding variable.

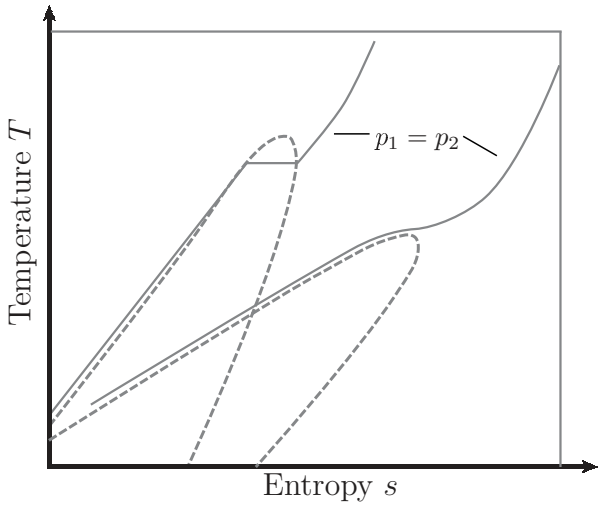

Figure 3.9: Effect of using absolute pressure as optimized variable: Changes in the pure component parameters change the shape of the working fluids' two-phase region (dashed lines); Accordingly, an isobar for the same pressure (solid lines) can pass the two-phase region of the fluid (grey) or become supercritical (black).

are considered, reduced pressures are used as variables in the optimization (i.e., the pressure relative to the critical pressure $p_i^{\text{red}} = \frac{p_i}{p_c}$).

The selection of the reduced pressure as optimized variable opposed to the absolute value is related to the robustness of the optimization: when the absolute pressure is used as optimized variable, changes in the pure component parameters z can lead to situations, where the cycle calculation fails, because the phase calculations cannot be performed, i.e., when the pure component parameters change and the pressure p_{evap} selected by the optimizer is not subcritical (figure 3.9). Though the resulting super-critical cycle is possible in general, the calculation of the boiling point that corresponds to this pressure is not possible. The selection of the reduced pressure for the optimization prevents this situation. When the properties of the fluid change due to a change in the pure component parameters, the reduced pressure level will still correspond to a subcritical pressure. A constraint $p_{\text{evap}}^{\text{red}}\, p_c \leq p_{\max}$ is added to the problem to allow for setting bounds for feasible pressure levels. The reduced pressure is bound by $0.05 \leq p_{\text{evap}}^{\text{red}} \leq 0.8$. These bounds are used to ensure a subcritical cycle. Near critical pressure levels are prevented.

A minimal temperature difference in the evaporator $\Delta T_{\min}$ is imposed to ensure feasible heat transfer (table 3.5). Additionally, minimal and maximal allowed pressures $p_{\min}$ and $p_{\max}$ are defined. The pressure levels in the cycle are further constrained

Table 3.5: Specifications and constraints for the geothermal ORC system.

Parameter	Symbol	Value
minimal temperature difference	$\Delta T_{\min}$	10 K
turbine efficiency	$\eta_{s,\text{turb}}$	0.8
pump efficiency	$\eta_{s,\text{pump}}$	0.6
minimal absolute pressure	$p_{\min}$	1 bar
minimal reduced pressure	$p_{\min}^{\text{red}}$	10^{-5}
maximal absolute pressure	$p_{\max}$	20 bar
maximal reduced pressure	$p_{\max}^{\text{red}}$	0.8
minimal temperature	$T_{\min}$	20 °C

by minimal and maximal reduced pressures $p_{\min}^{\text{red}}$ and $p_{\max}^{\text{red}}$, respectively. A minimal allowed temperature $T_{\min}$ is chosen to allow for cooling in the condenser.

The model is implemented in Fortran. The derivatives of the model needed during optimization are obtained from automatic differentiation using Adifor 2.0 (Bischof et al., 1996; Bücker and Corliss, 2006).

3.4.4 Results of the targeting

The net power output of a geothermal ORC is considered as an objective function here. In a preparatory step, the database of fluids is assessed for simple constraints and infeasible components are deleted, as discussed in section 3.2.2 . The constraints g_{s} used for the refinement of the database are

$$\begin{aligned} T_{\text{c}} - T_{\min} &\geq 0 \\ p^{\text{sat}}(T_{\text{HC}}^{\text{in}}) - p_{\min} &\geq 0 \\ p_{\text{c}}\, p_{\max}^{\text{red}} - p_{\min} &\geq 0 \\ p_{\max} - p^{\text{sat}}(T_{\min}) &\geq 0 \\ p_{\max} - p_{\text{c}}\, p_{\min}^{\text{red}} &\geq 0\ . \end{aligned} \tag{3.21}$$

These constraints ensure a subcritical cycle and the existence of feasible pressure levels. After the refinement, the convex hull around the feasible working fluids is defined. Fig. 3.3 shows the actual result for the present case thereby showing that simple constraints in process settings translate into clear regions in the parameter space.

Table 3.6: Result of the integrated design of working fluid and process.

Variable	Symbol	Value
segment number	m	5.7
segment diameter	σ	2.9 Å
segment energy parameter	$\frac{\epsilon}{k}$	133 K
condensation pressure	$p_{\text{cond}}^{\text{red}}$	0.1
evaporization pressure†	$p_{\text{evap}}^{\text{red}}$	0.8
working fluid flow rate	$\dot{m}_{\text{wf}}$	65 $\frac{\text{kg}}{\text{s}}$
degree of superheating†	ΔT_{sh}	0 K

†parameter at bound

The CoMT optimization with the relaxed pure component parameters is performed. The optimization is performed using sequential quadratic programming (SQP) implemented in Matlab (2012) based on Han (1977), Powell (1978), and Powell (1979). The computations took less than 50 s on a standard desktop PC (Core i5 CPU, 1.7 GHz with 4 GB RAM) demonstrating the advantage of avoiding discrete degrees of freedom. The result of the optimization (table 3.6) is a subcritical cycle with no superheating. The net power output of the optimal cycle is 3.2 MW. The result of the optimization is both an optimal process and an optimal hypothetic working fluid.

This combination is the target for the following structure-mapping. Using the Taylor-approximation around the optimum $\hat{f}(z)$ (eq. (3.5)), the database of feasible fluids is assessed and ranked according to the expected net power output. The high-ranked working fluids are further assessed by a process optimization, where only the process degrees of freedom $x = (p_{\text{cond}}^{\text{red}}, p_{\text{evap}}^{\text{red}}, \Delta T_{\text{sh}}, \dot{m}_{\text{WF}})^{\text{T}}$ are optimized. Table 3.7 summarizes the results for the 10 working fluids ranked highest in the structure-mapping.

In order to evaluate the optimization result, it is compared to the result from an individual process optimization for all 200 fluids in the database. The real ranking list (#Real) of the 200 substances is unambiguous and serves as a measure for how well the CoMT-CAMD method identifies the most optimal working fluids. A rich set of promising working fluids is identified (table 3.7). The highest-ranked working fluid in the structure-mapping is dinitrogen tetraoxide. The prediction for this fluid is highest, but the actual performance is low. It should be noted that this component is actually not available in pure form due to its reactive nature at process conditions. The second and third ranked fluids (R124 and R227ea) are the actual best and second best fluids

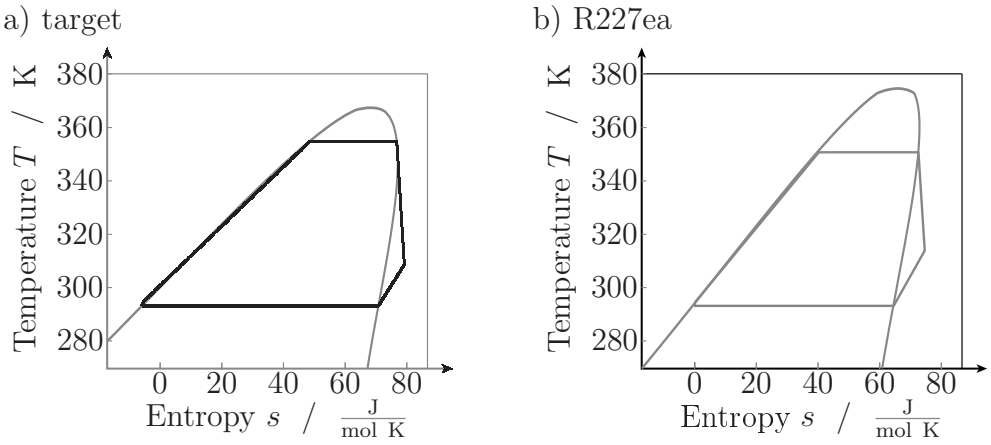

Figure 3.10: The optimal working fluid from the CoMT-optimization (a, target) and the best working fluid (b, R227a) compared in a temperature–entropy chart.

from the complete database. The optimal hypothetical working fluid and the optimal real working fluid R227ea are similar with respect to the shape of the 2-phase-region and the critical temperature (Fig. 3.10). The predicted top ten contains the top six fluids from the database. These fluids identified by the CoMT-CAMD approach can now be assessed for other properties that are not covered by the process optimization (e.g., toxicity, flammability, global warming potential, or legal prescriptions (Andersen and Bruno, 2005; Kuo et al., 2011; Kosmadakis et al., 2009)).

The results from the structure-mapping show that CoMT-CAMD enables the selection of a working fluid and the optimization of the key process parameters in one optimization problem. However, some of the high-ranked working fluids in the structure-mapping have low performance (e.g., dinitrogen tetroxide, cyanogen). The observed difference in the predicted and the actual performance can be explained by analyzing the process performance with respect to changes in the working fluid properties.

3.4.5 Influence of working fluid properties on process performance

Process models of the ORC can provide insight into the influence of process parameters (e.g., pressure levels, temperature of the heat source) on the process performance (Tchanche et al., 2009; Heberle and Brüggemann, 2010; Aljundi, 2011; Hung et al., 2010; Liu et al., 2004; Fernández et al., 2011). The presented framework employs a holistic model of the ORC process by integrating a model of the working fluid into

Table 3.7: Ranked list of the most promising working fluids from the structure-mapping (#Mapping) and comparison to the real rank (#Real) and the real power output. The pure component parameters (m, σ, and $\frac{\epsilon}{k}$) are listed for comparison.

#Mapping	Name	P_{net} / MW	#Real	m / −	σ / Å	$\frac{\epsilon}{k}$ / K
-	hypothetical optimum	3.2	-	5.7	2.9	133
1	dinitrogen tetraoxide	1.6	18	6.7	2.2	146
2	R1243	2.5	2	3.9	3.0	151
3	R227ea	2.7	1	3.5	3.3	162
4	R134a	2.1	6	3.1	3.1	166
5	R236ea	1.9	10	3.7	3.2	178
6	R152a	1.8	16	2.6	3.2	180
7	R124	2.1	4	3.0	3.3	184
8	cyanogen	0.2	41	2.9	2.9	192
9	R142b	2.1	5	3.5	3.5	202
10	propane	2.1	3	3.6	3.6	209

the process model. Thereby, this holistic model allows analyzing both the influence of process parameters and working fluid properties on the process performance. Thus, a detailed analysis of the influence of working fluid properties on the process performance is possible.

In figure 3.11, the net power output P_{net} of the optimal process is shown as function of the segment number m and the segment diameter σ. The segment energy $\frac{\epsilon}{k}$ is kept constant at the optimal value of 133 K. Each point of the surface represents a solution f^{opt} from eq. (3.4) and thus, an optimal process, where x has its optimized value for each z. The surface has a distinct maximum at $m = 5.7$ and $\sigma = 2.9$ Å. The absence of flat regions of almost constant objective function values indicates that there is no degeneracy of the PC-SAFT parameters. Figure 3.11 only shows a two-dimensional cut of the design space, however, none of the results indicate that parameter degeneracy is a problem for the presented ORC design approach. The gradients and the curvature of the surface change drastically for different points of the surface. These abrupt changes in the gradient hinder an optimization of the model using finite differences. Convergence therefore improved significantly by using automatic differentiation to obtain exact gradients of the objective function and the constraints.

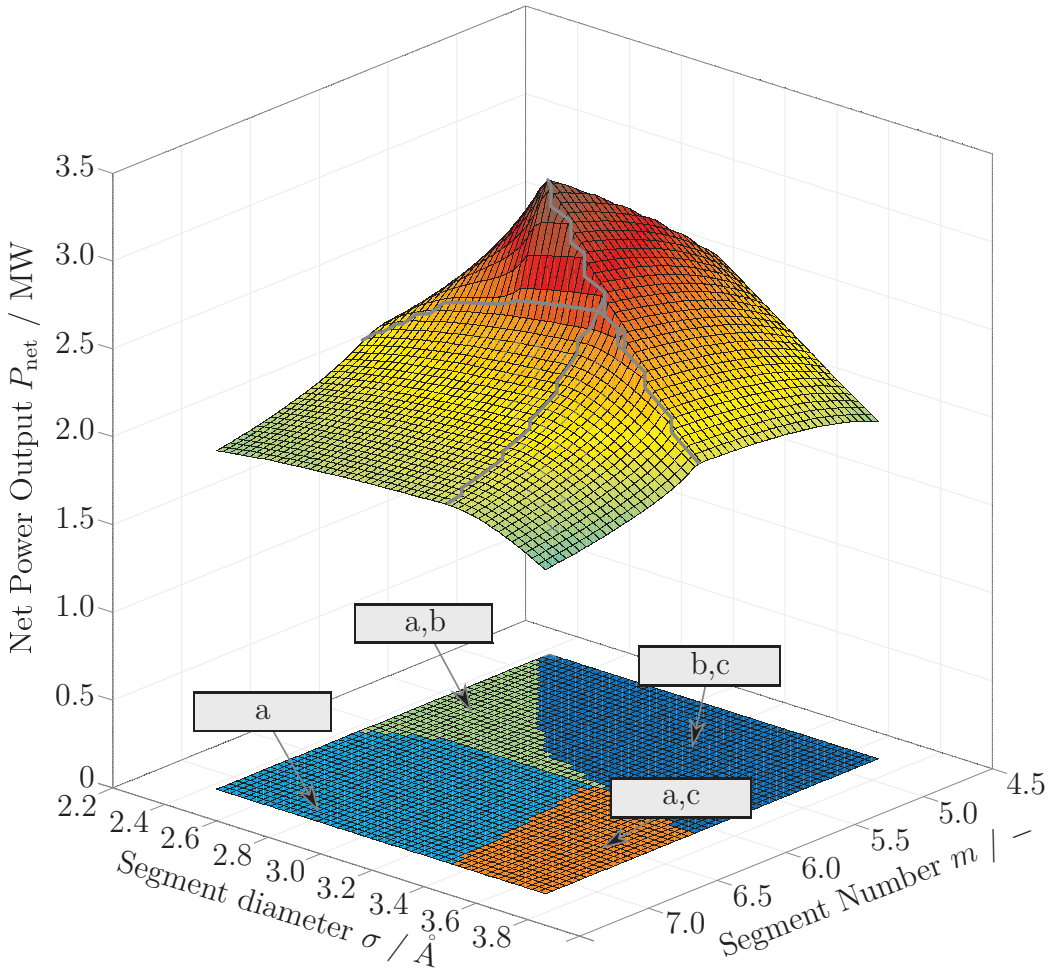

Figure 3.11: Optimal net power output as function of the segment number m and the segment diameter σ for constant segment dispersion energy $\frac{\epsilon}{k} = 133\ K$. The projected regions on the bottom represent different active set of constraints. Active constraints are a) minimal temperature difference at preheater entry, b) upper absolute pressure level, c) minimal temperature difference at evaporator entry.

In figure 3.11, regions are indicated representing different active sets of constraints. The active set is the subset of constraints, which are at their respective bound for the optimal process (i.e., $g_{i,1}(x^{\mathrm{opt}}, z) = 0$). The active constraints in the different regions are (a) the minimal temperature difference at the preheater entry, (b) the upper absolute pressure and (c) the minimal temperature difference in the evaporator entry. The different active constraints determine how changes in the fluid parameters act on

the objective function. As a result, one can observe that the gradients and curvature change abruptly, when a switchover of one to the other active set is reached. For small values of the segment number m, the net power output is rising for rising m, until the pinch at the preheater entry is reached. When the new constraint becomes active, a sharp drop of the net power output can be observed. Changes in the working fluid properties affect the cycle in many different ways and the active constraints are not known in advance. These observations show that metaobjective functions (cf. section 2.3.1) intended to guide the selection of working fluids are difficult to develop a priori and require a deep understanding of the process. The appearance of many faces in the objective function (Fig. 3.11) clearly shows the limitations of metaobjective functions and, in the view of the author, Fig. 3.11 supports the integrated optimization of working fluid and process parameters.

The Taylor-approximation in eq. (3.5) employed for the structure-mapping does not account for changes in the active set. The insight gained by Fig. 3.11 enables us to explain the appearance of dinitrogen tetroxide high in the ranking list: fluids that are overestimated in the structure-mapping can be expected when the set of active constraints changes along the path of the Taylor expansion (see also section 3.2). To account for the changes of the active set in the structure-mapping the improvements of the structure-mapping are used in the following chapters. However, the results show that the list of high-ranked fluids from the current structure-mapping already gives a rich set of good fluid candidates that can be assessed further.

3.5 Summary

A method is presented allowing for the integrated optimization of working fluids and ORC processes. The method exploits the molecular picture underlying the PC-SAFT equation of state: the pure component parameters of the working fluid are relaxed during the optimization allowing solving the integrated problem in a single NLP. However, the resulting pure component parameters are, in general, not corresponding to any real working fluid. Thus, a structure-mapping is introduced to identify real working fluids from a database of PC-SAFT pure component parameters.

The proposed method for the working fluid selection is applied to an illustrative example. The resulting optimization problem can be solved efficiently. The basic structure-mapping was used for to rank real working fluids after the optimization. Some of the working fluids enter the ranking despite a process optimization of those working fluids proves that the actual performance is low.

The influence of the working fluid properties on the performance of the cycle is analyzed in detail. The objective function has kinks and regions of different curvature. Thus, the Taylor-approximation used for the basic structure-mapping overestimates the objective in certain regions of the search space. Methods to overcome the shortcoming of the basic structure-mapping are presented and will be used in the following.

Chapter 4

Computer-aided molecular design for structure-mapping

The presented method for the integrated design is based on two steps: the identification of an optimal hypothetical working fluid by continuous-molecular targeting and the structure-mapping to identify real working fluids. The structure-mapping presented in section 3.2 can be used for the identification of optimal working fluids from a database of known fluids. The design of novel working fluids is enabled by computer-aided molecular design (CAMD). The CAMD approaches discussed in section 2.4.1 are based on thermo-physical properties of the working fluid. In this section, a new CAMD is presented based on continuous-molecular targets.

The CoMT-CAMD method decomposes the integrated design introduced in section 3.1. The decomposition is not done in terms of the physical properties θ of the working fluid, but in the pure component parameters z. The optimization problems considered are:

Contents of this chapter have been published in:

Lampe, M., Stavrou, M., Schilling, J., Sauer, E., Gross, J., Bardow, A. (2015) "Computer-aided Molecular Design in the Continuous-Molecular Targeting Framework using Group-Contribution PC-SAFT". *Computers & Chemical Engineering*, 81:278–287.

The molecular structure is represented by the discrete variables y^s. The objective function of the CAMD-optimization is the estimated performance of the fluid using the Taylor-approximation from eq. (3.5) (sec. 3.2). As discussed in 3.2.2, the Taylor-approximation of the objective function is only valid for a certain region of the molecular search space. The region is limited to pure component parameters for which the same set of constraints is active in the optimal solution. This active-set $AS(z)$ is unknown in advance for all values of z other than the optimal values z^*. Thus, the constraint from eq. (3.7) is added to the problem ensuring that no additional process constraints compromise the estimated performance for the designed fluid.

The linear formulation of the GC-method ($GC \cdot y^s = z$) calculates the pure component parameters z from the molecular structure y^s of the working fluid. As no second order information is used in the GC-method, the pure component parameters z of the designed fluid can be calculated as linear function of y^s (sec. 4.3). If the CoMT-optimization problem is formulated in terms of the pure component parameter combinations used by the GC-method, e.g., $z = (m, m\sigma^3, m\epsilon/k)^T$, the CAMD problem has only linear constraints and a quadratic objective function. The set of constraints $F \cdot y^s = 0$ ensures proper connectivity of the molecule. The formulation of these chemical feasibility constraints is adopted from the implementation of Struebing (2011) and Struebing et al. (2011). The linear inequality constraints $A\,z \leq b_{\text{rel}}$ are a relaxed version of the convex hull constraints introduced in section 3.1. These constraints prevent extrapolation of the GC-method beyond the region of fit (section 4.3.1). The MIQP allows for efficient assessment of potential fluids and avoids a process optimization for every candidate.

4.2 Chemical feasibility of structures

The presented approach for the optimization-based CAMD is based on concepts proposed by Struebing (Struebing, 2011; Struebing et al., 2011). Their implementation has successfully been applied to the design of solvents using the solvatochromic performance of the designed fluid as an objective function.

The chemical feasibility of the designed fluid has to be considered in every CAMD-approach. In the presented formulation, the structure of a designed fluid is defined by a vector of integers $n \in \mathbb{Z}^o$ that denote the number of occurrences of the group in the designed fluid. First, constraints are introduced that allow for the definition of a certain type of structure, i.e., linear or ring structure, branched molecules or addition of functional groups. Then, constraints are introduced for the proper connectivity of

the designed molecular structure, i.e., the octet rule, additional bonding rules and the size of the designed molecular structure.

Depending on the type of the designed structure (i.e., cyclic or linear) different types of groups are allowed to occur in the structure. Thus, variables for the selection of the type of structure are introduced. The concept is already described in Struebing (2011); Struebing et al. (2011) and extended here to include all considered structures as well as structural limitations. A set of binary variables y^{s} is used as flags for the different types. The variable $y^{\mathrm{s}}_{\mathrm{linear}}$ and $y^{\mathrm{s}}_{\mathrm{cyclic}}$ are used for discriminating linear or cyclic structures[1]. Each structure has to be either one of them. Thus,

$$y^{\mathrm{s}}_{\mathrm{linear}} + y^{\mathrm{s}}_{\mathrm{cyclic}} = 1 \tag{4.4}$$

is added to the problem. For the design of ring structures ($y^{\mathrm{s}}_{\mathrm{cyclic}} = 1$), sub-types for the discrimination of ring types are introduced. Cyclopentanes $y^{\mathrm{s}}_{\mathrm{pent}}$, cyclohexanes $y^{\mathrm{s}}_{\mathrm{hex}}$ and aromate $y^{\mathrm{s}}_{\mathrm{arom}}$ rings are considered. Each ring structure has one of these types. This is ensured by the constraint

$$y^{\mathrm{s}}_{\mathrm{pent}} + y^{\mathrm{s}}_{\mathrm{hex}} + y^{\mathrm{s}}_{\mathrm{arom}} = y^{\mathrm{s}}_{\mathrm{cyclic}} \ . \tag{4.5}$$

For each sub-type, there are two groups and a fixed number of these groups forms a ring (i.e., 5 groups for cyclopentanes, and 6 groups for cyclohexanes and aromates). This gives one equation for each type of ring

$$n_{\mathrm{CH}^{\mathrm{pent}}} + n_{\mathrm{CH}_2^{\mathrm{pent}}} = 5\, y^{\mathrm{s}}_{\mathrm{pent}} \tag{4.6}$$

$$n_{\mathrm{CH}^{\mathrm{hex}}} + n_{\mathrm{CH}_2^{\mathrm{hex}}} = 6\, y^{\mathrm{s}}_{\mathrm{hex}} \tag{4.7}$$

$$n_{\mathrm{C}^{\mathrm{arom}}} + n_{\mathrm{CH}^{\mathrm{arom}}} = 6\, y^{\mathrm{s}}_{\mathrm{arom}} \ . \tag{4.8}$$

These equations ensure both: the ring-groups are prevented from being selected, when linear structures are considered; and the correct number of groups for forming a suitable ring is ensured.

In a similar way, subtypes for the linear structures are defined to signal double ($y_{\mathrm{db}} = 1$) and triple bond structures ($y_{\mathrm{tb}} = 1$), respectively. In contrast to the ring structures, where each ring is part of a certain subgroup, a linear structure is not necessarily double or triple bonded. However, double or triple bonds are only allowed in linear structures, which is modeled by the inequality

$$y_{\mathrm{db}} + y_{\mathrm{tb}} \leq y^{\mathrm{s}}_{\mathrm{linear}} \ . \tag{4.9}$$

[1] These values are commonly referred to as y_5 for $y^{\mathrm{s}}_{\mathrm{linear}}$ and y_6 for $y^{\mathrm{s}}_{\mathrm{cyclic}}$ (Odele and Macchietto, 1993; Buxton et al., 1999; Struebing, 2011; Struebing et al., 2011). For consistency of notation, the variables are renamed here.

Additionally, rings as well as double and triple bonded structures must not have polar groups, as this was not considered in the fitting of the GC-method. The set

$$\begin{aligned} P := \{&\text{—CH=O; }\rangle\text{C=O; —O—CH}_3\text{; —O—CH}_2\text{—;} \\ &\text{—O—CH=O; —O—(C=O)—; —OH; —NH}_2\} \end{aligned} \tag{4.10}$$

of functional groups is defined. The groups are not considered for ring structures ($y^{\mathrm{s}}_{\mathrm{cyclic}} = 1$), double bonded structures ($y_{\mathrm{db}} = 1$), and triple bonded structures ($y_{\mathrm{tb}} = 1$) and may only occur in linear structures

$$\sum_{p \in P} n_p \leq 1 - y^{\mathrm{s}}_{\mathrm{cyclic}} - y_{\mathrm{tb}} - y_{\mathrm{db}} \tag{4.11}$$

Not every combination of groups can lead to a structurally feasible fluid, e.g., selecting one $-CH_3$ and one $-CH_2-$ group leads to an open bond at the $-CH_2-$ group and is thus infeasible. The condition of *open* bond results from the, so-called, octet rule or, more precisely, to the concept of valence as defined by IUPAC (Muller, 1994), as also the *duet rule* is considered for smaller segments. The basic idea is that every group has a specific valency, i.e., a specific number of other groups, that can be attached to the group. If the number of connections of other groups equals the valency of the group, every open bond of the group is used and the group is connected properly. In general, the valence is not corresponding to the number of bonds, when double or triple bonds are considered, as multiple bonds saturate multiple valences of the group. The number of open bonds for each group v_i is a given parameter (table 4.1).

The octet rule for the correct number of bonds on each group can be formulated as (Odele and Macchietto, 1993)

$$\sum_{i \in I} n_i \left(2 - v_i\right) = 2 \ , \tag{4.12}$$

where the set I is the conjunction of all considered groups

$$\begin{aligned} I := \{&\text{—CH}_3\text{; —CH}_2\text{—; }\rangle\text{CH—; }\rangle\text{C}\langle\text{; =CH}_2\text{; =CH—; }\rangle\text{C=; —C}\equiv\text{CH;} \\ &\text{/CH}_2^{\mathrm{Hex}}\text{—; }\rangle\text{CH}^{\mathrm{Hex}}\text{—; /CH}_2^{\mathrm{Pent}}\text{—; }\rangle\text{CH}^{\mathrm{Pent}}\text{—; /CH}^{\mathrm{Arom}}\text{=; }\rangle\text{C}^{\mathrm{Arom}}\text{=;} \\ &\text{—CH=O; }\rangle\text{C=O; —O—CH}_3\text{; —O—CH}_2\text{—; —O—CH=O;} \\ &\text{—O—(C=O)—; —OH; —NH}_2\} \ . \end{aligned} \tag{4.13}$$

The left hand side of eq. (4.12) corresponds to the number of open ends on a linear molecular structure. Besides the ends of the chain, each group of the chain is connected

Table 4.1: Number of open bonds on considered groups

Group	open bonds v_i	Group	open bonds v_i
$-CH_3$	1	$-CH_2-$	2
$>CH-$	3	$>C<$	4
$=CH_2$	1	$=CH-$	2
$>C=$	3	$-C\equiv CH$	1
$/CH_2^{Hex}-$	2	$>CH^{Hex}-$	3
$/CH_2^{Pent}-$	2	$>CH^{Pent}-$	3
$/CH^{Arom}=$	2	$>C^{Arom}=$	3
$-CH=O$	1	$>C=O$	2
$-O-CH_3$	1	$-O-CH_2-$	2
$-O-CH=O$	1	$-O-(C=O)-$	2
$-OH$	1	$-NH_2$	1

to two neighboring groups. Adding a group i with valency $v_i = 2$ lengthens the chain and does not change the value of the right hand side of eq. (4.12). A group with higher valency ($v_i \geq 2$) adds a branch to the chain. A corresponding number of *chain ends* (i.e., a group with a single open bond, $v_i = 1$) is needed to close the branch again. Every branch adds 1 to the right hand side. A group with $v_i = 1$ closes a branch and 1 is substracted from the right hand side. The 2 on the left hand side corresponds to the two ends of a linear unbranched chain. However, if ring structures are considered, two open bonds are used for the ring-closure and eq. (4.12) becomes infeasible. Thus the modified version

$$\sum_{i \in I} n_i \, (2 - v_i) = 2 \, y^{\mathrm{s}}_{\mathrm{linear}} \tag{4.14}$$

is applied, where the right hand side is zero for ring structures. Additionally, disjunct molecular structures are not allowed: A single connected molecule is enforced. This is assured with the following equation (Odele and Macchietto, 1993; Buxton et al., 1999), where analogously to the octet rule the right hand side is modified for ring-structures

$$\left(\sum_{i \in I} n_i \right) - n_j \, (v_j - 1) \geq 2 \, y^{\mathrm{s}}_{\mathrm{linear}} \quad \forall j \in I \; . \tag{4.15}$$

For the size of the molecular structure, constraints are set for the maximal and

List of Tables

ketones; —O—CH_3 and —O—CH_2— for ethers, and —O—CH=O for formates and —O—(C=O)— for esters.. Parameters for the different groups are calculated by Sauer et al. (2014) and found in Tab. 4.2.

The GC-method is fitted to VLE (vapor-liquid equilibrium) data and densities from a database for a range of fluids (Sauer et al., 2014). The quality of the GC-method is assessed by the agreement with experimental data and not by the agreement of pure component parameters. Sauer et al. (2014) give the average absolute deviation for the liquid densities as $AAD_{\rho^{\mathrm{L}}} = 4.96$ % and for saturation pressures $AAD_{p^{\mathrm{sat}}} = 9.16$ % over all considered data-points. The highest deviations occur in the prediction of the VLE for highly branched alkanes (e.g., tri- and tetramethylalkanes).

The group-contribution method is based on a rich set of considered groups and structures. However, the work of Sauer et al. (2014) is concerned with the comparison of different GC-approaches, rather than with the fitting the method for as many groups and fluids as possible. Thus, certain limitations apply to the database used for the fitting of the GC-method. To prevent the extrapolation of the results to structures, which have not been considered in the fitting, the CAMD-approach is limited to structures similar to those considered for the fitting of the GC-method: the number of branches in a molecule is limited to three, only one double bond is allowed in alkenes, only alkynes with a triple bond on the chain-end (1-alkynes) are considered, only alkyl side-groups are allowed on ring structures, only a single polar group is allowed, and occurrence of functional groups excludes double bonds, triple bonds and ring-structures.

4.3.1 Construction of the convex hull

The convex hull limits the search space of working fluids in both steps of the presented method. When the structure-mapping in the second step is based on a database of working fluids as in chapter 3, the construction of the convex hull is based on the range of pure component parameters of the database. This includes all working fluids that can be selected in the structure-mapping. This clear and explicit definition of the search-space for the second step, the structure-mapping, allows to bound the search space to the same region in the first step, the CoMT optimization. In the CAMD approach presented in this chapter, there is no explicit definition for the search space of the structure-mapping. The feasible region of the pure component parameters in CAMD is defined implicitly, i.e., by limiting the number of groups in a molecular structure. Thus, the convex hull cannot be constructed on the basis of this definition. The convex hull constructed on the basis of the database can, in general, also be used

Table 4.2: Group-contributions for the employed groups from (Sauer et al., 2014).

Group	m_i / −	σ_i / Å	$\left(\frac{\epsilon}{k}\right)_i$ / K
—CH_3	0.61198	3.7202	229.90
—CH_2—	0.45606	3.8900	239.01
$\rangle$CH—	0.14304	4.8597	347.64
$\rangle$C$\langle$	-0.66997	-1.7878	107.68
=CH_2	0.36939	4.0264	289.49
=CH—	0.56361	3.5519	216.69
$\rangle$C=	0.86367	3.1815	156.31
—C≡CH	1.32790	2.9421	223.05
$\diagup CH_2^{Hex}$—	0.39496	3.9126	289.03
$\rangle CH^{Hex}$—	0.02880	8.9779	1306.70
$\diagup CH_2^{Pent}$—	0.46742	3.7272	267.16
$\rangle CH^{Pent}$—	0.02214	7.7190	1297.70
$\diagup CH^{Arom}$=	0.42335	3.7270	274.41
$\rangle C^{Arom}$=	0.15371	3.9622	527.20
—CH=O	1.57740	2.8035	242.99
$\rangle$C=O	1.22300	2.8124	249.04
—O—CH_3	1.65390	3.0697	196.05
—O—CH_2—	1.13490	3.2037	187.13
—O—CH=O	1.75250	2.9043	229.63
—O—(C=O)—	1.50630	2.8166	222.52
—OH	0.40200	3.2859	488.66
—NH_2	0.40558	3.6456	467.59

for the CAMD based structure-mapping. However, the aim of the CAMD approach is to identify new molecular structures. These new structures can correspond to pure component parameters outside of this search space. These structures would be excluded from consideration, when the database is used to construct the convex hull.

The selection of fluids used for fitting the GC-method corresponds to a smaller range of pure component parameters then the database used in chapter 3. If the convex hull around the database components is used as a search space for the CAMD method, this means a significant extrapolation of the GC-method. Thus, the convex hull is constructed on the basis of the set of fluids that were used for fitting the GC-method. However, the convex hull around these components is small for the current implementation of the GC-approach. The limitation of the pure component parameters to this smaller search space in the CoMT-optimization can prohibit the identification of the optimal parameters. The objective function is still increasing in the direction limited by the convex hull. Thus, a relaxed version of the convex hull around the fitted components is used for the CAMD in this work. The relaxation is not necessary, if the optimal hypothetical working fluid is not at the bounds presented by the convex hull. Thus the targeting in the first step is based on the non-relaxed version of the convex hull.

When CoMT is applied to real applications, the GC-method should be extended to allow for the design of more classes of working fluids (e.g., refrigerants or siloxanes). Extensions of the GC-method enlarge the convex hull, when the additional working fluids are represented by pure component parameters that are not inside the convex hull yet. A sufficient extension of the range of predictable pure component parameters thus overcomes the shortcoming of the construction of the convex hull.

4.4 Illustrative example

The CAMD method for the structure mapping is applied to the illustrative example from 3.4 to demonstrate the merits. The molecular search space is limited to components consisting of the groups presented in the work of Sauer et al. (2014). The search space is further limited by the relaxed version of the convex hull (eq. (4.2)).

4.4.1 CAMD-results

In general, the CoMT-optimization used for the Illustrative Example in section 3.4 can directly be reused for the revisited example. With Hessian and gradient of the

Table 4.3: Optimal process x^* and optimal hypothetical working fluid y^* from the CoMT optimization.

Variable	Symbol	Value
segment number	m	2.13
segment diameter	σ	3.78 Å
segment energy parameter	$\frac{\epsilon}{k}$	233 K
condensation pressure	p_{cond}	2.17 bar
evaporization pressure	p_{evap}	7.84 bar
working fluid flow rate	$\dot{m}_{\text{wf}}$	39.15 $\frac{\text{kg}}{\text{s}}$
degree of superheating†	ΔT_{sh}	0 K

†parameter at bound

objective, the CAMD problem can be formulated based on the results from section 3.4. However, the database employed for the first visit of this example is considerably larger than the list of fluids represented in the GC-method (section 4.3.1). Thus, the CoMT-optimization is performed again using the smaller convex hull.

The result of the first optimization step, the CoMT-step, is presented in table 4.3. The optimal net power output for the considered range of PC-SAFT parameters is 1.7 MW. Please note that in section 3.4, a higher value of 3.2 MW could be achieved by the target due to the larger parameter space. The strength of the CAMD approach is that new fluids can be designed. Thus, the limitation of the search space of pure component parameters by the convex hull was relaxed for the CAMD step in eq. (3.2).

The results of the CAMD optimization are small structures, which can all be identified as existing components (Table 4.4). As the pure component parameters representing polar and associating interactions are not considered in the CoMT optimization, the associating as well as the polar functional groups are not considered in the CAMD for ORC working fluids. Thus, none of the designed structures contains these groups. For the verification of the ranking predicted by the CAMD-method, each of the designed fluids has been assessed in a process optimization.

Though all identified components are well-known, not all of these components are contained in the database used for fitting of the GC-method. In this sense, these components are newly designed by the CAMD method. One of these components is propane. Propane has a higher objective function value than the target in both the Taylor-approximation and the validation. This can happen, when the convex hull is limiting the CoMT-optimization and the objective function is still improving in the

Table 4.4: Ranked list of the most promising working fluids from CAMD (#CAMD) and comparison to the real rank (#Real) and the real power output. The pure component parameters (m, σ, and $\frac{\epsilon}{k}$) are listed for comparison.

#CAMD	Name	P_{net} / MW	#Real	m / −	σ / Å	$\frac{\epsilon}{k}$ / K
1	ethane	1.77	3	1.22	3.72	230
2	propane	2.12	2	1.68	3.77	233
3	prop-1-ene	2.15	1	1.52	3.76	244
4	neopentene	1.76	4	2.17	3.91	226
5	but-1-ene	1.70	5	1.97	3.79	242
6	n-butane	1.70	7	2.13	3.80	234
7	isobutane	1.70	6	1.91	3.88	248
8	isobutylene	1.69	8	2.33	3.67	225
9	but-2-ene	1.69	9	2.35	3.64	224
10	neohexane	1.22	10	2.62	3.91	228

constraint direction. The convex hull is relaxed in the CAMD problem to allow for the design of new components. The high ranking of propane is a promising result for the design of new components, which are not included in the database. Furthermore, propane ranked third best working fluid also for the complete database. The best two working fluids identified in section 3.4 are refrigerants, which are not included in the GC-method employed here.

This observation illustrates the main advantage of CAMD-based structure-mapping: CAMD enables the design of novel, better performing working fluids without excluding already existing structures. Therefore, the CAMD mapping based on GPC-SAFT is a powerful development within the CoMT-CAMD framework leading to the optimal molecules independent from a given component database.

4.5 Summary

A method is presented for the computer-aided molecular design of ORC working fluids based on continuous-molecular targets. The method uses the first step of the CoMT-CAMD framework, the CoMT optimization, for the identification of design targets as presented in section 3.1. The the second step of the framework, the structure-mapping, is not based on a database of existing working fluids (sec. 3.2). Instead, CAMD is used for the design of working fluids. Existing CAMD approaches (as presented in

section 2.4.1.1) are based on the thermo-physical properties of the working fluid. In the presented approach, the optimal pure component parameters represent targets based on the molecular structure of the working fluid as well as the energy between segments. These design targets are well suited for a CAMD-based approach. By employing a group-contribution method for the pure component parameters allows for an assessment of a working fluid described by the structure of the working fluid (sec. 4.3). In order to allow for the optimization of the structure criteria for the feasibility of the working fluid's molecular structure have to be defined (sec. 4.1).

The proposed CoMT-CAMD framework has advantages over thermo-physical properties as design targets: First, the designed fluids are assessed with a process-level objective function in both steps. Thus, the potentially ambiguous definition of process-specific target properties is avoided. Process-level trade-offs are fully captured. Secondly, the approach is based on an extended PC-SAFT equation providing the full Helmholtz function of the designed fluids. Thereby, all equilibrium thermodynamic properties are modeled in a thermodynamically consistent way by a single equation using only the PC-SAFT pure component parameters as input. This also enables the use of a single GC-method in the actual computer-aided molecular design (CAMD). The GC-method calculates the PC-SAFT pure component parameters from the molecular structure. The resulting CAMD problem can be formulated and efficiently solved as MIQP.

model for a radial inflow turbine. They conclude that the influence of the geothermal heat source temperature on the efficiency of the turbine should not be neglected. However, while both efficiencies vary with the geothermal heat source temperature, the difference in the turbine efficiency of R134a and R245fa at the same geothermal source temperature is smaller than 0.006 %-points. Furthermore, Sauret and Rowlands (2011) have employed a preliminary design model for a radial inflow turbine and compared the resulting efficiencies and turbine designs for five working fluids (four refrigerants and n-pentane). The authors conclude that the variation of the efficiency of the turbine is indeed small, while the design of the turbine shows significant variation. This is an important result, as the design of a turbine can be infeasible in terms of either operational parameters (i.e., speed of rotation, Mach numbers) or manufacturing issues (i.e., infeasible blade height). From the case studies of Wang et al. (2013) and Sauret and Rowlands (2011), the assumption of a constant efficiency of the turbine seems to hold. However, the working fluid and the process conditions will influence the design and the feasibility of the turbine.

5.1 Process model

In this chapter, a recuperated solar ORC (figure 5.1) is considered (Casati et al., 2011): The working fluid vapor leaving the solar field in state 1 is expanded in the turbine, which delivers work to the generator transforming it into useful power. This work focuses on a single stage 90° radial inflow turbine. Inside the turbine, the fluid passes the nozzle ring and enters the rotor in state 2. The rotor is left in state 3 and the working fluid passes the diffuser. After passing the diffuser, the working fluid leaves the turbine in state 4. Then, the fluid enters the recuperator and is cooled down to state 5. After passing the condenser the working fluid is in state 6, which is assumed to be saturated liquid. Then, the fluid is pumped to the upper pressure level (state 7). The pressurized fluid is preheated in the recuperator using the heat extracted from the vapor exiting the turbine and leaves the evaporator in state 8. Finally, the solar field is passed, where the working fluid is evaporated and possibly superheated. The working fluid is cooled in the condenser using ambient air. The air is entering the system in state C1 passes the compressor and is fed to the condenser in state C2. The air leaves the system in C3. The state points for the description of the air flow are introduced for the calculation of the energy needed to supply the cooling, which is the work entering the compressor to overcome the pressure drop of the condenser. Additionally, pressure drops are considered in the solar field, the recuperator (both sides) and the cold side of the condenser. The turbomachinary

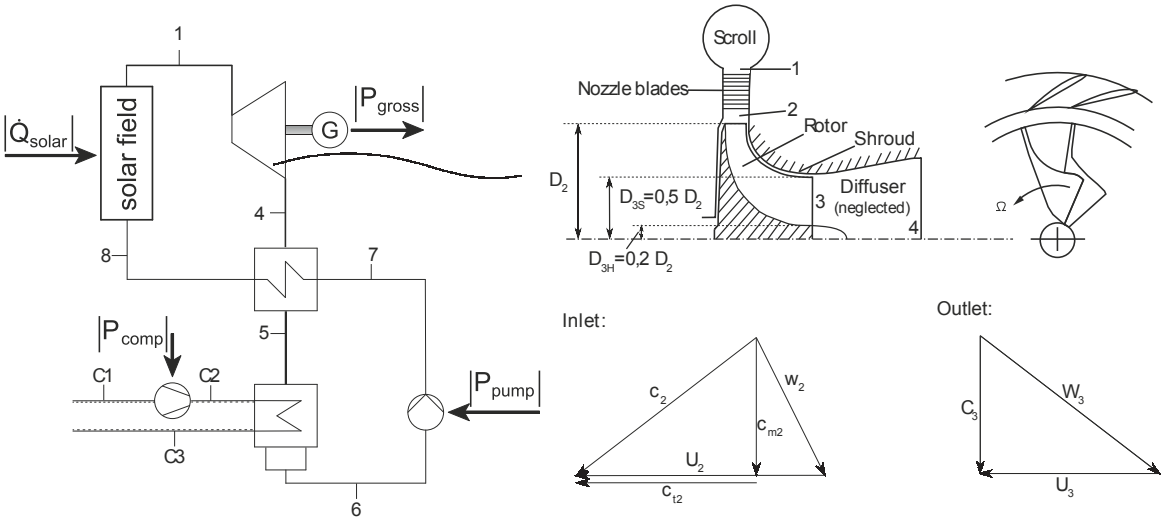

Figure 5.1: State points and configuration of the solar ORC a) process flowsheet and b) radial turbine including the corresponding velocity triangles

is considered to be adiabatic and no additional losses are included in the model. A detailed list of the parameters of the model including values for all pressure losses, mechanical and isentropic efficiencies for pump and compressor, and the minimal temperature differences is found in section 5.3 (table 5.2).

The chapter aims to show the merits of employing more detailed technology models for the working fluid selection. The objective function $f(x, z)$ in eq. (3.1) is to maximize the net power output P_{net}. The geothermal example presented in 3.4 neglects the parasitic load[1] of the blower of the cooling system. For the solar system, the parasitic load can be significant for the net power output of the system and should be

[1]Power used internally for the ORC system itself for, e.g., blower of the cooling system or control utilities.

Table 5.1: Degrees of freedom for the optimization of the solar ORC (Colonna, 2013)

Parameter	**Symbol**	**Bounds**		
degree of superheating	ΔT_{sh}	$0\ \text{K} \leq$	ΔT_{sh}	$\leq 200\ \text{K}$
pressure at evaporator outlet	$p_{\text{out,evap}}$	$p_{\text{out,cond}} \leq$	$p_{\text{out,evap}}$	$\leq 30\ \text{bar}$
pressure at condenser outlet	$p_{\text{out,cond}}$	$0.05\ \text{bar} \leq$	$p_{\text{out,cond}}$	$\leq p_{\text{out,evap}}$
mass flow rate	$\dot{m}_{\text{wf}}$	$0.01\ \frac{\text{kg}}{\text{s}} \leq$	$\dot{m}_{\text{wf}}$	$\leq 100\ \frac{\text{kg}}{\text{s}}$

considered. The parasitic load of the compressor P_{comp} reduces the net power output

$$\max_{x,z} P_{\text{net}} = |P_{\text{gross}}| - |P_{\text{pump}}| - |P_{\text{comp}}| \,. \tag{5.1}$$

The free process variables x (table 5.1) and vector z the relaxed PC-SAFT pure component parameters are the same as in the geothermal example in section 3.4. As in the geothermal example[2], energy balances around turbine, pump and compressor, and the definition of the isentropic efficiency yield

$$\begin{aligned} P_{\text{net}} =& \dot{m}_{\text{wf}} \left[(h_1 - h_4) - (h_7 - h_6) - (h_{\text{C2}} - h_{\text{C1}}) \right] \\ =& \dot{m}_{\text{wf}} \big[\eta_{\text{gen}} \eta_{s,\text{turb}} (h_{3ss} - h_1) \\ & - \eta_{\text{mech,pump}}^{-1} \eta_{s,\text{pump}}^{-1} (h_{7s} - h_6) \\ & - \eta_{\text{mech,comp}}^{-1} \eta_{s,\text{comp}}^{-1} (h_{C2s} - h_{C1}) \big] \,. \end{aligned} \tag{5.2}$$

The efficiecies $\eta_{\text{mech,pump}}$,$\eta_{s,\text{pump}}$, $\eta_{\text{mech,comp}}$ and $\eta_{s,\text{comp}}$ are constant. The state points are calculated as

$$h_6 = \text{h}(p_6, \text{T}^{\text{sat}}(p_6), z) \tag{5.3}$$

$$h_{7s} = \text{h}(p_7, s_6, z) = \text{h}(p_7, \text{s}(p_6, \text{T}^{\text{sat}}(p_6), z), z) \tag{5.4}$$

$$h_{C1} = \text{h}(p_{\text{amb}}, \text{T}_{\text{amb}}, z) \tag{5.5}$$

$$\begin{aligned} h_{C2s} =& \text{h}(p_{\text{amb}} + \Delta p_{\text{cond,cold}}, s_{\text{C1}}, z) \\ =& \text{h}(p_{\text{amb}} + \Delta p_{\text{cond,cold}}, \text{s}(\text{T}_{\text{amb}}, p_{\text{amb}}, z), z) \end{aligned} \tag{5.6}$$

$$h_1 = \text{h}(p_1, \text{T}^{\text{sat}}(p_1) + \Delta T_{\text{sh}}, z) \tag{5.7}$$

$$h_{3ss} = \text{h}(p_4, s_1, z) = \text{h}(p_4, \text{s}(p_1, \text{T}^{\text{sat}}(p_1) + \Delta T_{\text{sh}}, z), z) \,. \tag{5.8}$$

The pressures p_6, p_7, p_1 and p_4 can be calculated directly from the variables $p_{\text{out,evap}}$ and $p_{\text{out,cond}}$ using the pressure losses. However, P_{net} depends on the turbine efficiency $\eta_{s,\text{turb}}$. A model for the efficiency of the turbine is embedded depending on the cycle and the working fluid properties. The model also allows for preliminary design of the turbine. Thus, constraints on the design of the turbine can be embedded. Here, the process itself is constrained by the amount of heat transferred into the process $\dot{Q}_{\text{evap}}^{\text{max}}$, a maximal temperature that can be achieved using the solar field $T_{\text{evap}}^{\text{out,max}}$, a minimal condensation temperature $T_{\text{cond}}^{\text{min}}$, and the minimal allowed approach temperatures in

[2]Note that the definition of state points has changed compared to the geothermal example in section 3.4 due to the detailed model for the ORC system (cf. figure 5.1).

Notation

Latin symbols

a	free Helmholtz energy	$\frac{\mathrm{J}}{\mathrm{mol}}$
AS	Active set	(generic)
b	blade height	m
c	absolute velocity	$\frac{\mathrm{m}}{\mathrm{s}}$
C_0	sprouting velocity	$\frac{\mathrm{m}}{\mathrm{s}}$
d	database of fluids	-
D	diameter	m
e	threshold value	(generic)
f	objective function	(generic)
F	constituting equation for molecular structure	-
g	process model	(generic)
h	specific enthalpy	$\frac{\mathrm{J}}{\mathrm{mol}}$
h	equality constraints	(generic)
I	set of groups	-
m	segment number	-
$\dot{m}$	mass flow rate	$\frac{\mathrm{kg}}{\mathrm{s}}$
p	pressure	bar
P	power	W
R	degree of reaction	-
s	specific entropy	$\frac{\mathrm{J}}{\mathrm{mol\ K}}$
T	temperature	K
T	Taylor-approximation	(generic)
U	speed of rotation	$\frac{1}{\mathrm{s}}$
v	specific volume	$\frac{\mathrm{m}^3}{\mathrm{mol}}$
v	valency	-
w	weighting factor	(generic)
w	relative velocity	$\frac{\mathrm{m}}{\mathrm{s}}$
x	process variables	(generic)

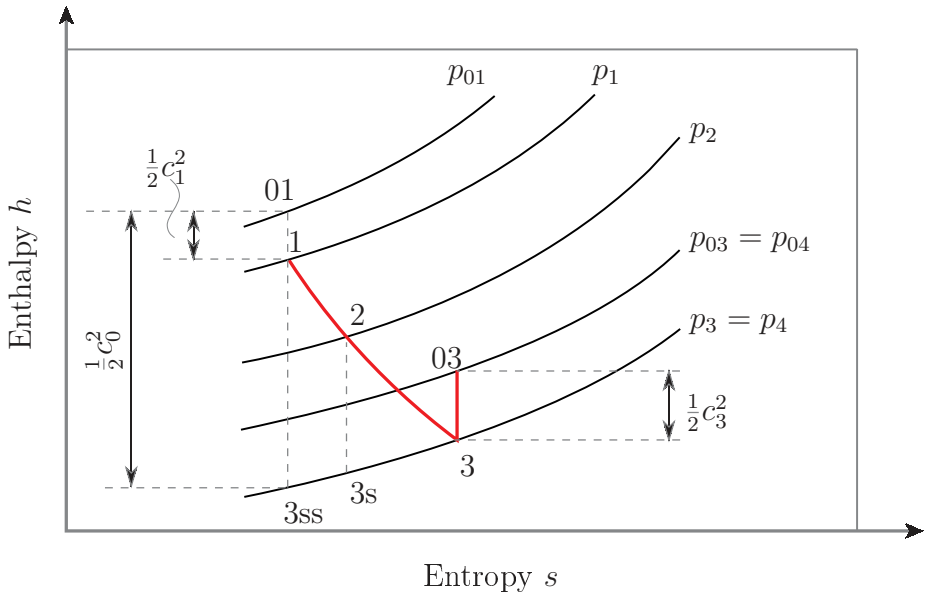

Figure 5.2: Enthalpy-entropy chart of the expansion process in the turbine. The flow enters the turbine in state 1 (Fig. 5.1), passes through the nozzle and enters the rotor in state 2. The fluid leaves the rotor in state 3 and leaves the turbine in the same state, as the diffuser is neglected. The states 0X denote the stagnation state of the fluid, when it recovers all kinetic energy from state X. The state 3ss corresponds to the fluid passing an ideal (isentropic) turbine. State 3s corresponds to the fluid passing the real nozzle, but an isentropic rotor.

in the rotor and the isentropic enthalpy drop in the complete stage (nozzle and rotor). The degree of reaction is commonly between 0 and 0.5 for a radial inflow turbine. Small values of the degree of reaction (e.g., an pure impulse stage, where $R = 0$), lead to supersonic inflow conditions even for moderate volume ratios (SVR ≥ 5). For higher degrees of reaction, the volume ratio can be higher, while still ensuring subsonic flow condition. However, higher values of R can yield prohibitive rotor blade height variations, sealing problems and might be impractical for a single stage turbine design (Dixon and Hall, 2010; Fiaschi et al., 2012). Thus, a moderate degree of reaction of

$$R = \frac{h_2 - h_3}{h_1 - h_3} = 0.15 \tag{5.10}$$

is considered.

For the exit velocity ratio Φ and the blade loading coefficient Ψ, relations for the optimal values are known (Rodgers and Geiser, 1987) and the optimal values are assumed. The exit velocity ratio (Φ, or flow coefficient) is defined as the ratio of the absolute velocity at the rotor exit c_3 and the tip rotor speed at the rotor inlet U_2

$$\Phi = \frac{c_3}{U_2} = 0.25 \ . \tag{5.11}$$

The blade loading coefficient (Ψ, or sprouting velocity ratio) is the speed of rotation to sprouting velocity ratio, where the sprouting velocity C_0 is the artificial velocity corresponding to the enthalpy drop from state 01 to state $3ss$ $\left(C_0 = \sqrt{2\left(h_{01} - h_{3ss}\right)}\right)$

$$\Psi = \frac{U_2}{C_0} = 0.7 \ . \tag{5.12}$$

The definition of the isentropic efficiency of a turbine can be obtained from textbooks (Dixon and Hall, 2010) and is calculated from loss coefficients and fluid velocities as

$$\eta_{s,\mathrm{turb}} = \frac{h_{01} - h_{03}}{h_{01} - h_{3ss}} = \frac{\Delta w}{\Delta w + \frac{1}{2}\left(c_3^2 + w_3^2\zeta_\mathrm{R} + c_2^2\zeta_\mathrm{N}\frac{T_3}{T_2}\right)}, \tag{5.13}$$

where h_{0x} is the stagnation enthalpy of the fluid[3]. h_{03ss} is the reference state after an isentropic nozzle and rotor and $\Delta w = h_{01} - h_{03}$ is the specific work. The loss coefficients for nozzle ζ_N and for rotor ζ_R are defined as

$$h_3 - h_{3s} = \tfrac{1}{2} w_3^2 \zeta_\mathrm{R} \tag{5.14}$$

[3]The stagnation enthalpy $h_{0x} = h_x + \frac{1}{2}c_x^2$ is the enthalpy that the fluid would have in total stagnation, when all kinetic energy from the velocity c_x is recovered.

$$h_{3s} - h_{3ss} = \tfrac{1}{2} c_2^2 \zeta_\mathrm{N} \tfrac{T_3}{T_2} \ . \tag{5.15}$$

The loss coefficients are considered constant ($\zeta_\mathrm{R} = 1$ and $\zeta_\mathrm{N} = 0.1$). Furthermore, diameter ratios $\frac{D_{3h}}{D_2}$ and $\frac{D_{3s}}{D_{3h}}$ are assumed to be constant. For the calculation of the efficiency, eq. (5.13) is reformulated as an implicit function for turbine efficiency $\eta_{s,\mathrm{turb}} = f\left(p_{01}, T_1, p_3, z\right)$.

Using assumptions eqs. (5.10), (5.11) and (5.12), the velocities in eq. (5.13) can be calculated. c_2 can be expressed as

$$c_2 = \sqrt{2 \ \left(h_{02} - h_2\right)} \ . \tag{5.16}$$

An energy balance around the nozzle yields $h_{01} = h_{02}$. Using eq. (5.10) and neglecting the diffuser (state 3 = state 4) yields

$$c_2 = \sqrt{2 \ \left(h_{01} - h_3 - R \ \left(h_1 - h_3\right)\right)} \ , \tag{5.17}$$

where $h_{01} = h_1 + \tfrac{1}{2}\overset{0}{\cancel{c_1^2}} = \mathrm{h}\left(p_1, T_1, z\right)$, as the inlet velocity is neglected. The enthalpy $\mathrm{h}\left(p, T, z\right)$, defined by pressure p, temperature T and the pure component parameters z, can be calculated using PC-SAFT. The next velocity in eq. (5.13), c_3, can be expressed from the definition of Φ, Ψ (in eq. (5.11) and eq. (5.12), respectively) and the sprouting velocity $C_0 = \sqrt{2\left(h_{01} - h_{3ss}\right)}$, which is the artificial velocity corresponding to a kinetic energy equal to the total enthalpy drop of an isentropic turbine

$$c_3 = \Phi \Psi C_0 = \Phi \Psi \sqrt{2\left(h_{01} - h_{3ss}\right)} \ . \tag{5.18}$$

The relative velocity at the rotor outlet w_3 can be expressed using the velocity triangle in fig. 5.1 as

$$w_3 = \sqrt{U_3^2 + c_3^2} = \sqrt{\left(U_2 \tfrac{D_3}{D_2}\right)^2 + c_3^2} \tag{5.19}$$

$$= \sqrt{\left(\Psi C_0 \tfrac{D_3}{D_2}\right)^2 + c_3^2} \tag{5.20}$$

and c_3 can be expressed as shown above. Inserting in eq. (5.13), using $h_{01} - h_{03} = \eta_{s,\mathrm{turb}}\left(h_{01} - h_{3ss}\right)$ and canceling $h_{01} - h_{3ss}$ yields

$$\eta_{s,\mathrm{turb}} = \frac{\eta_{s,\mathrm{turb}}}{\eta_{s,\mathrm{turb}} + \Phi^2\Psi^2 + \zeta_\mathrm{R}\Psi^2\left(\Phi^2 + \left(\frac{D_2}{D_3}\right)^2\right) + \zeta_N\left(1 - R\right)\left(\eta_{s,\mathrm{turb}} + \Phi^2\Psi^2\right)\frac{T_3}{T_2}} \tag{5.21}$$

Ignoring the trivial solution of no power output $\eta_{s,\text{turb}} = 0$ yields

$$\eta_{s,\text{turb}} = \frac{1 - \Phi^2\Psi^2 - \zeta_\text{R}\Psi^2\left(\Phi^2 + \left(\frac{D_2}{D_3}\right)^2\right) - \zeta_N\left(1-R\right)\Phi^2\Psi^2\frac{T_3}{T_2}}{1 + \zeta_\text{N}\left(1-R\right)\frac{T_3}{T_2}} \tag{5.22}$$

The only free variable is the temperature ratio $\frac{T_3}{T_2}$. While this term depends on the process conditions and the selection of the working fluid, the ratio is known to have limited influence on the numerical value of the efficiency (Dixon and Hall, 2010). However, the model also allows for the calculation of crucial design parameters and for the identification of infeasible turbine design. In addition to the assumptions above, the velocity at the inlet is neglected ($c_1 = 0$) for the preliminary design. The model calculates the fluid velocities at all stages, the diameter of the turbine and the thermodynamic conditions of the fluid. The model defines constraints for: blade height b_2, volume ratio, Mach numbers and the speed of rotation.

The blade height can be calculated from the mass flow at the rotor inlet.

$$b_2 = \frac{\dot{m}}{\rho_2 c_{m2}\pi D_2} \tag{5.23}$$

The diameter of the inlet, in turn, can be calculated from conservation of mass flow rate through the rotor

$$\dot{m} = \dot{m}_3 = \dot{m}_2 \tag{5.24}$$

$$\Leftrightarrow D_2 = \sqrt{\frac{4\ \dot{m}}{\rho_3\Phi U_2\pi\left(\frac{D_{3s}}{D_2}\right)^2\left(1-\left(\frac{D_{3h}}{D_{3s}}\right)^2\right)}} \tag{5.25}$$

where $\frac{D_{3s}}{D_2}$ and $\frac{D_{3h}}{D_{3s}}$ are fixed. The unknown meridonal velocity c_{m2} can be calculated from the velocity triangle, as

$$c_{m2}^2 = c_2^2 - c_{t2}^2 \tag{5.26}$$

and velocity c_2 is known from eq. (5.17). The tangential velocity c_{t2} can be calculated from

$$c_{t2} = \frac{h_{01} - h_{03}}{\Psi\sqrt{2(h_{01} - h_{3s})}} \tag{5.27}$$

Finally, Eqs. (5.17), (5.23), (5.25), (5.27) yield

$$b_2^2 = \frac{\dot{m}\rho_3\Phi\Psi\sqrt{h_{01}-h_{3s}}\left(\frac{D_{3s}}{D_2}\right)^2\left(1-\left(\frac{D_{3h}}{D_{3s}}\right)^2\right)}{4\rho_2^2\left(2\left(h_{01}-h_3\right) - R\left(h_1-h_3\right)\right) - \frac{\left(h_{01}-h_{03}\right)^2}{2\Psi^2(h_{01}-h_{3s})}}\ , \tag{5.28}$$

where $\rho_2 = \rho(p_2, T_2, z)$ and $\rho_3 = \rho(p_3, T_3, z)$.

The speed of rotation can easily be calculated as

$$\mathrm{RPM} = \frac{U_2}{D_2} \tag{5.29}$$

with eq. (5.25) and $U_2 = \Psi\sqrt{2\,(h_{01} - h_{3ss})}$. Finally, as all velocities are known, the Mach numbers in stage x can be calculated as

$$\mathrm{M}_x = \frac{v_x}{w_x}\ , \tag{5.30}$$

where the sonic velocity in state i ($w_i = \mathrm{w}_i(p_i, T_i, z)$) is also modeled by PC-SAFT for each working fluid. The inclusion of the turbine model into the CoMT-CAMD framework is straight forward. The turbine design constraints are integrated into the process model by substituting eq. (5.22) in eq. (5.2) and combining the process and the turbine constraints to $g(x, z) = (g_{\mathrm{process}}(x, z), g_{\mathrm{turb}}(x, z))^T$ with

$$g_{\mathrm{turb}} = \begin{pmatrix} b_2 - b_2^{\max} \\ SVR - SVR^{\max} \\ RPM - RPM^{\max} \\ M_i - M^{\max} \end{pmatrix} \quad \forall i \in \{1, 2, 3\}\ . \tag{5.31}$$

No additional degrees of freedom are added to the optimization. Thus, the vector x from tab. 5.1 remains unaltered.

5.3 Illustrative example

The presented framework for the integrated design of working fluid, process and turbine is applied to the optimization of a small-scale solar ORC. The case study is adopted from Casati et al. (2011). Please note that their study did not focus the selection of an optimal working fluid, but was concerned with the modeling of the solar field. However, the application of the presented framework for the working fluid selection and turbine design seems promising for this application, because for small-scale applications the design of suitable turbines is challenging and should be considered in the working fluid selection. The application of Casati et al. (2011) is used as a base-case to compare the results and parameter values are adopted from their study. The detailed model for the dynamics of the solar field from Casati et al. (2011), however, is not considered here, because this level of detail is beyond the scope of this work.

Here, the solar field is considered as a heat source with a maximal amount of heat $\dot{Q}_{\mathrm{evap}}^{\max}$ that can be supplied at temperatures up to a limit of $T_{\mathrm{evap}}^{\mathrm{out,max}} = 380$ °C

Table 5.2: Parameter values for the model of the solar ORC

Parameter	Symbol	Value
Turbine		
generator efficiency	η_{gen}	0.95
maximal expansion ratio	$SVR^{\max}$	150
maximal rotational speed	$RPM^{\max}$	70,000
maximal blade height	$b_2^{\max}$	1 mm
maximal Mach number	$M^{\max}$	0.9
Solar Field		
pressure loss	Δp_{solar}	200 kPa
transfered heat	$\dot{Q}_{\text{evap}}^{\max}$	463 kW
max. temperature at outlet	$T_{\text{evap}}^{\text{out,max}}$	380 °C
Pump		
mechanical efficiency	$\eta_{\text{mech,pump}}$	0.9
isentropic efficiency	$\eta_{s,\text{pump}}$	0.7
Regenerator		
minimal Temperature difference	$\Delta T_{\text{regen}}^{\min}$	30 °C
pressure loss (hot side)	$\Delta p_{\text{regen,hot}}$	5 kPa
pressure loss (cold side)	$\Delta p_{\text{regen,cold}}$	30 kPa
Condenser		
minimal condensation temperature	$T_{\text{cond}}^{\min}$	80 °C
minimal Temperature difference	$\Delta T_{\text{cond}}^{\min}$	20 °C
pressure loss (hot side)	$\Delta p_{\text{cond,hot}}$	0 kPa
pressure loss (cold side)	$\Delta p_{\text{cond,cold}}$	0.5 kPa
Air Cooling Compressor		
mechanical efficiency	$\eta_{\text{mech,comp}}$	0.9025
isentropic efficiency	$\eta_{s,\text{comp}}$	0.85

(table 5.2). Minimal approach temperatures for the regenerator $\Delta T_{\text{regen}}^{\text{min}}$ and condenser $\Delta T_{\text{cond}}^{\text{min}}$ are employed. Additionally, a minimal condensation temperature $T_{\text{cond}}^{\text{min}}$ is set to allow for air cooling of the system.

5.3.1 Results of the targeting

The first step of the holistic design approach is the CoMT optimization, where process and working fluid are optimized simultaneously. The PC-SAFT pure component parameters are considered as continuous variables in the optimization. The result of the optimization is an optimal combination of working fluid and process (the target). For the solar application, the optimization yields a subcritical cycle with net power output of $P_{\text{net}} = 125$ kW. The cycle uses the maximal amount of heat available and reaches the maximal allowed temperature as well as the minimal allowed condensation temperature. The preliminary turbine design is feasible and reaches an efficiency of ($\eta_{s,\text{turb}} = 82$ %). The turbine design is at its bound for the speed of rotation RPM and the Mach number M (table 5.3).

5.3.2 Results of the structure-mapping

The basic structure-mapping (section 3.2) is employed to identify real working fluids. The result of the basic structure-mapping (table 5.4) is qualitative similar to the result of the illustrative example in section 3.4: Well-suited and, in fact, optimal working fluids are identified. Four out of the best ten working fluids are identified and the best 3 fluids are in the correct order. For this example, the space of near optimal working fluids is dense and the performance the worst working fluid (cyclohexane) in table 5.4 is only 10 % lower than the best identified working fluid (1-trans-3,5-trimethylcyclohexane). However, the real ranking based on a process optimization performed for each fluid ranks cyclohexane only on position 80 of the database.

To refine the ranking, the adaptive structure-mapping (section 3.2.4) is employed starting with the result of the basic structure-mapping in table 5.4. The current ranking is traversed starting with the working fluid with the highest predicted performance. For each working fluid, a process optimization is performed. The result of the process optimization is compared to the estimated performance. If the difference in the result and the estimate exceeds a predefined threshold value, then an additional Taylor-approximation is performed at the pure component parameters of this fluid, else the next fluid is considered. The method stops, when the threshold value is not exceeded for the complete list.

Table 5.3: Results of the case study for the target process and working fluid, and the TMCH process including the pure component parameters, the work and heat load of all components and the results of the preliminary design of the turbine

Parameter	**Symbol**	**Value**	
		Target	**TMCH**
Working Fluid			
segment number	m / –	1.9	2.4
segment diameter	σ / Å	4.2	4.5
segment energy	$\frac{\epsilon}{k}$ / K	389	325
Process Conditions			
pressure evaporator	$p_{\text{evap}}^{\text{out}}$ / bar	28	25
pressure condenser	$p_{\text{cond}}^{\text{out}}$ / bar	0.2	0.2
mass flow rate	$\dot{m}_{\text{wf}}$ / $\frac{\text{kg}}{\text{s}}$	0.8	0.9
degree of superheating	ΔT_{sh} / K	45	41
Work and Heat			
generator	P_{gen} / kW	135	127
pump	P_{pump} / kW	4.4	5.3
compressor	P_{comp} / kW	5.1	5.3
evaporator	$\dot{Q}_{\text{evap}}$ / kW	463	463
recuperator	$\dot{Q}_{\text{recup}}$ / kW	338	573
condenser	$\dot{Q}_{\text{cond}}$ / kW	324	333
net	P_{net} / kW	125	117
Turbine			
efficiency	$\eta_{\text{s,turb}}$ / –	.82	.81
blade height	b_2 / mm	2.4	2.8
volume ratio	SVR / –	125	150
speed of rotation	RPM / $\frac{1000}{\text{min}}$	65	51
Mach number (rotor in)	M_2 / –	0.9	0.9
diameter (rotor inlet)	d_2 / mm	134	156
diameter (rotor outlet)	d_3 / mm	47	54

Table 5.4: Results from the basic structure-mapping: working fluids and corresponding PC-SAFT pure component parameters. Ranks in brackets are the real rank given by $\mathbf{P}_{\text{net}}$.

Rank	**Component**	**m** / −	σ / Å	$\frac{\epsilon}{\mathbf{k}}$ / **K**	$\mathbf{P}_{\text{net}}$ / **kW**
/	D4 (Casati et al., 2011)	5.77	4.11	214	104.0
/	hypothetic optimum	1.85	4.24	389	124.5
1 (1)	1-trans-3,5-trimethylcyclohexane	2.40	4.53	325	117.1
2 (2)	cycloheptane	2.68	3.94	297	117.0
3 (3)	1,3,5,7-cyclooctatetraene	2.83	3.80	308	116.8
4 (22)	methylcyclohexane	2.63	4.01	284	112.3
5 (19)	1,4-dioxane	2.91	3.39	279	112.8
6 (11)	1,1-dimethylcyclohexane	2.78	4.11	287	114.9
7 (66)	benzene	2.44	3.65	289	107.9
8 (6)	trans-1,2-dimethylcyclohexane	2.80	4.11	288	115.5
9 (34)	cis-1,2-dimethylcyclopentane	2.82	3.91	272	111.1
10 (80)	cyclohexane	2.47	3.86	282	105.6

Table 5.5: Results from adaptive structure-mapping: working fluids and PC-SAFT parameters. As Benchmark, D4 (octamethylcyclotetrasiloxane) used by Casati et al. (2011) and the hypothetical optimal working fluid are given. Ranks in brackets are the real rank given by $\mathbf{P}_{\text{net}}$.

Rank	**Component**	**m** / −	σ / Å	$\frac{\epsilon}{\mathbf{k}}$ / **K**	$\mathbf{P}_{\text{net}}$ / **kW**
/	D4 (Casati et al., 2011)	5.77	4.11	214	104.0
/	hypothetical optimum	1.85	4.24	389	124.5
1 (1)	1-trans-3,5-trimethylcyclohexane	2.40	4.53	325	117.1
2 (2)	cycloheptane	2.68	3.94	297	117.0
3 (3)	1,3,5,7-cyclooctatetraene	2.83	3.80	308	116.8
4 (4)	ethylcyclohexane	3.01	4.00	284	116.4
5 (5)	p-xylene	3.13	3.78	286	115.7
6 (6)	trans-1,2-dimethylcyclohexane	2.80	4.11	288	115.5
7 (7)	isopropylcyclopentane	2.97	4.03	281	115.5
8 (8)	cis-1,4-dimethylcyclohexane	2.92	4.04	282	115.3
9 (9)	trans-1,3-dimethylcyclohexane	2.96	4.02	281	115.3
10 (11)	1,1-dimethylcyclohexane	2.78	4.11	287	114.9

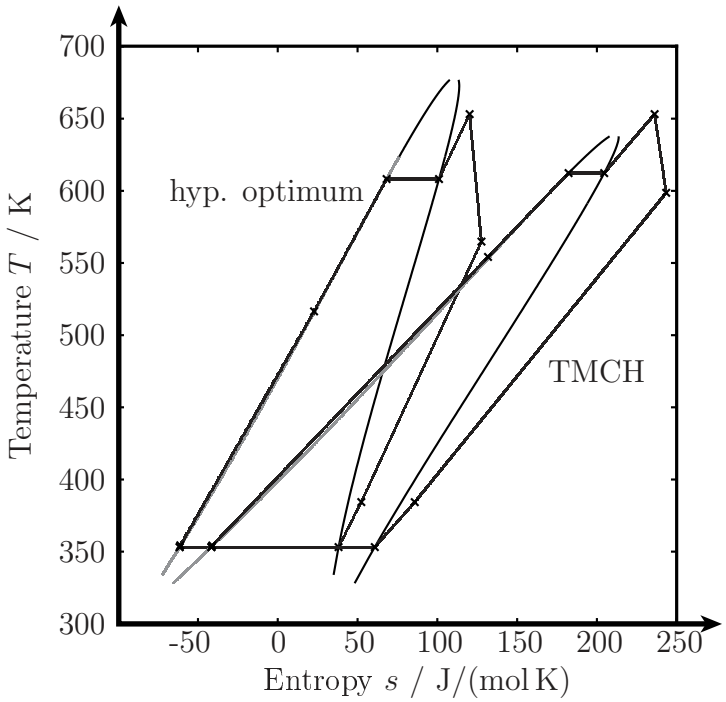

Figure 5.3: Comparison of the hypothetical, optimal process (the target, left) and the TMCH process (right) in Temperature-Entropy chart

The resulting ranking (table 5.5) of the adaptive structure-mapping ranks the best nine working fluids in their correct order. The tenth and eleventh working fluid are flipped in the final ranking. The calculation for the final ranking are based on 8 adaption-steps, which involved 5,660 function evaluations in total[4]. The optimization of all fluids from the database used 32,211 function evaluations.

The best identified working fluid is 1-trans-3,5-trimethylcyclohexane (TMCH) with $P_{\text{net}} = 117$ kW (increase of 12 % compared to basecase). TMCH has not yet been considered for ORC applications. The T–s diagram for the hypothetical, optimal fluid and TMCH are similar with respect to the temperature levels and the overall cycle (figure 5.3 and table 5.3). TMCH has higher molecular wheight and thus, the saturation curve is more overhanging than the curve for the hypothetical optimal fluid. This results in a higher temperature after the turbine and a bigger size of the recuperator. Due to more preheating, the temperature at the inlet of the evaporator is higher.

[4]Function evaluations include those used for the CoMT-optimization, the process optimizations during the adaptive structure-mapping, and the evaluations used for the calculations of the new Taylor-approximation.

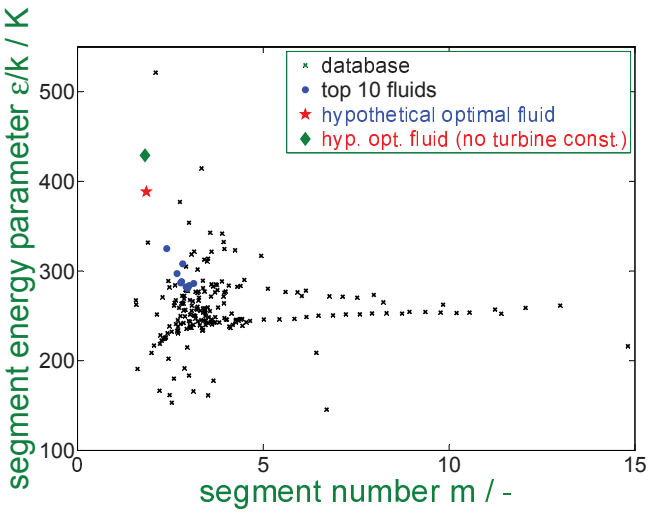

Figure 5.4: Working fluid database and results of the structure-mapping. The original 3-dimensional data $z = (m, \sigma, \epsilon/k)^{\mathrm{T}}$ is projected in a 2-dimensional m–$\frac{\epsilon}{k}$ plane.

5.3.3 Turbine model results

A thermodynamically optimal cycle for a given working fluid can lead to an infeasible turbine design. A feasible turbine design can still be achieved for the same working fluid by adjustment of the process parameters. However, this means turning away from the optimal values and accordingly loosing performance. To demonstrate this point, consider the optimization of process and working fluid in eq. (3.1), but without constraints on turbine design (i.e., removing g_{turb} from the constraints): the CoMT-optimization yields a net power output of $P_{\mathrm{net}} = 128$ kW (before: 125 kW) and a different optimal fluid $\hat{z}^*$ is chosen (figure 5.4). The turbine is infeasible in terms of both volume ratio and Mach number (SVR = 268 and M = 0.97). When reactivating g_{turb} and fixing the selected fluid $z = \hat{z}^*$ in the optimization, the pressure ratio is decreased (figure 5.5) and a net power output of $P_{\mathrm{net}} = 119$ kW is reached, which is less than the optimal hypothetical working fluid reaches.

Thus, while assuming a constant turbine efficiency during working fluid selection seems justified, neglecting turbine design constraints can lead to suboptimal solutions.

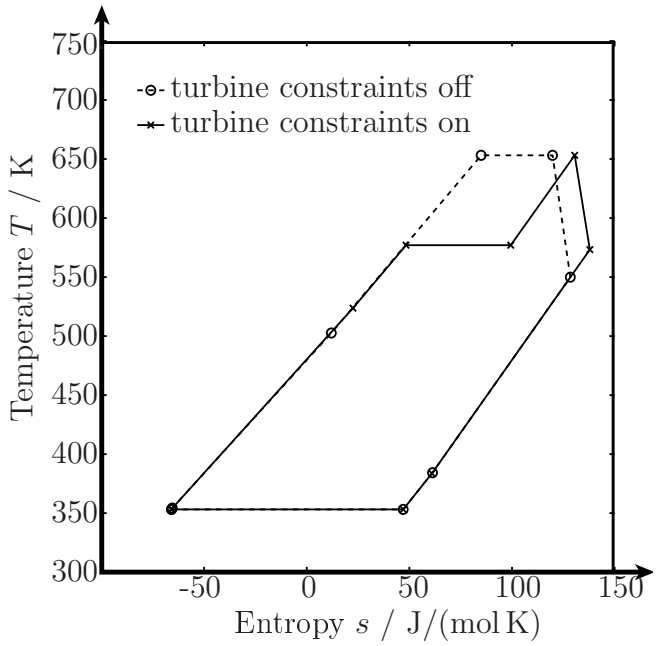

Figure 5.5: Comparison of the optimal fluid without turbine constraints (dotted line, $P_{\text{net}} = 119$ kW) and optimal cycle for the same fluid but optimized including turbine design constraints (solid line, $P_{\text{net}} = 119$ kW) in a Temperature-Entropy chart.

5.4 Summary

Commonly, the efficiency of the turbine is considered as a constant parameter during the design of an ORC system. However, the turbine design and efficiency are important to consider, as the turbine design can become infeasible for the conditions and working fluids selected. Thus, a preliminary turbine design model is proposed to constrain the search space of the optimization to regions where the assumptions are valid. The application to a small-scale solar system shows that the inclusion of the turbine design into the integrated process and working fluid design indeed changes the result of the optimization: If the turbine design is neglected in the optimization, a different optimal working fluid is selected.

Furthermore, the adaptive structure-mapping is used for the refinement of the ranking of working fluids. In the example, 8 adaption steps are used to obtain the final ranking, in which the best nine fluids are identified in their correct order. Compared to the optimization of every single fluid from the database, this corresponds to saving ≈ 80 % of the function evaluations.

y^{s}	molecular structure variables	-
z	parameters of working fluid model	(generic)

Greek symbols

η	efficiency	-
η	dynamic viscosity	Pa s
β	auxiliary variable	- (if not stated otherwise)
$\frac{\epsilon}{k}$	segment energy parameter	K
γ	auxiliary variable	- (if not stated otherwise)
γ	surface tension	$\frac{\mathrm{kg}}{\mathrm{s}^2}$
λ	thermal conductivity	$\frac{\mathrm{W}}{\mathrm{m\ K}}$
μ	viscosity	Pa s
Φ	exit velocity ratio	-
Ψ	sprouting velocity ratio	-
ρ	density	$\frac{\mathrm{kg}}{\mathrm{m}^3}$
σ	segment diameter	$\mathring{\mathrm{A}}$
θ	fluid property	(generic)

Subscripts and superscripts

*	optimal value
’	boiling liquid
”	saturated vapor
0	stagnation
2	euclidean
I	first law
II	second law
amb	ambient conditions
arom	aromatic ring
c	property at critical point
C	Carnot
cond	condenser
comp	compressor
db	double bond

y^{s}	molecular structure variables	-
z	parameters of working fluid model	(generic)

Greek symbols

η	efficiency	-
η	dynamic viscosity	Pa s
β	auxiliary variable	- (if not stated otherwise)
$\frac{\epsilon}{k}$	segment energy parameter	K
γ	auxiliary variable	- (if not stated otherwise)
γ	surface tension	$\frac{\mathrm{kg}}{\mathrm{s}^2}$
λ	thermal conductivity	$\frac{\mathrm{W}}{\mathrm{m\ K}}$
μ	viscosity	Pa s
Φ	exit velocity ratio	-
Ψ	sprouting velocity ratio	-
ρ	density	$\frac{\mathrm{kg}}{\mathrm{m}^3}$
σ	segment diameter	$\mathring{\mathrm{A}}$
θ	fluid property	(generic)

Subscripts and superscripts

*	optimal value
’	boiling liquid
”	saturated vapor
0	stagnation
2	euclidean
I	first law
II	second law
amb	ambient conditions
arom	aromatic ring
c	property at critical point
C	Carnot
cond	condenser
comp	compressor
db	double bond

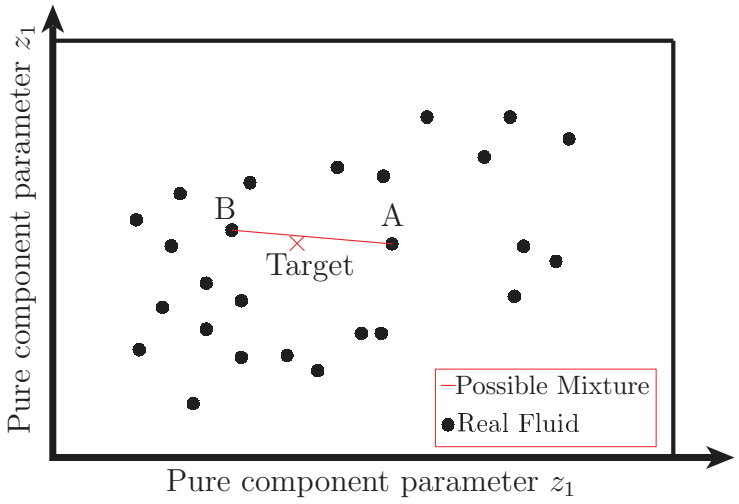

Figure 6.1: Intuitive idea of targeting a pure component and finding a mixture of A and B that has the target properties. The pure component parameter search space is projected in an arbitrary 2-dimensional space for illustration.

The selection of an optimal pure component working fluid is already non-trivial (Quoilin et al., 2013; Bao and Zhao, 2013). The selection of an optimal working fluid *mixture* introduces further complexity. Approaches based on trial and error are prohibitive as the combinatorial nature of the problem cannot be tackled efficiently. Thus, systematic methods for the design of working fluid mixtures are needed. Papadopoulos et al. (2013) identify high-performance working fluid mixtures by computer-aided molecular design (CAMD). In their approach, the constituting equations enforcing the feasibility of the component are skipped for one component and an optimal second component is identified. The result is used to cluster the search space for the second component and the problem is solved to identify a mixture for each of the clusters. Mavrou et al. (2015) compared the resulting mixtures to other proposed mixtures and confirm that the designed mixtures perform better. Furthermore, methods have been developed to select a mixture from a database of components by genetic algorithms (Andreasen et al., 2014).

In this chapter, the first step of the integrated design, the CoMT optimization, is extended for the optimization of binary working fluid mixtures. The extension allows for the integrated design of an optimal working fluid mixture and the process itself. The mixture components, the composition and the key process parameters are the degrees of freedom for the optimization. In section 6.1, the formulation of the integrated mixture and process design is introduced. The continuous-molecular targeting framework is used to identify the optimal working fluid mixture. The resulting op-

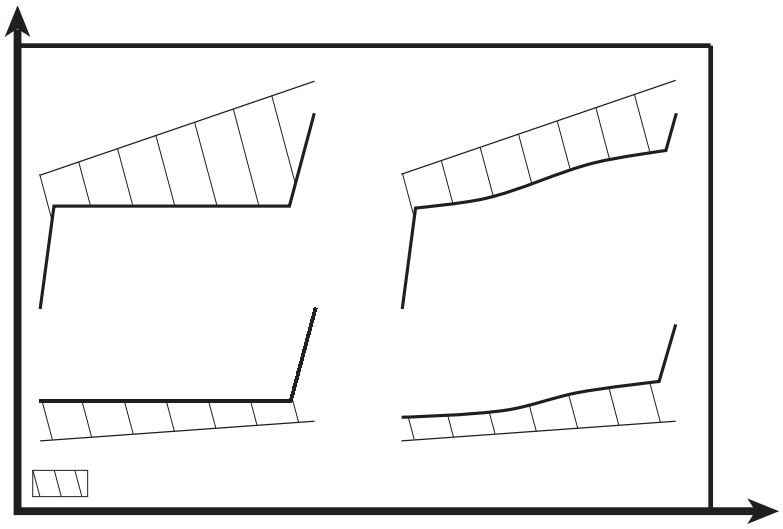

To identify an optimal working fluid mixture for the ORC, the CoMT-optimization given in eq. (3.1) is extended to account for a mixture as degree of freedom. Thus, variables are introduced for the composition x_{wf}, and two sets of pure component parameters z_1 and z_2 to model both fluids. The CoMT-optimization for mixtures is

$$\begin{aligned} \min_{x,z_1,z_2,x_{\mathrm{wf}}} \quad & f(x,\theta) \\ \text{s.t.} \quad & g_1(x,\theta) \leq 0 \\ & g_2(x,\theta) = 0 \\ & \theta = h(x,z_1,z_2,x_{\mathrm{wf}}) \\ & A\,z_1 \leq b \\ & A\,z_2 \leq b \\ & x_{\min} \leq x \leq x_{\max} \\ & 0 \leq x_{\mathrm{wf}} \leq 1 \\ & z_{\min} \leq z_1 \leq z_{\max} \\ & z_{\min} \leq z_2 \leq z_{\max} \\ & x, z_1, z_2, x_{\mathrm{wf}} \in \mathbb{R}\ . \end{aligned} \tag{6.1}$$

This formulation is based on the CoMT for pure components in eq. (3.1). The objective function f and equations g_1, g_2 (process model) remain unaltered. The equations of PC-SAFT h now additionally depend on the second set of pure component parameters z_2 and the mixture composition x_{wf}. The linear constraints for the pure component parameters of the convex hull $A\,z_i \leq b$ are employed for each mixture component. Thus, the complete search space of working fluids is feasible for each components. The search space is thus symmetrical in the compounds of the mixture: For any combination of two components z_1 and z_2, and their composition x_{wf}, an identical symmetric solution can be obtained by exchanging the fluids (i.e., $\bar{z}_1 = z_2$ and $\bar{z}_2 = z_1$) and adapting the composition (i.e., $\bar{x}_{\mathrm{wf}} = 1 - x_{\mathrm{wf}}$). The symmetry of the search space can be prevented by a symmetry breaking constraint, e.g., bounding the mixture composition to $x_{\mathrm{wf}} \leq 0.5$. Symmetry breaking constraints should be employed when global optimization is used to speed up the optimization (Liberti and Ostrowski, 2014). For local search algorithms, the symmetry breaking constraints are not always beneficial (Prestwich and Roli, 2005), as additional local minima can be introduced to the problem. In this work, local optimization is employed for all optimizations. Thus, no symmetry breaking constraints are employed.

Similar to the result of eq. (3.1), the optimal mixture components z_1^* and z_2^* of problem (6.1) do not correspond to any real fluid. The CoMT-optimization for mixtures thus yields a target mixture, which corresponds to an optimal hypothetical mixture.

Table 6.1: Specification of the heat source for the generic example.

Parameter	Symbol	Value
heat source mass flow rate	$\dot{m}_{\mathrm{HS}}$	50 $\frac{\mathrm{kg}}{\mathrm{s}}$
heat source specific heat capacity	$c_{p,\mathrm{HS}}$	4.185 $\frac{\mathrm{kJ}}{\mathrm{kg\ K}}$
heat source inlet temperature	$T_{\mathrm{in,HS}}$	270 °C

6.2 Illustrative example

The comparison of mixtures of existing working fluids to existing pure components in the literature shows advantages for the mixtures compared to pure components. However, this comparison can be misleading when a good mixture is compared to a bad pure component. Eq. (6.1) yields an optimal hypothetical mixture and the corresponding process parameters. The same optimization can be performed for a pure working fluid by enforcing a composition of $x_{\mathrm{wf}} = 0$. This allows for the identification of an optimal hypothetical pure working fluid. The results of both optimizations can be used for an unbiased assessment of the potential benefit of mixtures.

To assess the potential of mixtures, a generic example of an ORC system is used. Changing the model for the cooling of the cycle allows to identify how the cold side effects the optimal mixture. The model of the solar ORC system presented in chapter 5. Here, the model for the turbine as well as pressure losses are neglected. The minimal temperature difference to heat source and heat sink are $\Delta T_{\mathrm{min}} = 0$ K. The heat source is defined by a mass flow rate of hot water (see table 6.1). The degrees of freedom x for the process are the pressure levels for evaporization p_{evap} and condensation p_{cond} as well as the mass flow rate of working fluid $\dot{m}_{\mathrm{wf}}$. Again, the system is optimized for an optimal net power output P_{net}.

For the cooling of the system, different options and model formulations are employed in the following to demonstrate their effect on the optimal working fluid mixture.

6.2.1 Constant cooling temperature

The most simple model of a cooling system assumes a constant lower temperature limit. The lower limit is selected according to a considered cooling system. For this example, a lower temperature limit of 70 °C is considered. Eq. (6.1) is used to optimize two sets of pure component parameters z_1 and z_2 as well as the optimal mixture composition x_{wf}.

evap	evaporator
feas	feasible
gross	gross value
hex	hexane ring
HS	heat source
ig	ideal gas
lb	lower bound
m	meridonal
mech	mechanical
min	minimal value
max	maximal value
net	net value
opt	optimal process
pent	pentane ring
pred	prediction of thermo-physical property (where distinction necessary)
pump	pump
rel	relaxed
res	residual
regen	regenerator
s	isentropic
sh	superheating
sat	saturation
red	reduced property
tb	triple bond
turb	turbine
th	thermal
ub	upper bound
wf	working fluid

Abbreviations and Acronyms

CAMD	Computer-Aided Molecular Design
CoMT	Continuous-Molecular Targeting
const.	constant
CHP	Combined Heat and Power
FOM	Figure of Merit

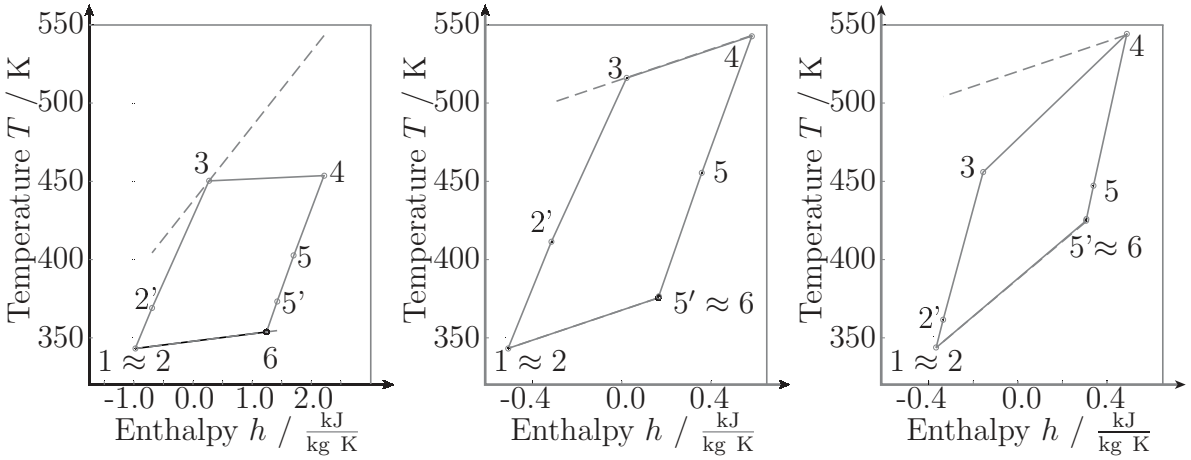

Figure 6.4: Resulting ORC from the CoMT-optimization for a cooling source with constant mass flow rate of a) 500 $\frac{\text{kg}}{\text{s}}$, b) 50 $\frac{\text{kg}}{\text{s}}$ and c) 20 $\frac{\text{kg}}{\text{s}}$.

6.2.2 Fixed mass flow rate of cooling agent

In this section, the cooling system is modeled in the same way as the heat source; i.e., a mass flow rate of cooling agent is supplied with a specified temperature. Three different mass flow rates are assessed to show the effect of a variation of the value of this parameter (500 $\frac{\text{kg}}{\text{s}}$, 50 $\frac{\text{kg}}{\text{s}}$, and 20 $\frac{\text{kg}}{\text{s}}$). The value of 50 $\frac{\text{kg}}{\text{s}}$ corresponds to the same heat capacity flow rate $(\dot{m}\, c_p)_{\text{HS}}$ as for the heat source.

In figure 6.4a, the result of the optimization is shown for a flow rate of $\dot{m}_{\text{CS}} = 500\ \frac{\text{kg}}{\text{s}}$. The result is a mixture with a composition of $x_{\text{wf}} = 0.29$ (see table 6.2). The temperature glide follows the cooling agent exactly. To enable the perfect match of cooling agent and working fluid the condensation pressure p_{cond} and the mass flow rate $\dot{m}_{\text{CS}}$ are selected to the according values. The evaporization pressure p_{evap} is chosen to exploit the minimal allowed temperature difference to the heat source.

The results for the varied mass flow of cooling source are similar to this result (figures 6.4b and 6.4c). The cooling agent is dominating the value for the temperature glide, regardless of the heat source properties. The optimal match of cooling agent and working fluid leads to a thermodynamically optimal cycle. However, only a comparison based on an economic objective function would give a final answer to the question, if mixtures can outperform pure components: the optimal cycles in this and the previous section exploit a perfect match of working fluid and cooling agent in the condenser. This leads to low temperature differences for the heat transfer and accordingly to large required heat exchange area. The larger heat exchange area might lead to prohibitive investment cost to employ the cycle in a ORC system.

Table 6.2: Resulting mixtures from the CoMT-optimization for different mass flow rates of cooling agent

Parameter	Unit	Values		
$\dot{m}_{\mathrm{CS}}$	$\frac{\mathrm{kg}}{\mathrm{s}}$	500	50	20
x_{wf}	–	0.29	0.1	0.16
m_1	–	1.84	1.91	1.85
σ_1	Å	3.41	4.32	4.15
$\left(\frac{\epsilon}{k}\right)_1$	K	503	489	543
m_2	–	2.04	1.84	1.84
σ_2	Å	4.36	3.91	3.32
$\left(\frac{\epsilon}{k}\right)_2$	K	392	400	392
p_{evap}	bar	1.26	8.68	5.13
p_{cond}	bar	0.05	0.13	0.25
$\dot{m}_{\mathrm{wf}}$	$\frac{\mathrm{kg}}{\mathrm{s}}$	57.0	15.2	12.5

6.2.3 Modeling of an air-cooled system

The comparison based on a constant mass flow rate of cooling agent in section 6.2.2 might lead to the conclusion that mixtures are performing better for real ORC systems. However, the assumption of a constant mass flow rate of the cooling agent might still be misleading. Besides the negative effect on the heat exchange area, the assumption of a constant mass flow rate of cooling agent is not valid for many applications: When an air-cooled system is employed, the amount of air for cooling the system is not limited by any constraint, in general. The amount of air that is fed to the system results from a tradeoff between cost for the compression of the air and the effectiveness of the cooling-system.

To reflect this tradeoff, a model of an air-cooling system is employed (figure 6.5). The air-cooling system is modeled as a compressor that has to overcome a pressure drop Δp in the condenser. The air from the environment (state C1) is compressed (state C2) and fed to the condenser for cooling exiting the condenser in state C3. A constant isentropic efficiency of the compressor $\eta_{\mathrm{comp}} = 0.75$ is assumed. The mass flow rate of air is the minimal mass flow rate allowing for the cooling of the cycle. Thus, effort for cooling at lower temperatures is considered in the optimization. The air is entering the compressor at $T_{\mathrm{air,in}} = 15$ °C and fed to an heat exchanger. The pressure drop to be overcome by the compressor is $\Delta p = 0.01$ bar.

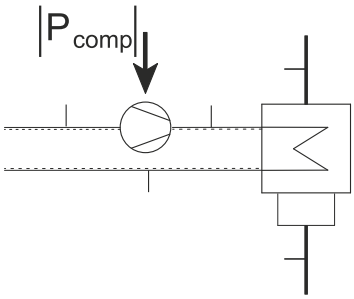
P comp

When the mass flow rate of the cooling agent is constant, mixtures are preferable due to their ability to adapt to the temperature profile of the cooling agents.

The results also show that pure component working fluids are competitive with mixtures and indeed optimal in some cases. By employing a model of the cooling system, the trade-off between the efficiency of the cycle and power consumption of the cooling system is reflected. For this case, a mixture is the optimal solution. However, the difference to the optimal pure component working fluid is below 3 %. For the construction of a real ORC system, the small difference might favor the selection of a pure component for simplicity of the system design.

The comparison of mixtures to pure working fluids indicates that there are pure components that can compete with mixtures in terms of thermodynamical performance. The fact that most comparisons identify mixtures that are favorable, might be due to the limited set of pure components that these mixtures have been compared to.

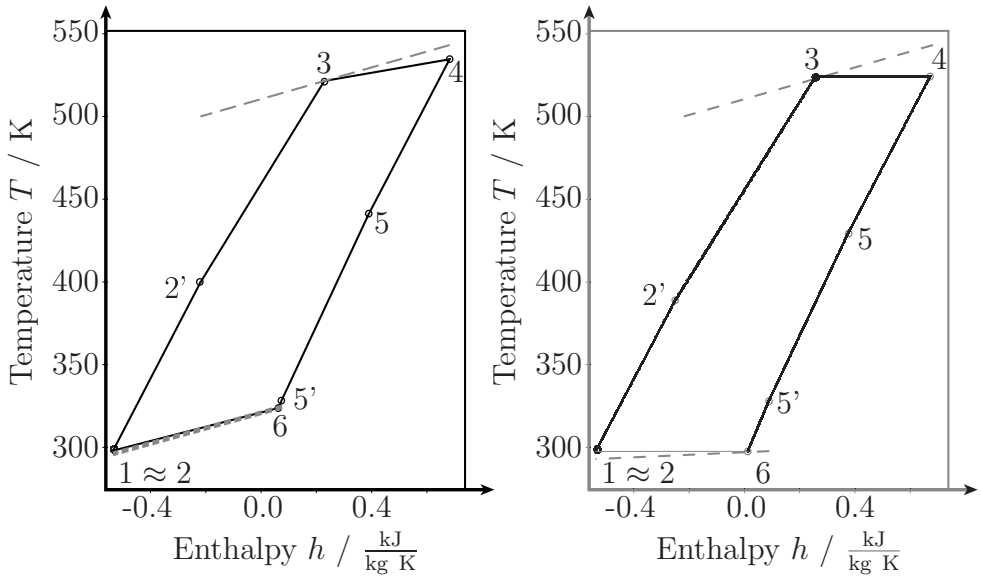

Figure 6.6: a) Result of the CoMT-optimization employing a model of and air-cooling system. b) Result of the CoMT-optimization for a pure component employing a model of and air-cooling system.

GC	Group-Contribution
infeas.	infeasible
MILP	Mixed Integer Linear Program
MINLP	Mixed Integer Nonlinear Program
MIQP	Mixed Integer Quadratic Program
NLP	Nonlinear Program
ORC	Organic Rankine Cycle
OTEC	Ocean Thermal Energy Conversion
(PC-)SAFT	(Perturbed Chain) Statistically Associating Fluid Theory

Chapter 7

Summary, conclusions and future perspective

This thesis presents systematic extensions of the continuous-molecular targeting framework for the integrated design of working fluids and ORC processes. In the first step of the proposed method, a simultaneous optimization of working fluid and process allows for the identification of an optimal hypothetical working fluid. The second step of the method is used to search for real working fluids that lead to similar performance.

7.1 Summary and conclusions

The major findings and merits of the design method are highlighted in the following separately.

7.1.1 Integrated design of ORC working fluids and processes

In chapter 2 of the thesis, the literature on working fluid selection for ORC systems and fluid design is reviewed. The review reveals shortcomings in existing methods: So far, the selection of ORC working fluids is mainly led by heuristic rules and experience of the designer. The heuristic knowledge is used for the preselection of promising candidate fluids for the ORC system. If the heuristics underlying the preselection fail, this approach yields suboptimal solutions.

The design of fluids specifically for a process is difficult due to the inherent interdependency of process and fluid properties. The fluid design yields a mixed-integer nonlinear program of prohibitive size and complexity. To overcome the complexity of the integrated process and fluid design, commonly, methods for problem decom-

position are employed. Decomposing the problem in the fluid properties can yield contradicting objective functions for the fluid design.

This thesis presents a method for the integrated working fluid and process design (chapter 3). The method exploits the coarse-grained molecular picture underlying the PC-SAFT equation of state. The use of binary variables in the integrated fluid and process design is circumvented by relaxation of the PC-SAFT pure component parameters. The relaxation allows for solving the integrated fluid and process design in a single nonlinear program (NLP) using standard solvers.

For the ORC process, it was essential to supplement the PC-SAFT equation of state with a good predictor of the heat capacity $c_p^{\mathrm{ig}}(T)$ of substances in the ideal gas state. More specifically, it is required that $c_p^{\mathrm{ig}}(T)$ can be estimated from the pure component parameters of the PC-SAFT model only. A QSPR model for the ideal gas heat capacity was developed with a determination coefficient of 0.99 for 8 parameters adjusted to 500 pure components (section 3.3). The new relation for the ideal gas contribution to the heat capacity broadens PC-SAFT to a fundamental equation reflecting the full Helmholtz energy. Thus, the presented CoMT-CAMD approach to can be applied also to many other applications.

The presented CoMT-CAMD approach has successfully been applied to optimizing an ORC for a geothermal application (section 3.4). The method was used to generate a ranking list of the 10 most promising working fluids out of a database of 200 substances. The net power output was considered as the only objective function. No heuristics were considered. A rigorous optimization was run for the 200 substances in order to unambiguously assess the proposed ranking list. It was seen that the topmost 6 working fluids were indeed members of the CoMT-CAMD (top 10) ranking list.

A subsequent analysis of the objective function showed kinks in the surface of the objective function, caused by the switchover from one set of active process constraint to another. These kinks in the objective function surface are responsible for some less promising working fluids entering the ranking list. At the same time, the kinks explain why heuristics or metaobjectives can only be applicable in small ranges (in fact ranges unknown a priori) of working fluid properties.

7.1.2 Computer-aided molecular design based on continuous-molecular targets

The integrated design of process and working fluid in the CoMT-CAMD approach has been based on a selection of real fluids from a database. The selection of working fluids from a database relies on measurement data for the fluids and does not allow for the design of new working fluids. A CAMD method is presented to overcome the selection and allow for the design of possibly new working fluids in chapter 4. The results of the integrated optimization serve as design targets for a subsequent CAMD problem in the second step of the method.

The CAMD method still employs the result from the integrated fluid and process design to allow for a sound identification of optimal fluid properties. The heuristic definition of targets using guidelines or knowledge of the process is overcome. In the presented approach, the characteristic fluid properties considered throughout the method are the relaxed pure component parameters of the hypothetical optimal fluid. The proposed CAMD based on continuous-molecular targets has advantages over predefined property targets: First, the designed fluids are assessed with a process-level objective function in both steps. Thus, the potentially ambiguous definition of process-specific target properties is avoided. Process-level trade-offs are fully captured. Secondly, the approach is based on an extended PC-SAFT equation providing the full Helmholtz function of the designed fluids. Thereby, all equilibrium thermodynamic properties are modeled in a thermodynamically consistent way by a single equation using only the PC-SAFT pure component parameters as input. This also enables the use of a single GC-method in the actual computer-aided molecular design (CAMD) independent of the problem. The GC-method calculates the PC-SAFT pure component parameters from the molecular structure. The resulting CAMD problem can be formulated and efficiently solved as MIQP (section 4.1).

7.1.3 Considering turbine design in working fluid selection

The ORC working fluid selection is strongly coupled to the selection and design of a suitable expander. Despite this coupling, the efficiency of the turbine is commonly considered a constant parameter in the working fluid literature. Aiming for a better integration of these aspects of the ORC design, a model for the preliminary design of a radial turbine is integrated into the process model in chapter 5. The preliminary turbine model allows for considering key constraints for the working fluid and process parameters posed by the feasibility of the optimal turbine design.

The model of the radial-inflow turbine is based on a 1-d meanline flow analysis. The calculation of the meanline-flow through the turbine is computationally cheap and allows for a preliminary design of the turbine. Here, a preliminary design model is used to calculate key design parameters of the turbine. The calculation is based on assumptions for the design of an optimal turbine. Constraints on critical design parameters of the turbine are employed. Thus, the design of the optimal turbine is ensured to be feasible for the optimal working fluid under the optimal process conditions.

The detailed turbine model was successfully applied to the design of a solar-driven, small-scale ORC. For the emerging field of solar ORCs, there is limited experience on working fluid selection and the design of suitable a expander for such system can be an obstacle in later design stages. The results show that the integration of the turbine design influences the selection of the working fluid.

7.1.4 Mixtures as ORC working fluids

The model for the integrated optimization of working fluid and process is extended in chapter 6 for the design of working fluid mixtures. The design of working fluid mixtures is achieved by introducing a second set of pure component parameters and the mixture composition as new degrees of freedom to the CoMT optimization. The resulting integrated optimization of process and mixture was successfully applied to an illustrative example.

The ability of the model to design an optimal working fluid mixture is exploited to analyze the effect of mixture on the performance of the cycle assuming different options for the cooling system. The result of the assessment shows that the higher performance of working fluid mixtures is due to the adaption of the mixtures temperature glide to the temperature profile of the cooling agent. Furthermore, the results indicate that a higher performance of a mixture compared to pure components is not guaranteed. The specification of the application can lead to pure components that are superior or at least competitive to any mixture.

7.2 Future research

In the following, recommendations are given for future research. For the recommendations, an estimation is made regarding effort expected for the implementation and uncertainty of the success. The classification is also presented in figure 7.1.

Kurzfassung

Die Verstromung von Niedertemperaturwärme ist ein Schlüssel zu einer nachhaltigen Energieversorgung. Eine der wesentlichen Technologien für die Erzeugung von Strom aus Niedertemperaturwärme sind Organic Rankine Cycles (ORC). Die in ORCs eingesetzten Arbeitsmittel werden heute in einem zweischrittigen Verfahren ausgewählt: Zuerst werden mit heuristischem Wissen geeignete Kandidaten ausgesucht. Im zweiten Schritt bewertet eine Prozessoptimierung jeden dieser Kandidaten. Dadurch kann der Beste unter den ausgewählten Kandidaten identifiziert werden. Wird das optimale Arbeitsmittel bei der Vorauswahl von den Heuristiken nicht erfasst, führt das zweischrittige Verfahren zu suboptimalen Lösungen. Dies kann durch eine simultane Optimierung von Arbeitsmittel und Prozess vermieden werden. Eine simultane Optimierung führt allerdings auf ein gemischt-ganzzahliges nicht-lineares Optimierungsproblem, dass aufgrund seiner Größe und Komplexität nicht direkt lösbar ist.

In dieser Arbeit wird eine systematische Methode für die simultane Optimierung von Arbeitsmittel und Prozess vorgestellt. Die Methode basiert auf der Darstellung der Arbeitsmittel in einem physikalisch-basierten Stoffmodell, der PC-SAFT (perturbed chain statistical associating fluid theory) Zustandsgleichung. Mit PC-SAFT werden hier Reinstoffe durch einen Satz von drei Parametern charakterisiert. Die Optimierung wird durch eine Relaxierung der Reinstoffparameter ermöglicht. Dadurch können Prozess und Arbeitsmittel simultan in einem Schritt, dem *Continuous-Molecular Targeting* (CoMT), optimiert werden. Durch die Relaxierung entsprechen die optimalen Werte der Reinstoffparameter im Allgemeinen keinem realen Fluid. Daher werden im nachgeschalteten *Structure-Mapping* reale Stoffe gesucht, deren Eigenschaften den Eigenschaften des optimalen Arbeitsmittels nahe kommen. Dazu wird mittels einer Taylor-Approximation der Zielfunktion aus dem CoMT-Schritt eine Bewertung von Stoffen aus einer Datenbank durchgeführt. Die Methode erlaubt somit die gleichzeitige Optimierung von ORC Prozessen und den darin eingesetzten Arbeitsmitteln.

Das Structure-Mapping zur Suche nach optimalen Fluiden aus einer Datenbank erlaubt es nicht neue Arbeitsmittel zu identifizieren. Daher wird die Methode durch einen Computer-Aided Molecular Design (CAMD) Ansatz erweitert, der die Datenbanksuche ersetzt. Dabei werden die Reinstoffparameter durch eine Gruppenbeitrags-

7.2.2 CAMD objective - Result of adaptive structure–mapping as objective function in CAMD

An adaptive approach is presented for the systematic refinement of the structure-mapping in section 3.2.4. The adaptive approach yields a nonlinear estimate of the objective function as a function of the pure component parameters. The resulting approximation was shown to allow for the identification of working fluids that have not been identified by the basic structure-mapping (section 3.2.1). As the approximation is already used and thus available, the expected effort of application is low.

The result of the CAMD method for the structure-mapping can only be as good as the approximation of the objective function. When an inaccurate approximation is used as objective of the design of working fluids, sub-optimal working fluids can be identified. Thus, the usage of the final approximation of the adaptive structure-mapping could contribute to the identification of more promising working fluids. However, the resulting function is highly nonlinear transforming the quadratic problem (MIQP) into a nonlinear program (MINLP).

7.2.3 Economic objective - Integration of Non-Equilibrium Properties to Allow for Economic Objective Functions

The consideration of non-equilibrium properties of the working fluid is a further refinement of the PC-SAFT equation of state. The non-equilibrium properties that should be included into the design of an ORC system are mainly the viscosity of the fluid to allow for calculation of pressure-losses and the thermal conductivity for the calculation of the heat transfer area. These two properties allow for the sizing of the heat exchangers. As the heat exchangers contribute a major share of the investment cost of an ORC system (Quoilin et al., 2011; Coskun et al., 2011), an economic evaluation of the designed system is not possible on the basis of only equilibrium properties of the fluid. Thus the integration of non-equilibrium properties allows for a thorough comparison of fluids and processes on the basis of economics.

However, the selection of suitable cost-functions for the considered equipment into the optimization problem is necessary for the implementation of economic objective functions. These cost-functions have to be valid for the complete search space of working fluids considered in the optimization. The CoMT optimization spans a variety of working fluids from various families, which complicates the compilation of cost-functions. Thus, the integration of economic objective function can be considered low-risk and high-effort.

7.2.4 Structure alterations - Discrete degrees of freedom for alterations of the flowsheet

In this thesis, the flowsheet of the ORC system is fixed for all applications. However, structural alterations of the flowsheet can lead to further improvement. Structural alterations can be integrated in form of a superstructure, where all considered structural solutions are combined to one flowsheet and the optimizer can select or deselect units from the superstructure using binary variables (Voll et al., 2013).

Furthermore, superstructure-free approaches can be employed that rely on evolutionary algorithms for the selection of optimal structures and rigorous mathematical optimization for the integrated process and fluid design problem (Voll et al., 2012). The integration of such techniques for the alterations of the flowsheet can be categorized as mid-risk, mid-effort. However, to obtain meaningful results, the evaluation of structural alternatives should be performed on the basis of economic objective functions. Thus this refinement of the method has limited value, until also economic objective functions are implemented (as recommended in section 7.2.3).

7.2.5 Solving the unsolvable - Towards solving the integrated process and fluid design

At first glace, the hypothesis that the MINLP formulation of the integrated process and fluid design is prevented from solving by prohibitive size and complexity is the fundamental justification of this work. However, in the view of the author, the results of the thesis encourage research towards solving the problem in a single optimization based on the continuous-molecular targeting framework.

The results of the targeting show, that the relaxed version of the integrated problem can be solved efficiently. The CAMD method presented for the structure-mapping exploits an approximation of the objective function for sound and efficient design of fluids. A combination of these approaches could allow for solving the problem iteratively, following the basic idea of the Outer-approximation approach for solving MINLP (Duran and Grossmann, 1986; Viswanathan and Grossmann, 1990).

Bibliography

Abrams, D. S. and Prausnitz, J. M. (1975). "Statistical thermodynamics of liquid mixtures: A new expression for the excess Gibbs energy of partly or completely miscible systems". *AIChE Journal*, 21(1):116–128.

Adjiman, C. S., Galindo, A., and Jackson, G. (2014). "Molecules Matter: The Expanding Envelope of Process Design". In Eden, M. R., Siirola, J. D., and Towler, G., editors, *Proceedings of the 8th International Conference on Foundations of Computer-Aided Process Design*, volume 34 of *Computer Aided Chemical Engineering*. Elsevier Science, Burlington.

Aljundi, I. H. (2011). "Effect of dry hydrocarbons and critical point temperature on the efficiencies of organic Rankine cycle". *Renewable Energy*, 36(4):1196–1202.

Andersen, W. C. and Bruno, T. J. (2005). "Rapid Screening of Fluids for Chemical Stability in Organic Rankine Cycle Applications". *Industrial & Engineering Chemistry Research*, 44(15):5560–5566.

Andreasen, J. G., Larsen, U., Knudsen, T., Pierobon, L., and Haglind, F. (2014). "Selection and optimization of pure and mixed working fluids for low grade heat utilization using organic Rankine cycles". *Energy*, 73:204–213.

Angelino, G. and Colonna, P. d. P. (1998). "Multicomponent Working Fluids For Organic Rankine Cycles (ORCs)". *Energy*, 23(6):449–463.

Apostolakou, A. and Adjiman, C. S. (2003). "Optimization Methods in CAMD - II". In Achenie, Luke E. K., Gani, R., and Venkatasubramanian, V., editors, *Computer aided molecular design*, volume 12 of *Computer-aided chemical engineering*, pages 63–93. Elsevier, Amsterdam and Boston.

Bao, J. and Zhao, L. (2013). "A review of working fluid and expander selections for organic Rankine cycle". *Renewable and Sustainable Energy Reviews*, 24:325–342.

Barber, C. B., Dobkin, D. P., and Huhdanpaa, H. (1996). "The quickhull algorithm for convex hulls". *ACM Transactions on Mathematical Software*, 22(4):469–483.

Bardow, A., Steur, K., and Gross, J. (2010). "Continuous-Molecular Targeting for Integrated Solvent and Process Design". *Industrial & Engineering Chemistry Research*, 49(6):2834–2840.

Beyer, H.-G. and Schwefel, H.-P. (2002). "Evolution strategies – A comprehensive introduction". *Natural Computing*, 1(1):3–52.

Bicerano, J. (2002). *Prediction of polymer properties*, volume 65 of *Plastics engineering*. Marcel Dekker, New York, 3rd ed., rev. and expanded. edition.

Bischof, C., Khademi, P., Mauer, A., and Carle, A. (1996). "Adifor 2.0: automatic differentiation of Fortran 77 programs". *IEEE Computational Science and Engineering*, 3(3):18–32.

Blas, F. J. and Galindo, A. (2002). "Study of the high pressure phase behaviour of CO2+n-alkane mixtures using the SAFT-VR approach with transferable parameters". *Fluid Phase Equilibria*, 194-197:501–509.

Bombarda, P., Invernizzi, C. M., and Pietra, C. (2010). "Heat recovery from Diesel engines: A thermodynamic comparison between Kalina and ORC cycles". *Applied Thermal Engineering*, 30(2-3):212–219.

Bommareddy, S., Chemmangattuvalappil, N. G., Solvason, C. C., and Eden, M. R. (2010). "Simultaneous solution of process and molecular design problems using an algebraic approach". *Computers & Chemical Engineering*, 34(9):1481–1486.

Borsukiewicz-Gozdur, A. (2013). "Pumping work in the organic Rankine cycle". *Applied Thermal Engineering*, 51(1-2):781–786.

Branchini, L., Pascale, A. d., and Peretto, A. (2013). "Systematic comparison of ORC configurations by means of comprehensive performance indexes". *Applied Thermal Engineering*, 61(2):129–140.

Brignole, E. A. and Cismondi, M. (2003). "Molecular Design - Generation & Test Methods". In Achenie, Luke E. K., Gani, R., and Venkatasubramanian, V., editors, *Computer aided molecular design*, volume 12 of *Computer-aided chemical engineering*, pages 23–41. Elsevier, Amsterdam and Boston.

Bücker, H. M. and Corliss, G. F. (2006). "A Bibliography of Automatic Differentiation". In Bücker, H. M., Corliss, G. F., Naumann, U., Hovland, P., and Norris, B., editors, *Automatic Differentiation: Applications, Theory, and Implementations*, volume 50 of *Lecture Notes in Computational Science and Engineering*, pages 321–322. Springer-Verlag, Berlin/Heidelberg.

methode berechnet: Das Fluid wird als Zusammensetzung aus verschiedenen Bausteinen, den sogenannten Gruppen dargestellt. Die Gruppen können einzelne Atome oder kleinere Verbindungen von Atomen sein (z.B. eine Methylgruppe). Im CAMD wird dann eine Kombination aus diesen Gruppen gesucht, die entsprechend der Taylor-Approximation die optimale Molekularstruktur darstellt. Somit ist die Suche nach optimalen Arbeitsmitteln nicht mehr auf eine Datenbank beschränkt sondern erlaubt auch die systematische Suche nach neuen Arbeitsmitteln. Die Anwendung auf das Beispiel eines solar-betriebenen ORC zeigt, dass für realistische Anwendungen tatsächlich neue Arbeitsmittel besser geeignet sein können als die bisher eingestzten.

Für die Arbeitsmittelauswahl werden in der Regel konstante Wirkungsgrade für die Turbine angenommen. Der Wirkungsgrad der Turbine hat einen entscheidenden Einfluss auf die Wahl von Arbeitsmitteln. Umgekehrt ist der erreichbare Wirkungsgrad der Turbine ist abhängig vom eingesetzten Arbeitsmittel. Daher wird das Prozessmodell des ORC um ein Turbinenmodell erweitert. Dieses eindimensionale Modell für eine Radialturbine erlaubt eine Berechnung des Wirkungsgrades und ein vorläufiges Design der Turbine. Das Design der Turbine kann dazu genutzt werden, um nicht erlaubte Wertebereiche für Designparameter (z.B. niedrige Blatthöhe oder hohe Rotationsgeschwindigkeit) auszuschließen. Die Ergebnisse zeigen, dass die Beschränkung der Designparameter einen wesentlichen Einfluss auf die Wahl des Arbeitsmittels hat.

Die bisher aufgeführten Arbeiten beziehen sich auf die Auswahl eines Reinstoffes als Arbeitsmittel im Kreisprozess. In der Literatur werden aktuell vermehrt auch Gemische als Arbeitsmittel vorgeschlagen, um den Wirkungsgrad des Prozesses weiter zu steigern. Daher wird die vorgestellte Methode für simultane Optimierung von Arbeitsmittel und Prozess auf Gemische erweitert. Die Optimierung identifiziert analog zu den Reinstoffen ein optimales, hypothetisches Arbeitsmittelgemisch, das wiederum keinem realen Gemisch entspricht. Das Optimum stellt allerdings eine obere Schranke für die Güte des Prozesses dar. Kein reales Gemisch kann besser sein, als das hypothetische, optimale Arbeitsmittelgemisch. Diese Beobachtung erlaubt einen konzeptionellen Vergleich von Gemischen und Reinstoffen als Arbeitsmitteln, der losgelöst von einzelnen Fluiden erfolgen kann. Dabei wird der Prozess jeweils mit einem Gemisch und einem Reinstoff als Arbeitsmittel optimiert. Die Differenz der Ergebnisse erlaubt es, die Vorteile des Einsatzes von Gemischen zu quantifizieren.

Die vorgestellte Methode eine glichzeitige Optimierung von Arbeitsmitteln und ORC Prozessen. Dabei können sowohl bereits existierende Stoffe aus Datenbanken berücksichtigt werden als auch neue Arbeitsmittel, die bisher nicht bekannt waren. Des Weiteren können auch Gemische aus Arbetsmitteln in der Optimierung berücksichtigt werden, was die Wirkungsgrade der ORC Prozesse noch weiter erhöhen kann.

Colonna, P., Casati, E., Trapp, C., Mathijssen, T., Larjola, J., Turunen-Saaresti, T., and Uusitalo, A. (2015). "Organic Rankine Cycle Power Systems: From the Concept to Current Technology, Applications, and an Outlook to the Future". *Journal of Engineering for Gas Turbines and Power*, 137(10):100801.

Coniglio, L. and Daridon, J. L. (1997). "A group contribution method for estimating ideal gas heat capacities of hydrocarbons". *Fluid Phase Equilibria*, 139(1-2):15–35.

Constantinou, L. and Gani, R. (1994). "New group contribution method for estimating properties of pure compounds". *AIChE Journal*, 40(10):1697–1710.

Coskun, C., Oktay, Z., and Dincer, I. (2011). "Modified exergoeconomic modeling of geothermal power plants". *Energy*, 36(11):6358–6366.

Dai, Y., Wang, J., and Gao, L. (2009). "Parametric optimization and comparative study of organic Rankine cycle (ORC) for low grade waste heat recovery". *Energy Conversion and Management*, 50(3):576–582.

Delgado-Torres, A. M. and García-Rodríguez, L. (2010). "Analysis and optimization of the low-temperature solar organic Rankine cycle (ORC)". *Energy Conversion and Management*, 51(12):2846–2856.

Derringer, G. C. and Markham, R. L. (1985). "A computer-based methodology for matching polymer structures with required properties". *Journal of Applied Polymer Science*, 30(12):4609–4617.

Desai, N. B. and Bandyopadhyay, S. (2009). "Process integration of organic Rankine cycle". *Energy*, 34(10):1674–1686.

Dixon, S. L. and Hall, C. A. (2010). *Fluid mechanics and thermodynamics of turbomachinery*. Butterworth-Heinemann/Elsevier, Burlington, MA, 6th edition.

Drescher, U. and Brüggemann, D. (2007). "Fluid selection for the Organic Rankine Cycle (ORC) in biomass power and heat plants". *Applied Thermal Engineering*, 27(1):223–228.

Dumitru, P. D., Plopeanu, M., and Badea, D. (2013). "Comparative study regarding the methods of interpolation". In Badea, A.-C., editor, *Recent advances in geodesy and geomatics engineering*, Energy, environmental and structural engineering series 17, pages 45–52. World Scientific and Engineering Academy and Society.

Duran, J.-L. and Grossmann, I. E. (1986). "An outer-approximation algorithm for a class of mixed-integer nonlinear programs". *Mathematical programming*, 36(3):307–339.

Duvedi, A. P. and Achenie, L. E. K. (1996). "Designing environmentally safe refrigerants using mathematical programming". *Chemical Engineering Science*, 51(15):3727–3739.

Eden, M. R., Jergensen, S. B., Gani, R., and El-Halwagi, M. M. (2003). "Reverse problem formulation based techniques for process and product synthesis and design". In *Process Systems Engineering 2003, 8th International Symposium on Process Systems Engineering*, volume 15 of *Computer Aided Chemical Engineering*, pages 451–456. Elsevier.

Eden, M. R., Jergensen, S. B., Gani, R., and El-Halwagi, M. M. (2004). "A novel framework for simultaneous separation process and product design". *Chemical Engineering and Processing: Process Intensification*, 43(5):595–608.

Ertl, P. (2003). "Cheminformatics Analysis of Organic Substituents: Identification of the Most Common Substituents, Calculation of Substituent Properties, and Automatic Identification of Drug-like Bioisosteric Groups". *Journal of Chemical Information and Modeling*, 43(2):374–380.

Fernández, F. J., Prieto, M. M., and Suárez, I. (2011). "Thermodynamic analysis of high-temperature regenerative organic Rankine cycles using siloxanes as working fluids". *Energy*, 36(8):5239–5249.

Fiaschi, D., Manfrida, G., and Maraschiello, F. (2012). "Thermo-fluid dynamics preliminary design of turbo-expanders for ORC cycles". *Applied Energy*, 97:601–608.

Fink, T., Bruggesser, H., and Reymond, J.-L. (2005). "Virtual Exploration of the Small-Molecule Chemical Universe below 160 Daltons". *Angewandte Chemie International Edition*, 44(10):1504–1508.

Fischer, J. (2011). "Comparison of trilateral cycles and organic Rankine cycles". *Energy*, 36(10):6208–6219.

Friedler, F., Fan, L. T., Kalotai, L., and Dallos, A. (1998). "A combinatorial approach for generating candidate molecules with desired properties based on group contribution". *Computers & Chemical Engineering*, 22(6):809–817.

Gani, R. (2004). "Chemical product design: challenges and opportunities". *Computers & Chemical Engineering*, 28(12):2441–2457.

Gani, R. (2007). "Case studies in chemical product design — use of CAMD techniques". In Gani, R., Ng, K. M., and Dam-Johansen, K., editors, *Chemical Product Design: Toward a Perspective through Case Studies*, volume 23, pages 435–458. Elsevier, Amsterdam and Boston.

Gani, R., Achenie, Luke E. K., and Venkatasubramanian, V. (2003). "Chapter 1: Introduction to CAMD". In Achenie, Luke E. K., Gani, R., and Venkatasubramanian, V., editors, *Computer aided molecular design*, volume 12 of *Computer-aided chemical engineering*, pages 3–21. Elsevier, Amsterdam and Boston.

Gani, R., Nielsen, B., and Fredenslund, A. (1991). "A group contribution approach to computer-aided molecular design". *AIChE Journal*, 37(9):1318–1332.

Gil-Villegas, A., Galindo, A., Whitehead, P. J., Mills, S. J., Jackson, G., and Burgess, A. N. (1997). "Statistical associating fluid theory for chain molecules with attractive potentials of variable range". *The Journal of Chemical Physics*, 106(10):4168.

Gross, J. (2005). "An equation-of-state contribution for polar components: Quadrupolar molecules". *AIChE Journal*, 51(9):2556–2568.

Gross, J. and Sadowski, G. (2001). "Perturbed-Chain SAFT: An Equation of State Based on a Perturbation Theory for Chain Molecules". *Industrial & Engineering Chemistry Research*, 40(4):1244–1260.

Gross, J. and Sadowski, G. (2002). "Application of the Perturbed-Chain SAFT Equation of State to Associating Systems". *Industrial & Engineering Chemistry Research*, 41(22):5510–5515.

Gross, J. and Vrabec, J. (2006). "An equation-of-state contribution for polar components: Dipolar molecules". *AIChE Journal*, 52(3):1194–1204.

Guo, T., Wang, H. X., and ShengJun Zhang (2010). "Working fluids of a low-temperature geothermally-powered Rankine cycle for combined power and heat generation system". *Science in China Series E: Technological Sciences*, 53(11):3072–3078.

Guo, T., Wang, H. X., and Zhang, S. J. (2011). "Fluids and parameters optimization for a novel cogeneration system driven by low-temperature geothermal sources". *Energy*, 36(5):2639–2649.

Han, S. P. (1977). "A globally convergent method for nonlinear programming". *Journal of Optimization Theory and Applications*, 22(3):297–309.

Harinck, J., Guardone, A., and Colonna, P. d. P. (2009). "The influence of molecular complexity on expanding flows of ideal and dense gases". *Physics of Fluids*, 21(8):086101.

Harper, P. M. (2000). *A Multi-Phase, Multi-Level Framework for Computer Aided Molecular Design*. PhD thesis, Technical University of Denmark, Lyngby.

Harper, P. M., Gani, R., Kolar, P., and Ishikawa, T. (1999). "Computer-aided molecular design with combined molecular modeling and group contribution". *Fluid Phase Equilibria*, 158-160:337–347.

Heberle, F. and Brüggemann, D. (2010). "Exergy based fluid selection for a geothermal Organic Rankine Cycle for combined heat and power generation". *Applied Thermal Engineering*, 30(11-12):1326–1332.

Heberle, F., Preißinger, M., and Brüggemann, D. (2012). "Zeotropic mixtures as working fluids in Organic Rankine Cycles for low-enthalpy geothermal resources". *Renewable Energy*, 37(1):364–370.

Hung, T.-C., Wang, S. K., Kuo, C. H., Pei, B. S., and Tsai, K. F. (2010). "A study of organic working fluids on system efficiency of an ORC using low-grade energy sources". *Energy*, 35(3):1403–1411.

Joback, K. G. and Reid, R. C. (1987). "Estimation of Pure-Component Properties from Group-Contributions". *Chemical Engineering Communications*, 57(1-6):233–243.

Jog, P. K. and Chapman, W. G. (1999). "Application of Wertheim's thermodynamic perturbation theory to dipolar hard sphere chains". *Molecular Physics*, 97(3):307–319.

Kang, S. H. (2012). "Design and experimental study of ORC (organic Rankine cycle) and radial turbine using R245fa working fluid". *Energy*, 41(1):514–524.

Kier, L. B. and Hall, L. H. (1986). *Molecular connectivity in structure-activity analysis*, volume 9 of *Chemometrics series*. Research Studies Press and Wiley, Letchworth, Hertfordshire, England and New York.

Chapter 1

Introduction

The depletion of fossil fuels is a well-known problem (Shafiee and Topal, 2009) and the concluding increase in energy cost (Nel and Cooper, 2009) leads to a trend to a more rational use of resources. Furthermore, the limited fossil fuel reserves urge the need to identify regenerative energy sources as a replacement. Here, this thesis is going to focus on systems used for the exploitation of heat sources.

Renewable heat sources are mainly used in two fashions: the direct use of heat and the conversion of heat to power. Direct use of renewable sources for heating is possible for many heat sources and allows for recovery of heat on high as well as low temperature levels. Most common is the direct use of geothermal heat. The highest share of geothermal heat directly used is heat pump systems (71 % of the installed capacities worldwide) as reviewed by Lund et al. (2011). The same authors identify bathing and swimming applications (13 %) and space heating (11 %) as major applications. However, the direct use of heat is only possible, if the heat source and the consumer are close to each other. Furthermore, the focus on heating limits the plant operation mainly to cold days. For this reason, the limited consumption can be the limiting factor for the exploitation of heat sources. Accordingly, the use factor for the direct use is estimated to be 27 % (Lund et al., 2011). In this work, the focus is on the indirect use of renewable heat, where the heat is converted to electrical power. The conversion allows for the efficient transportation using the existing power grid.

One conversion technology allowing for small-scale systems with high flexibility is the Organic Rankine Cycle (ORC). The ORC is based on the Rankine Cycle, which is used for the conversion of heat to power in almost every fossil-based power plant. The Rankine Cycle exploits a temperature difference between a heat source (e.g., hot flue gas from combustion) and a heat sink (e.g., the environment via a cooling tower). For this purpose, a pressurized working fluid is evaporated using heat from the heat source and run over a turbine, where work is extracted. After the turbine, the working

Löffler, M. K. (2008). "Flash Evaporation in Cyclones". *Chemical Engineering & Technology*, 31(7):1062–1065.

Lund, J. W., Freeston, D. H., and Boyd, T. L. (2011). "Direct utilization of geothermal energy 2010 worldwide review.". *Geothermics*, 40(3):159–180.

Mago, P. J., Chamra, L. M., Srinivasan, K., and Somayaji, C. (2008). "An examination of regenerative organic Rankine cycles using dry fluids". *Applied Thermal Engineering*, 28(8-9):998–1007.

Maizza, V. and Maizza, A. (1996). "Working fluids in non-steady flows for waste energy recovery systems". *Applied Thermal Engineering*, 16(7):579–590.

Maizza, V. and Maizza, A. (2001). "Unconventional working fluids in organic Rankine-cycles for waste energy recovery systems". *Applied Thermal Engineering*, 21(3):381–390.

Marcoulaki, E. C. and Kokossis, A. C. (2000). "On the development of novel chemicals using a systematic optimisation approach. Part II. Solvent design". *Chemical Engineering Science*, 55(13):2547–2561.

Marrero, J. and Gani, R. (2001). "Group-contribution based estimation of pure component properties". *Fluid Phase Equilibria*, 183-184:183–208.

Matlab (2012). *The MathWorks Inc., R2012b (8.0.0.783), 32-bit.*

Mavrou, P., Papadopoulos, A. I., Stijepovic, M. Z., Seferlis, P., Linke, P., and Voutetakis, S. (2015). "Novel and conventional working fluid mixtures for solar Rankine cycles: Performance assessment and multi-criteria selection". *Applied Thermal Engineering*, 75:384–396.

Mikielewicz, D. and Mikielewicz, J. (2010). "A thermodynamic criterion for selection of working fluid for subcritical and supercritical domestic micro CHP". *Applied Thermal Engineering*, 30(16):2357–2362.

Müller, E. A., Vega, L. F., and Gubbins, K. E. (1994). "Theory and simulation of associating fluids: Lennard-Jones chains with association sites". *Molecular Physics*, 83(6):1209–1222.

Muller, P. (1994). "Glossary of terms used in physical organic chemistry (IUPAC Recommendations 1994)". *Pure and Applied Chemistry*, 66(5).

Nafey, A. S. and Sharaf, M. A. (2010). "Combined solar organic Rankine cycle with reverse osmosis desalination process: Energy, exergy, and cost evaluations". *Renewable Energy*, 35(11):2571–2580.

Nannan, N. R., De Servi, Carlo M., van der Stelt, Teus, Colonna, P., and Bardow, A. (2013). "An Equation of State Based on PC-SAFT for Physical Solvents Composed of Polyethylene Glycol Dimethylethers". *Industrial & Engineering Chemistry Research*, 52(51):18401–18412.

Naser, S. F. and Fournier, R. L. (1991). "A system for the design of an optimum liquid-liquid extractant molecule". *Computers & Chemical Engineering*, 15(6):397–414.

Nel, W. P. and Cooper, C. J. (2009). "Implications of fossil fuel constraints on economic growth and global warming". *Energy Policy*, 37(1):166–180.

Odele, O. and Macchietto, S. (1993). "Computer Aided Moleclar Design: A Novel Method for Optimal Solvent Selection". *Fluid Phase Equilibria*, 82:47–54.

Oyewunmi, O. A., Taleb, A. I., Haslam, A. J., and Markides, C. N. (2014). "An Assessment of Working-Fluid Mixtures Using SAFT-VR MIE for Use in Organic Rankine Cycle Systems for Wastte-Heat Recovery". *Computational Thermal Sciences: An International Journal*, 6(4):301–316.

Paepe, M. d., D'Herdt, P., and Mertens, D. (2006). "Micro-CHP systems for residential applications". *Energy Conversion and Management*, 47(18-19):3435–3446.

Palma-Flores, O., Flores-Tlacuahuac, A., and Canseco-Melchor, G. (2015). "Optimal molecular design of working fluids for sustainable low-temperature energy recovery". *Computers & Chemical Engineering*, 72:334–349.

Papadopoulos, A. I. and Linke, P. (2005). "A Unified Framework for Integrated Process and Molecular Design". *Chemical Engineering Research and Design*, 83(6):674–678.

Papadopoulos, A. I. and Linke, P. (2009). "Integrated solvent and process selection for separation and reactive separation systems". *Chemical Engineering and Processing: Process Intensification*, 48(5):1047–1060.

Papadopoulos, A. I., Stijepovic, M. Z., and Linke, P. (2010). "On the systematic design and selection of optimal working fluids for Organic Rankine Cycles". *Applied Thermal Engineering*, 30(6-7):760–769.

Papadopoulos, A. I., Stijepovic, M. Z., Linke, P., Seferlis, P., and Voutetakis, S. (2013). "Toward Optimum Working Fluid Mixtures for Organic Rankine Cycles using Molecular Design and Sensitivity Analysis". *Industrial & Engineering Chemistry Research*, 52(34):12116–12133.

Pedrosa, N., Vega, L. F., Coutinho, J. A. P., and Marrucho, I. M. (2006). "Phase Equilibria Calculations of Polyethylene Solutions from SAFT-Type Equations of State". *Macromolecules*, 39(12):4240–4246.

Peng, D.-Y. and Robinson, D. B. (1976). "A New Two-Constant Equation of State". *Industrial & Engineering Chemistry Fundamentals*, 15(1):59–64.

Pereira, F. E., Keskes, E., Galindo, A., Jackson, G., and Adjiman, C. S. (2011). "Integrated solvent and process design using a SAFT-VR thermodynamic description: High-pressure separation of carbon dioxide and methane". *Computers & Chemical Engineering*, 35(3):474–491.

Pistikopoulos, E. N. and Stefanis, S. K. (1998). "Optimal solvent design for environmental impact minimization". *Computers & Chemical Engineering*, 22(6):717–733.

Poling, B. E., Prausnitz, J. M., and O'Connell, J. P. (2001). *The properties of gases and liquids*. McGraw Hill professional. McGraw-Hill, New York, 5th edition.

Powell, M. J. D. (1978). "A fast algorithm for nonlinearly constrained optimization calculations". In Watson, G., editor, *Numerical Analysis*, volume 630 of *Lecture Notes in Mathematics*, pages 144–157. Springer Berlin Heidelberg.

Powell, M. J. D. (1979). "Variable metric methods for constrained optimization". In Glowinski, R., Lions, J., and Laboria, I., editors, *Computing Methods in Applied Sciences and Engineering, 1977, I*, volume 704 of *Lecture Notes in Mathematics*, pages 62–72. Springer Berlin Heidelberg.

Preißinger, M. (2014). *Thermoökonomische Bewertung des Organic Rankine Cycles bei der Stromerzeugung aus industrieller Abwärme*, volume 25 of *Thermodynamik - Energie, Umwelt, Technik*. Logos Berlin, Berlin.

Prestwich, S. and Roli, A. (2005). "Symmetry Breaking and Local Search Spaces". In Barták, R. and Milano, M., editors, *Integration of AI and OR Techniques in Constraint Programming for Combinatorial Optimization Problems*, volume 3524 of *Lecture Notes in Computer Science*, pages 273–287. Springer Berlin Heidelberg.

Qadir, A., Chiesa, M., and Abbas, A. (2014). "In silico design of solvents for carbon capture with simultaneous optimisation of operating conditions". *International Journal of Greenhouse Gas Control*, 30:179–187.

Qiu, G. (2012). "Selection of working fluids for micro-CHP systems with ORC". *Renewable Energy*, 48:565–570.

Qiu, G., Liu, H., and Riffat, S. B. (2011). "Expanders for micro-CHP systems with organic Rankine cycle". *Applied Thermal Engineering*, 31(16):3301–3307.

Qiu, G., Shao, Y., Li, J., Liu, H., and Riffat, S. B. (2012). "Experimental investigation of a biomass-fired ORC-based micro-CHP for domestic applications". *Fuel*, 96:374–382.

Quoilin, S., Broek, Martijn Van Den, Declaye, S., Dewallef, P., and Lemort, V. (2013). "Techno-economic survey of Organic Rankine Cycle (ORC) systems". *Renewable and Sustainable Energy Reviews*, 22:168–186.

Quoilin, S., Declaye, S., Tchanche, B. F., and Lemort, V. (2011). "Thermo-economic optimization of waste heat recovery Organic Rankine Cycles". *Applied Thermal Engineering*, 31(14-15):2885–2893.

Raman, V. and Maranas, C. D. (1998). "Optimization in product design with properties correlated with topological indices". *Computers & Chemical Engineering*, 22(6):747–763.

Rayegan, R. and Tao, Y. X. (2011). "A procedure to select working fluids for Solar Organic Rankine Cycles (ORCs)". *Renewable Energy*, 36(2):659–670.

Redlich, O. and Kwong, J. (1949). "On the Thermodynamics of Solutions. V. An Equation of State. Fugacities of Gaseous Solutions". *Chemical Reviews*, 44(1):233–244.

Renon, H. and Prausnitz, J. M. (1968). "Local compositions in thermodynamic excess functions for liquid mixtures". *AIChE Journal*, 14(1):135–144.

Rodgers, C. and Geiser, R. (1987). "Performance of a High-Efficiency Radial/Axial Turbine". *Journal of Turbomachinery*, 109(2):151.

Roskosch, D. and Atakan, B. (2015). "Reverse engineering of fluid selection for thermodynamic cycles with cubic equations of state, using a compression heat pump as example". *Energy*, 81:202–212.

Rowley, R., Wilding, W. V., Oscarson, J. L., Yang, Y., Zundel, N. A., Daubert, T. E., and Danner, R. P. (2006). "DIPPR Data Compilation of Pure Chemical Properties". *Design Institute for Physical Properties*.

Sahinidis, N. V., Tawarmalani, M., and Yu, M. (2003). "Design of alternative refrigerants via global optimization". *AIChE Journal*, 49(7):1761–1775.

Saleh, B., Koglbauer, G., Wendland, M., and Fischer, J. (2007). "Working fluids for low-temperature organic Rankine cycles". *Energy*, 32(7):1210–1221.

Samudra, A. P. and Sahinidis, N. V. (2013). "Optimization-based framework for computer-aided molecular design". *AIChE Journal*, 59(10):3686–3701.

Sauer, E., Stavrou, M., and Gross, J. (2014). "Comparison between a Homo- and a Heterosegmented Group Contribution Approach Based on the Perturbed-Chain Polar Statistical Associating Fluid Theory Equation of State". *Industrial & Engineering Chemistry Research*, 53(38):14854–14864.

Sauret, E. and Rowlands, A. S. (2011). "Candidate radial-inflow turbines and high-density working fluids for geothermal power systems". *Energy*, 36(7):4460–4467.

Seader, J. D. and Henley, E. J. (2006). *Separation process principles*. Wiley, Hoboken, N.J., 2nd ed. edition.

Shafiee, S. and Topal, E. (2009). "When will fossil fuel reserves be diminished?". *Energy Policy*, 37(1):181–189.

Shepard, D. (1968). "A two-dimensional interpolation function for irregularly-spaced data". In Blue, R. B. and Rosenberg, A. M., editors, *Proceedings of the 1968 23rd ACM national conference*, pages 517–524.

Siddiqi, M. A. and Atakan, B. (2011). "Investigation of the Criteria for Fluid Selection in Rankine Cycles for Waste Heat Recovery". *International Journal of Thermodynamics*, 14(3).

Soave, G. (1972). "Equilibrium constants from a modified Redlich-Kwong equation of state". *Chemical Engineering Science*, 27(6):1197–1203.

Solms, N. v., Michelsen, M. L., and Kontogeorgis, G. M. (2003). "Computational and Physical Performance of a Modified PC-SAFT Equation of State for Highly Asymmetric and Associating Mixtures". *Industrial & Engineering Chemistry Research*, 42(5):1098–1105.

fluid is condensed and pressurized again.

As for every conversion between different forms of energy, there is a limit to the possible rate of conversion from heat to power. Carnot derived an upper bound for the efficiency of the conversion. Under his assumptions,

> "the motive power of heat is independent of the agents employed to realize it; its quantity is fixed solely by the temperatures of the bodies between which is effected, finally, the transfer of the caloric." Carnot (1824)

Thus, the efficiency of conversion directly depends on the temperature of the heat source. Once again, this observation favors fossil-based systems, as the high temperature level achieved by combustion allows for high efficiency. Another interesting observation in Carnot's statement is that efficiency does not depend on the agents employed to realize it. This statement is true under the idealizing assumptions Carnot made to derive an upper bound. However, in non-ideal, real world applications there is a significant influence of the working fluid on the performance of the conversion.

In large-scale power plants, water is used as a working fluid in the Rankine Cycle. Water can be handled easily, it is safe (i.e., not flammable, not toxic, not hazardous), available and cheap. However, the ORC is used for small-scale conversion of low-temperature heat to power. Technical restrictions prevent the usage of water for these applications. The low temperature level of the heat sources would lead to low turbine efficiency and low pressure levels enforcing vacuum technology for the condensation (Vankeirsbilck et al., 2011). Therefore, water is replaced by organic working fluids in the ORC. Organic fluids are typically more volatile than water, which allows for practical pressure levels. Furthermore, the higher molar mass of organic compounds allows for the design of more efficient turbine.

On the one hand side, turning away from water as a working fluid is a challenge for the design of the system. Additional to the design of the cycle itself (e.g., identification of optimal pressure and temperature levels, mass flow rates), a suitable working fluid has to be identified. The search-space of organic fluids is virtually unlimited. Estimates on the number of organic substances range from 10^{20} to 10^{24} (Ertl, 2003). Limited down to stable substances below a certain molar mass (160 Da) Fink et al. (2005) estimate $13,892,436$ compounds still leaving the designer of a system with an virtually unlimited number of options. On the other hand, the working fluid selection adds a new degree of freedom to the design. Thus, the design of the system becomes even more flexible allowing for a design specifically tailored to the application. Additional flexibility and gain in performance are awarded for overcoming the challenges of integrated working fluid and process design.

fluid is condensed and pressurized again.

As for every conversion between different forms of energy, there is a limit to the possible rate of conversion from heat to power. Carnot derived an upper bound for the efficiency of the conversion. Under his assumptions,

> "the motive power of heat is independent of the agents employed to realize it; its quantity is fixed solely by the temperatures of the bodies between which is effected, finally, the transfer of the caloric." Carnot (1824)

Thus, the efficiency of conversion directly depends on the temperature of the heat source. Once again, this observation favors fossil-based systems, as the high temperature level achieved by combustion allows for high efficiency. Another interesting observation in Carnot's statement is that efficiency does not depend on the agents employed to realize it. This statement is true under the idealizing assumptions Carnot made to derive an upper bound. However, in non-ideal, real world applications there is a significant influence of the working fluid on the performance of the conversion.

In large-scale power plants, water is used as a working fluid in the Rankine Cycle. Water can be handled easily, it is safe (i.e., not flammable, not toxic, not hazardous), available and cheap. However, the ORC is used for small-scale conversion of low-temperature heat to power. Technical restrictions prevent the usage of water for these applications. The low temperature level of the heat sources would lead to low turbine efficiency and low pressure levels enforcing vacuum technology for the condensation (Vankeirsbilck et al., 2011). Therefore, water is replaced by organic working fluids in the ORC. Organic fluids are typically more volatile than water, which allows for practical pressure levels. Furthermore, the higher molar mass of organic compounds allows for the design of more efficient turbine.

On the one hand side, turning away from water as a working fluid is a challenge for the design of the system. Additional to the design of the cycle itself (e.g., identification of optimal pressure and temperature levels, mass flow rates), a suitable working fluid has to be identified. The search-space of organic fluids is virtually unlimited. Estimates on the number of organic substances range from 10^{20} to 10^{24} (Ertl, 2003). Limited down to stable substances below a certain molar mass (160 Da) Fink et al. (2005) estimate $13,892,436$ compounds still leaving the designer of a system with an virtually unlimited number of options. On the other hand, the working fluid selection adds a new degree of freedom to the design. Thus, the design of the system becomes even more flexible allowing for a design specifically tailored to the application. Additional flexibility and gain in performance are awarded for overcoming the challenges of integrated working fluid and process design.

Wei, D., Lu, X., Lu, Z., and Gu, J. (2007). "Performance analysis and optimization of organic Rankine cycle (ORC) for waste heat recovery". *Energy Conversion and Management*, 48(4):1113–1119.

Wertheim, M. S. (1984a). "Fluids with highly directional attractive forces. I. Statistical thermodynamics". *Journal of Statistical Physics*, 35(1-2):19–34.

Wertheim, M. S. (1984b). "Fluids with highly directional attractive forces. II. Thermodynamic perturbation theory and integral equations". *Journal of Statistical Physics*, 35(1-2):35–47.

Wertheim, M. S. (1986a). "Fluids with highly directional attractive forces. III. Multiple attraction sites". *Journal of Statistical Physics*, 42(3-4):459–476.

Wertheim, M. S. (1986b). "Fluids with highly directional attractive forces. IV. Equilibrium polymerization". *Journal of Statistical Physics*, 42(3-4):477–492.

Zhai, H., Shi, L., and An, Q. (2014). "Influence of working fluid properties on system performance and screen evaluation indicators for geothermal ORC (organic Rankine cycle) system". *Energy*, 74:2–11.